SYNTHESIS OF HETEROCYCLIC POLY(ARYLENEETHYNYLENE)S

A Dissertation
Presented to
The Academic Faculty

By

Carlito Bangcuyo

In Partial Fulfillment
Of the Requirements for the Degree
Doctor of Philosophy in Chemistry

Georgia Institute of Technology
Fall 2006

SYNTHESIS OF HETEROCYCLIC POLY(ARYLENEETHYNYLENE)S

Approved by:

Dr. Uwe Bunz, Chair
School of Chemistry & Biochemistry
Georgia Institute of Technology

Dr. Marcus Weck
School of Chemistry & Biochemistry
Georgia Institute of Technology

Dr. Laren Tolbert
School of Chemistry & Biochemistry
Georgia Institute of Technology

Dr. Mohan Srinivasarao
School of Polymer, Textile & Fiber Engineering
Georgia Institute of Technology

Date Approved: Fall 2006

To my wife, Maureen

and my sons, Ripley and Carlito III

Acknowledgements

First of all, I would like to thank my wife and mother of my sons, Maureen. We have been through some very rough times together throughout my graduate career, and I could not have done this without your support and resolve. Your compassion, understanding, and sacrifice has gotten me to where I need to be today. I would also like to thank my sons, Ripley and Carlito III, for being around and making my life hectic. I cannot imagine what my life would be like without the two of you. You two bring so much joy and chaos into my life.

Next, I would like to thank the Bunz group for being a great group of people to work with. Special thanks to Sandra Shotwell, Selma Bakbak, and Belma Erdogan for being my lab mates and more than friends to me; my basketball rival, Yiqing Wang; my video game comrade, Brian Englert; the story teller, Glen Brizius; my drinking buddy, Jake Leech; the soup provider, Ikbum Kim; and my mutual symbiote, whom I do not know if I could have completed this without his administrative guidance, James Wilson. Other current/past Bunz group member that I would like to thank are: Joe Ellsworth, Brandon Emery, Paul Windschiefs, Shelby Schuler, Mike Nolan, Lynette Prophyl, Kirsten Matthews, Holly Ricks, Matt Laskoski, Jason Morton, Jimmy Gilbert, Dr. G., Steffan Scholz, Cindy Muenzenberg, and Pinghua Ge. A big thanks to the three people that helped me out the most when I first entered the Bunz group: Shane Waybright, Neil Pschirer, and Winfried Steffen.

I would like to thank my parents for helping me get through this ordeal. Without their support and patience over the years I do not think I would be in this position. Thanks to my brother Ronald for his companionship, humor, and generally keeping me a kid at heart. Thanks to my sister, her husband, and my niece. They are always there to lend a shoulder for me to rest my head on or an ear to listen when I need it the most.

I would like to thank my committee members: Dr. Marcus Weck, Dr. Laren Tolbert, Dr. Mohan Svirinsarao, Dr. Wally Scrivens, Dr. Cathy Murphy, Elise Vaughn, and Dr. Uwe Bunz. Uwe, you have been a great advisor and good friend to me and my family. I could not have enjoyed my grad school experience without you. Thank you to everyone and know that I love you all.

Table of Contents

Table of Contents (cont.)

List of Tables

List of Figures

List of Figures (cont.)

List of Schemes

List of Abbreviations

IR	Infrared
MS	Mass spectrometry
MP	Melting Point
NMR	Nuclear magnetic resonance
THF	Tetrahydrofuran
DMF	Dimethylforamide
TIPS	Triisopropylsilyl
TMS	Trimethylsilyl
UV-Vis	Ultraviolet-visible
XRD	X-ray diffraction
GPC	Gel permeation chromatography
PAE	Poly(arylenenethynylene)
PPE	Poly(phenyleneethynylene)
HCSH	Heck-Cassar-Sonogashira-Hagihara
LUMO	Lowest unoccupied molecular orbital
HOMO	Highest unoccupied molecular orbital
TFA	Trifluoroacetic acid
CV	Cyclic Voltammetry

Summary

Poly(aryleneneethynylene)s or PAEs are an interesting class of conjugated polymers that have potential uses in the field of thin film transistors, organic LEDs, sensors, and molecular wires. The field of PAEs have grown in recent years, however very few of its conjugated polymers have a heterocyclic motif contained within them. We have designed some conjugated heterocyclic polymers that contain quinoline, benzothiadiazole, and quinoxaline. These polymers show interesting ionochromic and solvochromic effects as well as unusual solid state properties. Some of these polymers will demonstrate their ability to form fascinating nanostructures by use of either mesoporous discs or gold mediated nanotubes. Finally, we also have produced peralkynylated heterocyclic molecules for use in potential n-semiconductive devices. These molecules are not only aesthetically pleasing, but versatile molecules that could be used in conjugated PAEs.

Chapter 1

Introduction

Poly(arylenenethynylene)s or PAEs are an interesting class of conjugated polymers that have potential uses in the field of thin film transistors, organic LEDs, sensors, and molecular wires. The field of PAEs have grown in recent years, however very few of its conjugated polymers have a heterocyclic motif contained within them. We have designed some conjugated heterocyclic polymers that contain quinolines, benzothiadiazoles, and quinoxalines. We also have produced peralkynylated heterocyclic molecules for use in potential *n*-semiconductive devices. These molecules are not only aesthetically pleasing, but are versatile molecules that could be used in conjugated PAEs.

Our initial goal of this project was to create a heterocyclic "self assembling ladder" PAE as an alternative to the pre-existing ladder polymers. Ladder polymers represent a unique class of highly stable, durable materials. An interesting example of the synthesis of these ladder polymers was first reported by Kimura (Scheme 1.1).[1] The polymerization produced a poly(enamine) structure. When this material was heated, a cyclization reaction occurred, known as the Conrad-Limpach reaction,[2, 3] with the elimination of ethanol to produce the ladder structure. However, due to the ladder polymer's insolubility, processing can be difficult and the structure is relatively undefined.

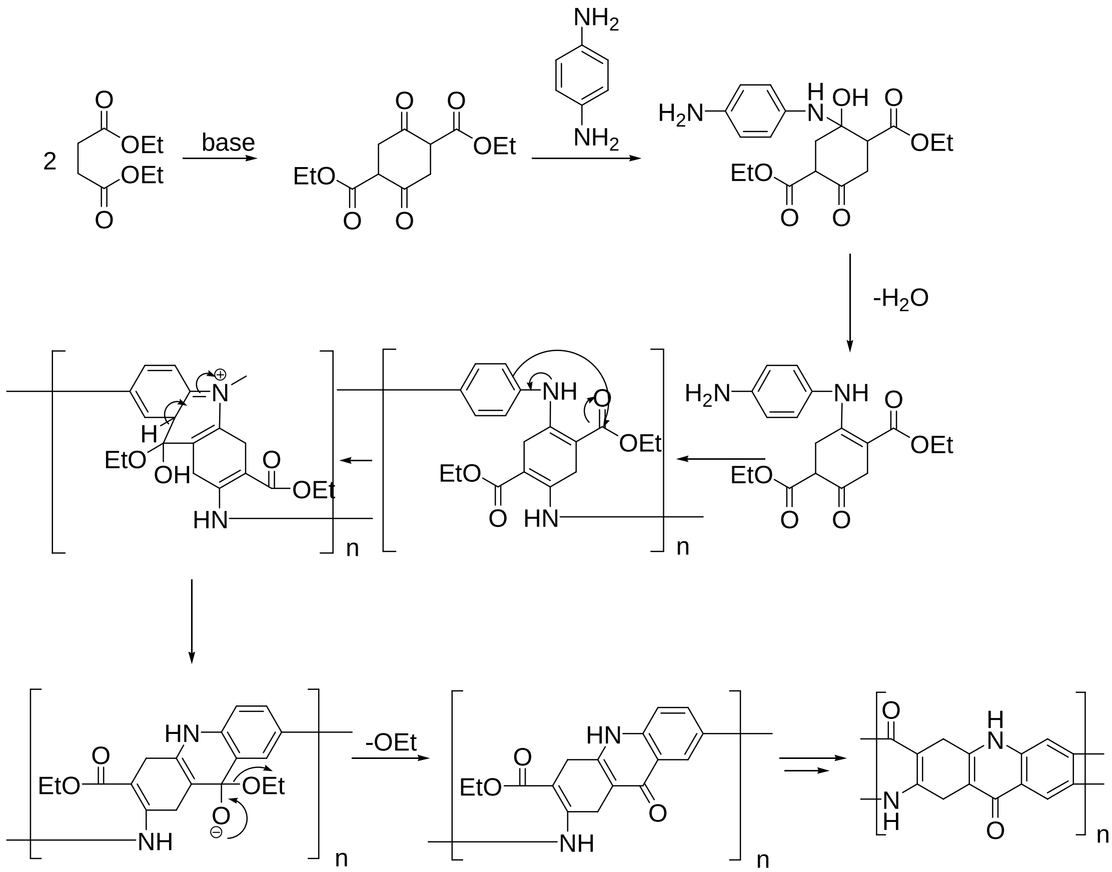

Scheme 1.1. Synthesis of a ladder polymer by Kimura.

With the synthesis of the quinoxaline based PAEs, we could theoretically form a polymer that would orient itself by placing a proton or cation species within the binding pockets (Figure 1.1). Through this route, we were able to gain some advantages over the traditional ladder polymers in that: (1) a predefined system would be established, (2) these materials would be better soluble than their counterparts thus increasing the ease of processibility, and (3) these PAEs would show interesting chromic effects.

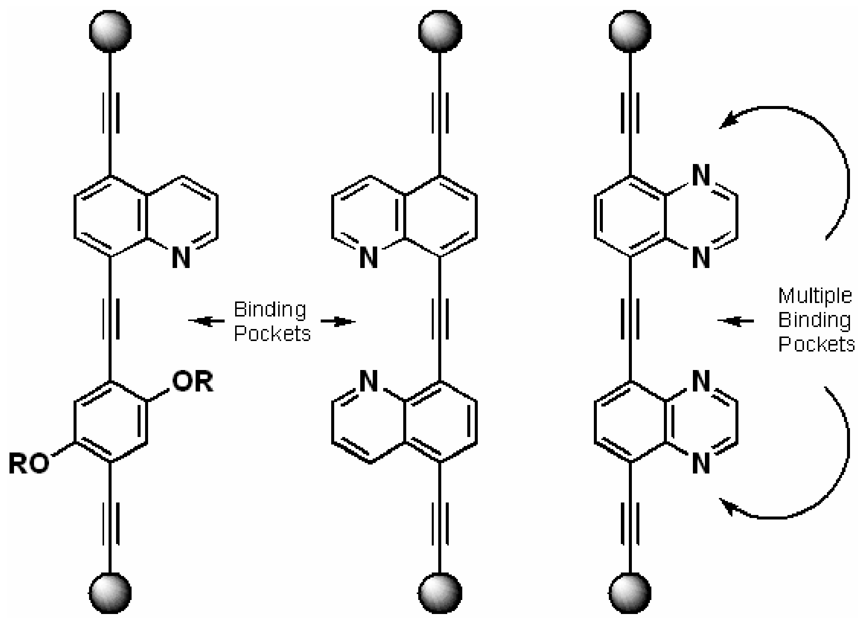

Figure 1.1. Models depicting the binding pocket in these heterocyclic PAEs. The binding pocket would increase from left to right. With the case of the quinoxaline model, the binding would theoretically produce an alignment orientation effect.

Arguably, the simplest model that we would synthesize would be the quinoline model (Figure 1.1). This copolymer would be soluble and would become the foundation for the current topic of heterocyclic PAEs. From these initial results, we will determine whether the quinoline copolymer would be soluble, and thus a smaller system of the quinoxaline copolymer would be synthesized and studied. The quinoxaline polymers would be made via a benzothiadiazole route that would allow the desired 5,8-positioning of the alkynes. The systematic approach to finding a solubilizing group for the quinoxaline PAEs would be realized by creating a small library of differing pendant side chains.

The creation of these novel heterocyclic PAEs yields interesting results that can be evidenced through the ionochromic and solvochromic behavior, and will be displayed in the following chapters. Coupled to the fact that these materials can form "pseudo" ladder copolymers, it would be of value to see if we can increase the solubility of these predefined systems. In addition to the heterocyclic based PAEs and our most recent work, we have also fabricated novel peralkynylated molecules that shifted our focus from the creation of linear copolymers to the expansion of a conjugated core system.

1.1. References

1. Kimura, S., *Makromol. Chem.* **1968,** *117*, 203.

2. Conrad, M.; Limpach, L., *Chem. Ber.* **1887,** *20*, 944.

3. Conrad, M.; Limpach, L., *Chem. Ber.* **1888,** *21*, 525.

CHAPTER 2

SYNTHESIS AND CHARACTERIZATION OF QUINOLINE-CONTAINING POLYARYLENEETHYNYLENES

2.1. Introduction

As previously stated in the introduction (Chapter 1), we intended to synthesize a quinoline monomer where the alkynes are situated in the 5 and 8 positions to for a binding pocket for sensing. However, our iodination conditions provided one isomer of the diiodoquinoline. In this chapter, we describe the synthesis of the unknown 3,6-diiodoquinoline and novel conjugated copolymers of the poly(arylenenethynylene) (PAE) type consisting of alternating benzene, acetylene, and 3,6-quinoline units (**8**, **10**, **12**). Upon protonation, the dialkyl-substituted copolymer **8** exhibits a bathochromically shifted yellow fluorescence from 399 nm to 524 nm.

Conjugated polymers (CP) are organic semiconductors and are important in applications that include: light-emitting diodes, thin film transistors, and plastic lasers.[1-17] They also have received ample attention as active components in sensors.[18,19-23] Bauerle, Swager, and others describes the ability of conjugated polymers to “sense” can be enhanced by the addition of an appendage as a recognition element.[22-24] Alternatively, the substitution of a C-H group by heteroatoms, preferably nitrogen in our case, into the main chain of the conjugated polymer could produce similar effects. Jenekhe, Schanze, Wasielewski, Eichen, Tour, Klemm, Meijer, and others have amply demonstrated this principle by introducing quinoline, pyridine, bipyridine, or phenanthroline moieties into conjugated polymers.[25-58] Wasielewski obtained interesting results and demonstrated that bispyridyl-poly(*p*-phenylenevinylene) hybrids show sensory properties for transition metal salts in both absorption and emission.[28,29,51] He discovered that Pd^{2+} and some lanthanides had a great effect upon λ_{max} in absorption. Intrigued by these results, we have prepared a series of unknown quinoline containing poly(aryleneethynylene)s (**8**, **10**, **12**), and studied their optical properties with respect to protonation and metal cation coordination.

2.2. Results and Discussion

The direct iodination of quinoline has been reported to give 5,8-diiodoquinoline (**4**).[39] According to the literature, Electrophilic iodination commences in the two most active positions of this interesting heterocycle (Scheme 2.1), however, we were unable to obtain **4**. Under the iodination conditions utilized ($I_2/KIO_4/H_2SO_4/CHCl_3$), an isomer of **4** where the halogens were substituted in the 3 and 6 positions formed according to NMR and analytical data. To obtain structural proof of the substitution pattern, we coupled the isolated diiodide with trimethylsilylacetylene under standard Pd catalysis, deprotected, and reacted the "naked" alkynyl quinoline in a second Pd-catalyzed coupling step with *o*-iodoanisole (Scheme 2.1). The generic trimeric product was highly crystalline, and we were able to isolate a suitable specimen for single crystal structure analysis from dichloromethane. Looking at the crystal structure, we were able to surmise that the iodination had occurred in the 3,6-position leading to the unknown 3,6-diiodoquinoline and subsequently to **6** (Figure 2.1).

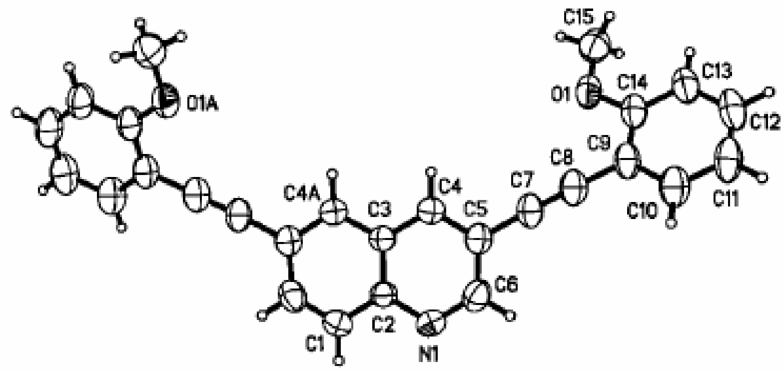

Figure 2.1. ORTEP plot of **6**. The anisotropic displacement parameters are shown at the 50% probability level. Bond length and bond angles are in excellent agreement with the expected values.

Originally, we had started our project under the premise to obtain 5,8-diiodoquinoline (**4**) to examine its oligomeric models and polymers. Even though we were unable to fabricate **4**, the synthetic access to **2** became the foundation to exploring the synthesis of novel poly(heteroaryleneethynylene)s.

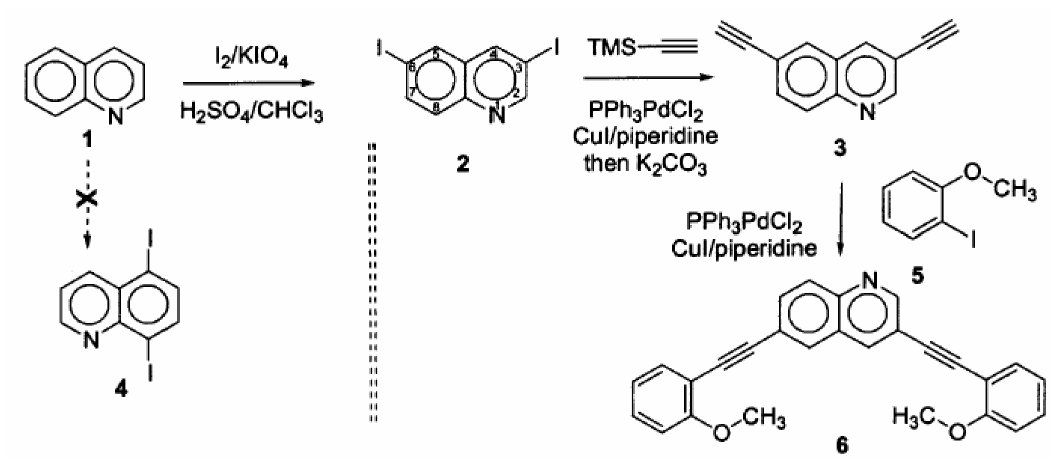

Scheme 2.1. Iodination of quinoline and synthesis of a quinoline bridged molecule

Reaction of **2** with 1,4-diethynyl-2,5-bis(2-ethylhexyl)benzene (**7**)[59] under Pd catalysis in piperidine furnished polymer **8** in a 93 % yield with a degree of polymerization (P_n) of 37 and a polydispersity (M_w/M_n, PDI) of 3.3. Polymer **10** was obtained by reaction of 3,6-diethynylquinoline (**3**) with 1,4-diiodo-2,5-bis(2-ethylhexyloxy)benzene **9** under identical conditions in an 88 % yield with a P_n of 95 (PDI = 3.1). In both polymers, **8** and **10**, the orientation of the quinoline units in the chain with respect to each other is random, as can be extracted from their ^1H and ^{13}C NMR spectra. The third, effectively nonconjugated polymer **12** (86 %; P_n = 11, M_w/M_n = 1.8) could be synthesized when **3** and **11** were coupled under Pd catalysis. Similarly, the orientation of the quinoline units in **12** is random according to NMR spectroscopy.

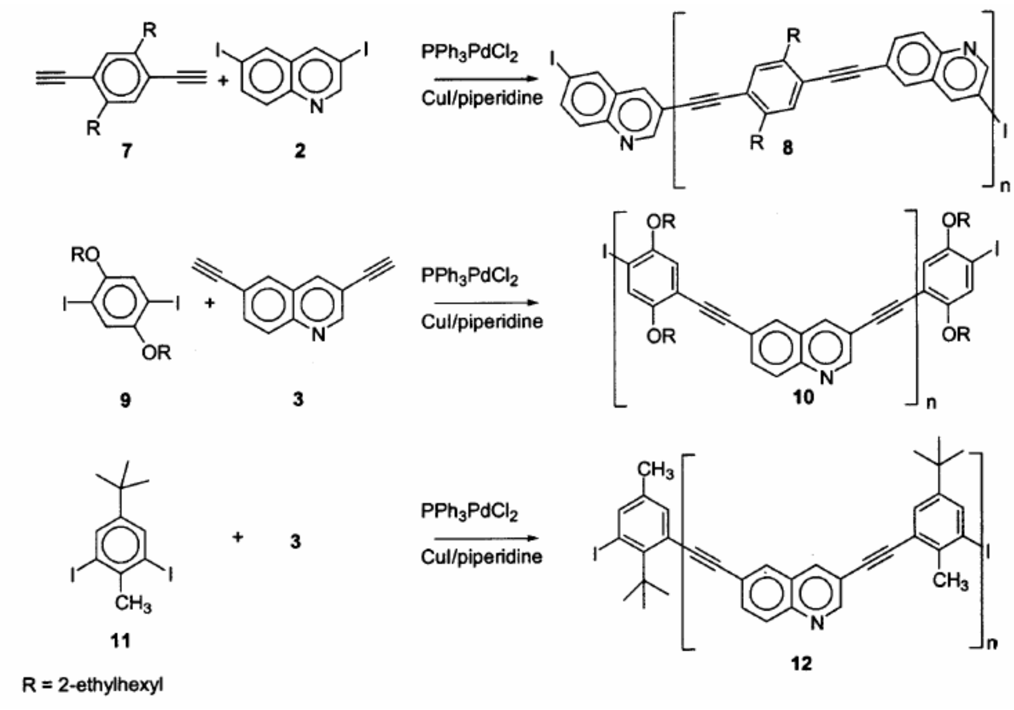

Scheme 2.2. Synthesis of quinoline containing polymers

The quinoline containing polymers were isolated by precipitation into methanol after careful washing with dilute ammonia solution. They are light-yellow or orange powders that are slightly soluble in chloroform and organic acids, such as trifluoroacetic acid (TFA) and acetic acid. To illustrate the solubility of these polymers, polymer **10** had to be heated for several hours in chloroform before it completely dissolved. All of these polymers are air, water, and light stable, but decompose above 150 ^{o}C under darkening as observed by polarizing microscopy. Samples of **8**, **10**, and **12** produce thin films and show shear-induced birefringence.

Absorption Behavior of Copolymers 8. 10, and 12

Dilute solutions of **8** in chloroform are light yellow with a λ_{max} at 380 nm. Addition of methanol induces aggregation and the development of a shoulder at 405 nm (Figure 2.2). The aggregation behavior of **8** are similar to aggregation studies performed on the dialkyl(*p*-polyphenyleneethynylene)s.[60, 61] In mixtures of acetic acid and chloroform, **8** displays UV-Vis spectra which are super imposable to those obtained by methanol addition. This suggests that the addition of a weak acid only induces aggregation.

Trifluoroacetic acid is more acidic than acetic acid, and its addition to a solution of **8** in chloroform leads to a substantial change in λ_{max} from 380 to 418 nm ($\Delta\lambda_{max}$ = 38 nm – protonated form Figure 1.3). Addition of metal cations (Table 1.1) to solutions of **8** leaves its absorption spectrum mostly unchanged. The nonconjugated polymer **12** resembles **8** in many respects in its UV-Vis spectrum, and also shows a bathochromic shift of 32 nm upon protonation with

TFA. Addition of metal salts leaves the absorption spectra of **12** unaltered as well (Table 2.1).

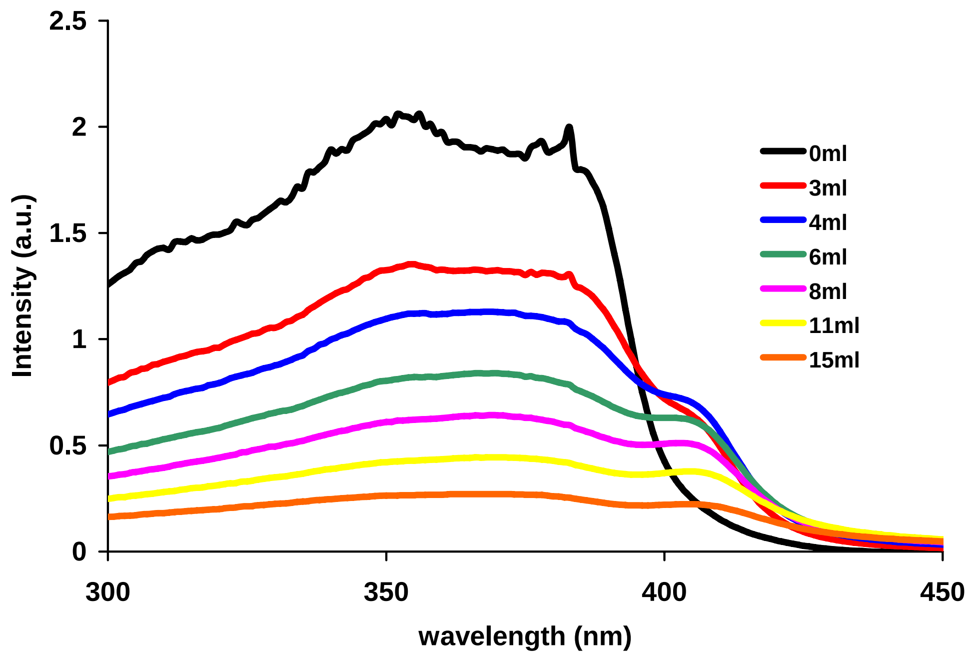

Figure 2.2. Addition of Methanol to polymer **8**. This Absorption spectra is similar when addition of acetic acid is used.

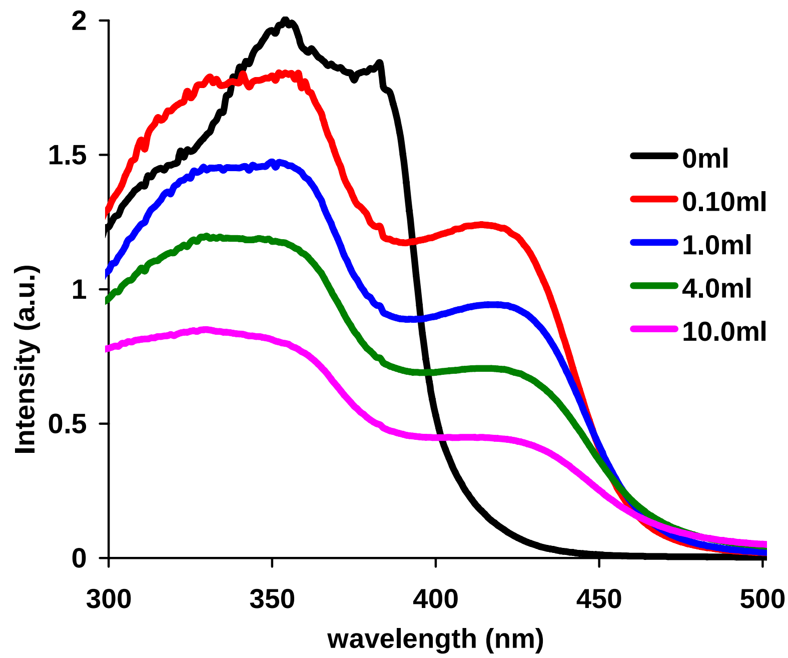

Figure 2.3. Addition of Trifluoroacetic Acid to **8.**

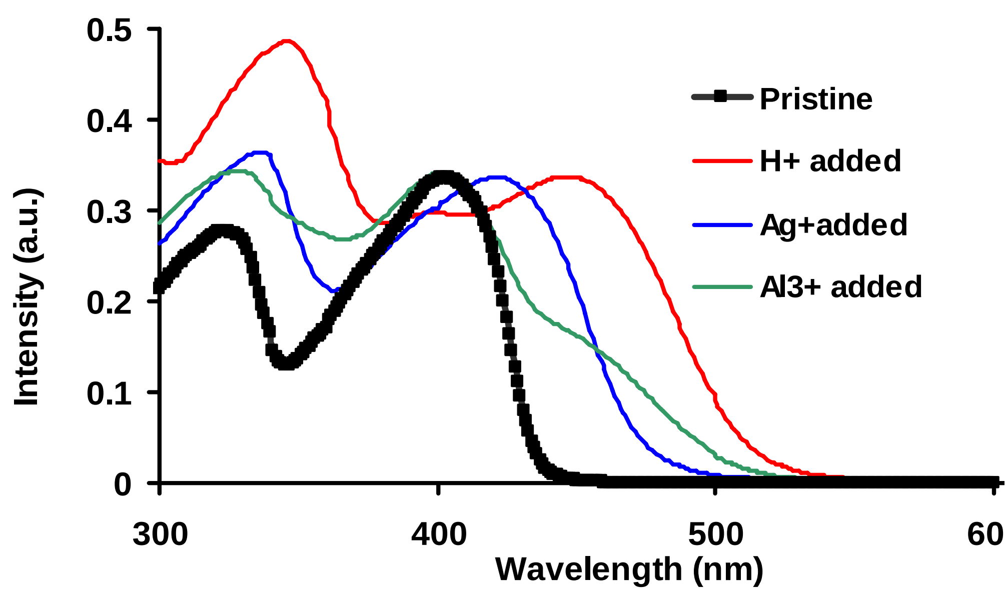

Figure 2.4. Absorption spectrum of polymer **10** pristine, after addition of trifluoroacetic acid, AgBF4, and Al2(SO4)3.

Table 2.1. Absorption Spectra (in nm) for Polymers **8**, **10**, and **12** at 298 K in Chloroform or Dichloromethane in Their Pristine Form and in the Presence and Absence of Metal Ions and Proton.

Run	Metal ion	Polymer **3**	Polymer **6**	Polymer **8**
1	Ion free	380 in $CHCl_3$ 406 in MeOH	401 in $CHCl_3$	310,368
2	Protonation H^+	408 with acetic acid 418 nm with TFA	347, 447	297, 333, 400
3	Pd^{++}	350, 402	442	327
4	Ag^+	361, 400	441	310,370
5	Fe^{++}	347, 381	331, 400	330
6	Fe^{+++}	----	404	327
7	Ni^{++}	350, 380	399	310,369
8	Mn^{++}	349, 381	399	303,370
9	La^{+++}	350, 380	400, 452	308,370
10	Cu^{++}	352, 381	399	326,371
11	Al^{+++}	352, 382	Nd	308,369
13	Zn^{++}	350, 389	399	308,369

Solutions of **10** display a light orange color and show a larger change in its λ_{max}, from 401 to 447 nm (ΔE = 0.32 eV) upon protonation with TFA (Figure 1.4). A second absorption at higher energy experiences a smaller bathochromic shift, from 331 to 344 nm (ΔE = 0.14 eV) upon protonation. Similar bathochromic shifts are observed when chloroform solutions of **10** are treated with solutions of Pd^{2+} or La^{3+} salts dissolved in a small amount of methanol (Table 2.1). However, if Ag^+ is added to a solution of **10,** an ionochromic effect is visible but less pronounced resulting in a λ_{max} of 422 nm (Figure 2.4). The cations Ni^{2+}, Mn^{2+}, Cu^{2+}, and Zn^{2+} do not change the absorption spectrum of **10** which are similar to the observations made for copolymers **8** and **12**. The UV-Vis spectrum of copolymer **10** is the one that is most affected of all the investigated polymers upon protonation or coordination of Pd^{2+}, La^{3+}, and Ag^{+} cations.

Fluorescence Behavior of Copolymers 8, 10, and 12

Polymer **8** is blue fluorescent in a solution of chloroform and emits at a λ_{max} of 399 nm. If **8,** in a moderately dilute solution (**8**: 5 mg/L), were treated with TFA, the original fluorescence disappeared and a broad emission at 509 nm emerged (Figure 2.5). Subsequent addition of more TFA led to a slight intensity decrease and a shift to 524 nm. No intermediate states could be detected even upon addition of very small amounts of TFA. If a much weaker acid, such as acetic acid, is used to titrate **8** then a decrease of the two bands at 399 and 413 nm is observed, while a new maximum appeared at 515 nm. Only after the addition of substantial amounts of acetic acid did the original emission features disappear (Figure 2.6).

Most metal ions weaken or quench the fluorescence of **8**, but Fe^{3+} and Al^{3+} show an effect upon the fluorescence (weak emission at 505 nm) which is similar to that observed upon protonation (Table 2.2). We attribute this behavior to the acidity of the hexaquo ions of iron(III) and aluminum(III) according to this equation: $M(H_2O)_6^{3+} + H_2O = M(H_2O)_5(OH)^{2+} + H_3O^{+}$. The emission behavior of **12** resembles that of **8** with respect to both protonation and metal salt complexation (Table 2.2).

To our surprise, the dialkoxy polymer **10** shows complete quenching of its fluorescence upon addition of TFA at a concentration of 5 mg/L (Figure 2.7). We did not see the appearance of a bathochromically shifted emission. Within this concentration range, self-absorption is not significant.[7] If the polymer solution of **10** was diluted to the concentration of 0.025 mg/L then we observed that fluorescence persisted upon addition of TFA and was slightly red-shifted with respect to the original emission. Metal salts either quenched the emission of **10** or left the emission relatively unchanged. Particularly interesting is that Al^{3+} and Fe^{3+} quench the emission of **10** in a protic environment which we can surmise to be the hydrolysis of their hexaquo ions.

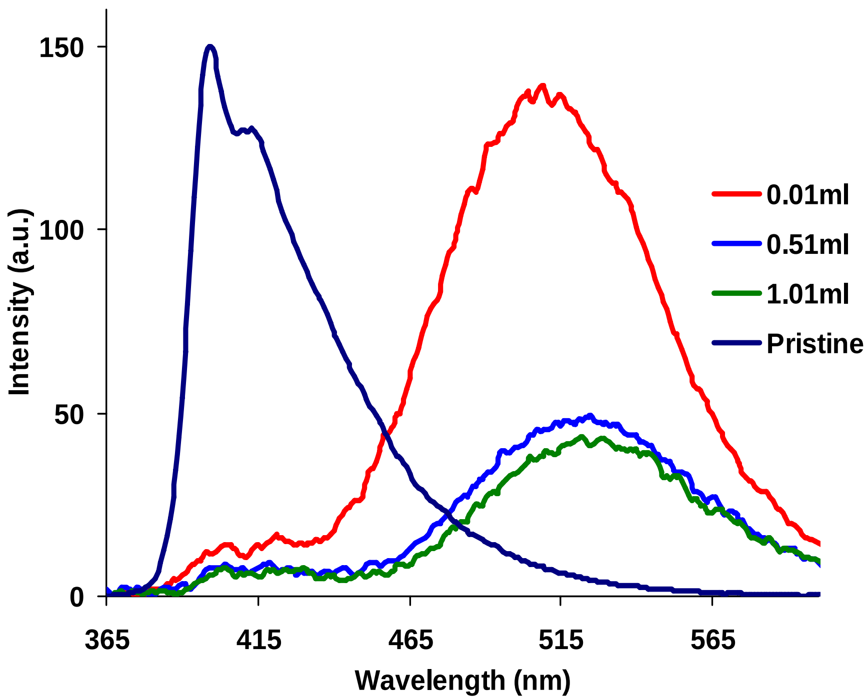

Figure 2.5. Emission spectrum of polymer **10** with the addition of TFA produces a bathochromic shift at 509 nm.

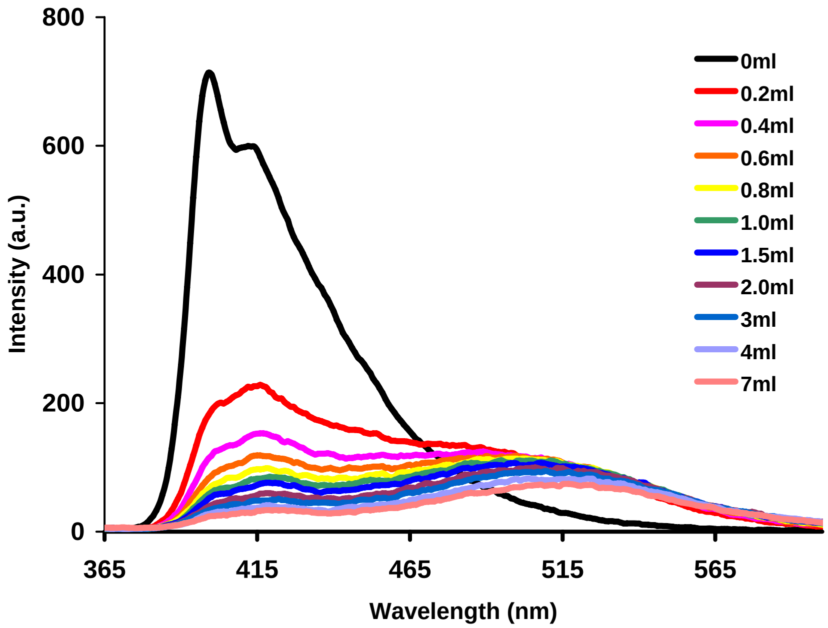

Figure 2.6. A decrease in fluorescence of **10** upon continuous addition of acetic acid.

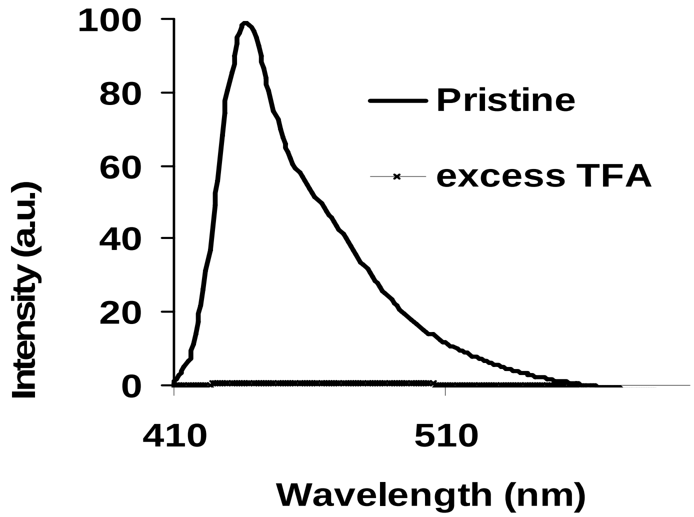

Figure 2.7. Emission spectra of polymer **10** with the addition of TFA. The fluorescence is quenched.

Table 2.2. Emission spectra for polymers **3, 6** and **8** at 298 K in chloroform or dichloromethane in their pristine form and in the presence and absence of metal ions and proton.

Run	Metal ion	Polymer **3**	Polymer **6**	Polymer **8**
1	ion free	399, 417	437	381
2	Protonation H^+	505-524, broad	Quenched	496
3	Pd^{++}	422	Quenched	Quenched
4	Ag^+	Quenched, 422 Weak intensity	Quenched	383
5	Fe^{++}	417	437	383
6	Fe^{+++}	504 (Weak Intensity)	Quenched	384
7	Ni^{++}	411	437	383
8	Mn^{++}	417	437	383
9	La^{+++}	417	437	383
10	Cu^{++}	417	437	383
11	Al^{+++}	520 (Weak Intensity)	Quenched	383
12	Pb^{++}	417	437	383, 589
13	Zn^{++}	417	437	383

Optical Studies Discussion

The alkyl chain substituted polymers **8** and **12** resemble each other in absorption and emission. We will discuss the optical properties of **8** which are almost superimposable to the optical properties of **12**, while the dialkoxy polymer **10** shows a distinctly different behavior. Polymer **12** is formally cross conjugated due to the presence of the meta-benzene linkages, but **8** shows similar conjugation to most poly(aryleneethynylene)s leading to a **12** nm bathochromic shift in its solution of UV-Vis spectrum if compared to **12**. As previously stated from the studies performed by UV-Vis, polymer **8** shows a distinct aggregation behavior (Figure 1.2a) upon addition of either methanol or acetic acid.[60-62] However, acetic acid is not acidic enough to protonate **8** in the ground state. The UV-Vis spectroscopic signature of the aggregates looks similar to those observed in other PPE types,[60-62] and is suggestive of planarization of the backbone under maximization of conjugation. The shift of 26 nm is comparatively small to the one recorded for the PPEs under similar conditions(380-439 nm, $\Delta\lambda = 59$ nm). If TFA is added to solutions of **8** in chloroform, protonation leads to a distinctly intense red shifted broad band at 420 nm (Figure 2.5). As a consequence, aggregation and protonation are decoupled in the electronic ground state of **8**. Polymer **12** behaves in a similar fashion. Pd^{2+} and Ag^{+} lead to a significant bathochromic shift in the absorption spectrum of **8.** This shift conforms to the observation upon the addition of methanol to **8**. However, the UV-Vis spectrum of **12** is virtually unchanged by the addition of those metal salts (Table 2.1).

The change in the emission spectrum of **8** upon protonation with TFA is remarkable because it features a brilliantly yellow emission band at 504 nm in acid that shifts to 524 nm with the addition of a large excess of TFA (Figure 2.5). The large half-width of the emission suggests that it is an intramolecular charge-transfer band. The lifetimes of polymer **8**'s emission in its protonated and unprotonated forms were both below 1 ns excluding excimer formation. The emission at 504 nm is due to the fact that only every second quinoline unit is protonated, while the feature at 524 nm would represent fluorescence of the fully protonated species **8**H^{+}. Small amounts of TFA (10-100 μL) are sufficient enough to switch the emission of **8**, but the presence of acetic acid leads to a gradual change in emission from 417 to 504 nm. This suggests that the partially protonated **8** is in equilibrium with its basic nonprotonated form. Acetic acid leads to aggregation of polymer **8** in its ground state but not to protonation. However, in the excited state, protonation occurs according to the fluorescence data previously shown, suggesting that **8** is considerably more basic in its excited that in its ground state. This polymer acts similar to the related dipyridophenazines in which the LUMO is centered mainly at the phenazine nitrogens.[63-66] The emission spectra of **8** in the presence of metal cations display a weak feature at >500 nm for Fe^{3+} and Al^{3+} both which can hydrolyzed to provide protons. Thus, we interpret the behavior of **8** as being primarily due to protonation and not metal complexation.

The alkoxy-substituted polymer **10** (Figure 1.8) features large bathochromic shifts upon protonation as well as metal salt coordination. An explanation for this behavior is not clear, but may involve a substantial intramolecular charge-transfer character in these donor-acceptor substituted polymers. Emission of **10** in its protonated form is critically dependent upon its concentration.[60, 61] Upon addition of TFA to solutions of **10** (5 mg/L), the fluorescence disappears, while at a concentration 0.025 mg/L a red-shifted emission is observed in strongly acidic solution. The emission is shifted from 437 to 462 nm due to formation of **10**H^+. This behavior was somewhat surprising, but the formation of an excimer complex with a nonemissive lowest lying excited state is known to occur in aggregates, and explains the behavior if the dimerizations of partially protonated chains of **10** into excimers is assumed.[63, 65, 66] At very low concentrations such excimers would not form, and thus emissions from single polymer chains would be expected and is observed.

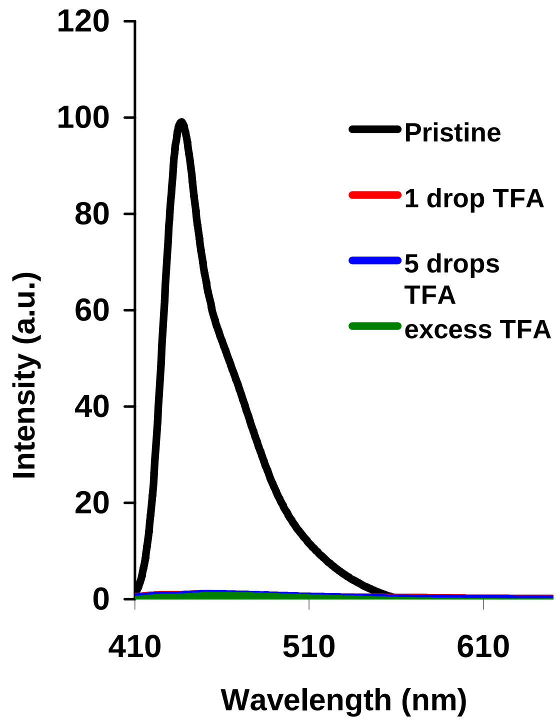

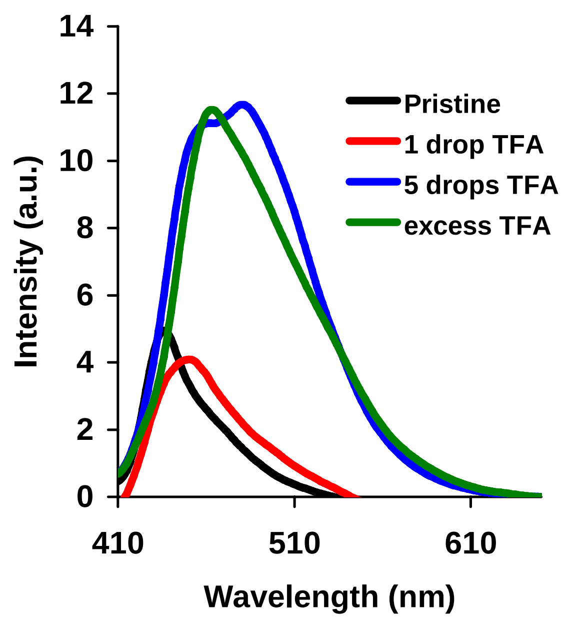

Figure 2.8. Emission spectrum of **10** in the presence of TFA at two different concentrations: (top) 5 mg/L, (bottom) 0.025 mg/L.

Conclusion

Novel quinoline containing poly(aryleneethynylene)s can be prepared by conventional Pd-catalyzed couplings. Depending upon their solubilizing groups, these polymers display a remarkable variation in their optical behavior with respect to emission and absorption. Protonation of these heterocyclic and basic polymers has a large effect upon their optical properties illustrated in the case of **10** to a bathochromically shifted absorption and to brilliant yellow and strong fluorescence in the case of **8**. While we were unable to synthesize the proposed conjugated quinoline system, the novel class of heterocyclic copolymers created laid the foundation for the rest of this thesis. In the future, quinoline copolymers featuring a 5,8 substitution pattern will hopefully be developed by future Bunz group members to clarify more of a single binding pocketed PAE. We now divert our attention to the synthesis of the quinoxaline based PAE, and do so by starting with the benzothiadiazoles in the next chapter.

2.3. Experimental

3,6-Diiodoquinoline (2). In a 1000 mL round bottom flask, quinoline (50.0 g, 387 mmol), iodine (100 g, 394 mmol), KIO_4 (50.0 g, 0.217 mol), acetic acid (200 mL), $CHCl_3$ (150 mL), concentrated H_2SO_4 (60 mL), and H_2O (60 mL) are stirred for 96 h at 90 ^oC. The solution is neutralized with sodium bicarbonate, washed with aqueous sodium sulfite, and extracted with hexanes (3 x 100 mL). Crystallization from ethanol produces yellow crystals of diiodoquinoline (26.1 g, 18 %).[1] Mp: 155 ^oC. IR (neat): υ 2956, 2922, 2852, 1567, 1455, 1376, 1324, 1053, 935, 908, 864, 822. ^1H NMR ($CDCl_3$): δ 9.03 (s, 1H), 8.42 (s, 1H), 8.11 (s, 1H), 7.96 (d, 1H), 7.78 (d, 1H). ^{13}C NMR ($CDCl_3$): δ 156.36, 145.40, 142.57, 138.98, 135.65, 1313.41, 93.41, 90.97. MS ($C_9H_5NI_2$): *m/z* 381.

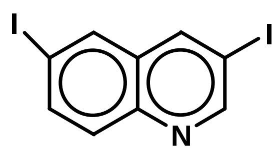

3,6-Bis(trimethylsilylethynyl)quinoline. A flame-dried 1000 mL schlenk flask containing 5,8-diiodoquinoline (11.0 g, 34.2 mmol), $Pd(PPh_3)_2Cl_2$ (0.150 g, 2.14 mmol), CuI (0.100 g, 0.525 mmol), and piperidine (10 mL) is degassed and evacuated. After drop-wise addition of TMS acetylene (5.50 g, 55.0 mmol) the resulting mixture is stirred for 16 h at ambient temperature. Addition of hexanes (150 mL) is followed by aqueous workup and purification by column chromatography (80:20 hexanes: dichloromethane) to furnish a clear oil (84 %). The adduct was subsequently deprotected, and only checked for purity by ^{13}C NMR. ^{13}C NMR ($CDCl_3$): δ 153.08, 146.43, 138.47,

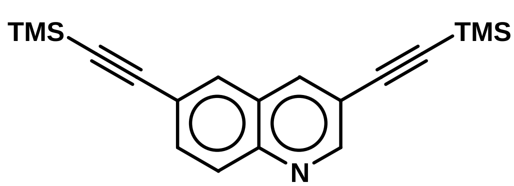

133.20, 131.40, 129.60, 126.91, 122.42, 118.20, 104.42, 101.99, 99.04, 96.56, 0.141.

3,6-Diethynylquinoline (3). To a 500 mL round bottom flask, 3,6-bis(trimethylsilylethynyl)quinoline (7.00 g, 21.8 mmol) and an excess amount of K_2CO_3 (15.0 g, 108 mmol) was added to methanol (200 mL) and stirred overnight. Addition of hexanes (150 mL) is followed by aqueous workup and purification by crystallization from ethanol to yield brownish crystals of **5** (4.67 g, 94 %). Mp: 116-118 ^{o}C. IR (neat): υ 3268, 3179, 2922, 1429, 1337, 984, 916, 832, 673, 627. ^{1}H NMR ($CDCl_3$): δ 8.93 (s, 1H), 8.24 (s, 1H), 8.04 (d, 1H), 7.95 (s, 1H), 7.77 (d, 1H), 3.31 (s, 1H), 3.22 (s, 1H). ^{13}C NMR ($CDCl_3$): δ 153.19, 146.79, 139.05, 133.33, 131.86, 129.83, 126.82, 121.53, 117.27, 83.04, 81.37, 80.80, 79.27. MS ($C_{19}H_{23}Ni_2$): *m/z* 177.

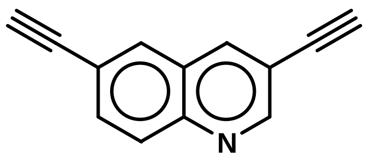

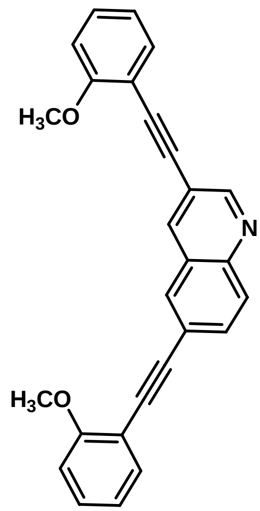

Synthesis of the Model Trimer 6: In a flame-dried 50 mL schlenk flask are placed 3,6-diethynylquinoline (0.750 g, 4.23 mmol), iodoanisole (2.69 g, 11.5 mmol), $Pd(PPh_3)_2Cl_2$ (39 mg, 0.05 mmol), CuI (50 mg, 0.263 mmol), and piperidine (7 mL). The reaction was stirred for 24 h at room temperature. For workup, chloroform (3 x 50 mL) followed by aqueous workup. Purification by column chromatography (80:20 hexanes:dichoromethane) followed by crystallization (80:15:5 hexanes:dichloromethane:ethyl acetate) produces colorless crystals (1.54 g, 93 %). Mp: 142 °C. IR (neat): υ 3071, 2958, 2924, 2851, 2211, 1593, 1575, 1492, 1462, 1433, 1358, 1275, 1181, 1162, 1131, 1101, 1023, 915, 835, 750. ^{1}H NMR ($CDCl_3$): δ 8.99 (d, 1H), 8.27 (d, 1H), 8.06-8.00 (m, 1H), 7.85-7.81 (m, 1H), 7.57-7.54 (m, 1H), 7.37-7.33 (m, 2H), 7.01-6.93 (m, 6H), 3.95 (d, 6H). ^{13}C NMR ($CDCl_3$): δ 160.08, 152.62, 146.00, 137.67, 133.69, 130.67, 130.45, 130.18, 129.33, 127.07, 122.53, 120.55, 118.42, 110.70, 92.77, 90.36, 89.53, 87.50, 55.83. λmax (abs, $CHCl_3$): 289, 328. λmax (em, $CHCl_3$): 387. MS ($C_{27}H_{19}NO_2$): *m/z* 389.

General Procedure for the Synthesis of the Quinoline Polymers. In a flame-dried 500 mL schlenk flask under inert atmosphere are placed 3,6-diethynylquinoline and the necessary comonomer, 1 mol % $Pd(PPh_3)_2Cl_2$, 1 mol % CuI, and piperidine (15 mL). The reaction mixture was stirred for 48 h. For workup, chloroform (3 x 50 mL) was added. The solution was washed three times with water and a 10% dilute ammonia solution to remove the transition metal containing catalyst residues. Removal of solvent and addition of methanol (400 mL) precipitates the polymers, which are isolated by filtration and vacuum dried.

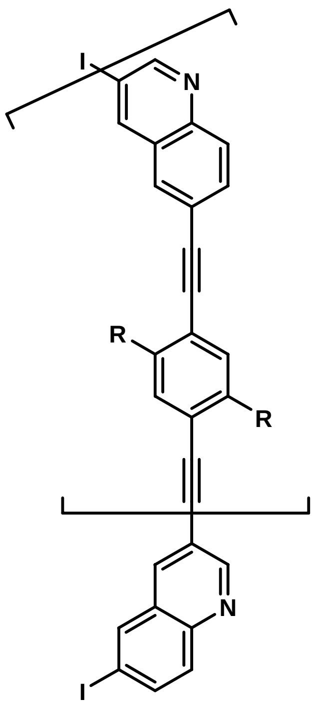

Polymer 8. 1,4-Diethynyl-2,5-bis(2-ethylhexyl)benzene (2.00 g, 5.70 mmol) and 3,6-diiodoquinoline (2.00g, 5.25 mmol) were reacted according to the general procedure to furnish a green-yellow powder (2.33 g, 93%) which was well soluble in chloroform. IR (neat): υ 3307, 2957, 2926, 2857, 2208, 1614, 1500, 1461, 1378, 1351, 1271, 1215, 1128, 908, 834, 758. 1H NMR (CDCl3): δ 8.94 (s, 1H), 8.20 (s, 1H), 8.05 (m, 1H), 7.93 (m, 1H), 7.77 (m, 1H), 7.29 (m, 2H), 2.74 (m, 2H), 1.77-0.79 (m, 13H). ^{13}C NMR ($CDCl_3$): δ 152.70, 147.12, 141.92, 137.64, 134.06, 132.84, 130.70, 129.91, 127.42, 123.03, 122.92, 92.81, 90.75, 82.98, 82.43, 82.07, 78.67, 40.73, 38.87, 32.79, 29.21, 29.16, 25.94, 23.32, 14.35, 11.10. GPC (polystyrene standards): Pn = 37, PDI 2.75. λmax (abs, $CHCl_3$): 380 nm. λmax (em, $CHCl_3$): 399, 417 nm.

Polymer 10. Application of the general procedure to 3,6-diethynylquinoline (0.500 g, 2.82 mmol) and 1,4-diiodo-2,5-bis(2-ethylhexyloxy)benzene (1.55 g, 2.64 mmol) furnished an orange powder (1.18 g, 88 %) which was not very

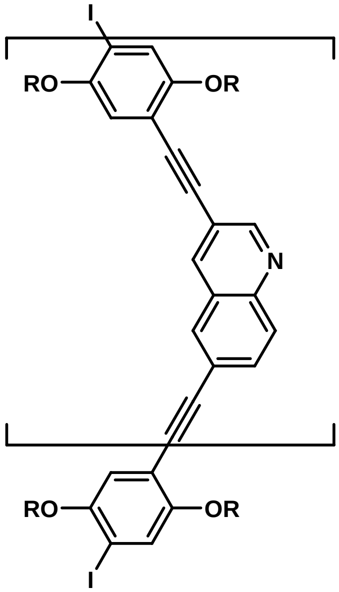

soluble in chloroform or any other organic solvent. IR (neat): υ 2956, 2858, 2210, 1613, 1504, 1463, 1418, 1380, 1276, 1213, 1125, 1033, 907, 855, 833, 627. ^{1}H NMR ($CDCl_3$): δ 9.00 (s, 1H), 8.24 (s, 1H), 8.07 (d, 1H), 7.98 (s, 1H), 7.82 (d, 1H), 7.11 (s, 1H), 3.99 (s, 2H), 1.86-0.89 (bm, 15H). ^{13}C NMR (CPMAS): δ 152.70, 145.71, 129.71, 121.84, 117.56, 113.48, 92.69, 70.81, 39.65, 23.15, 13.79, 11.53. GPC (polystyrene standards): Pn = 95, PDI 3.13. λ_{max} (abs, $CHCl_3$): 322, 401 nm. λ_{max} (em, $CHCl_3$): 437 nm.

Polymer 12. 1,3-Diiodo-2-methyl-5-tertbutylbenzene (1.05 g, 2.62 mmol) and

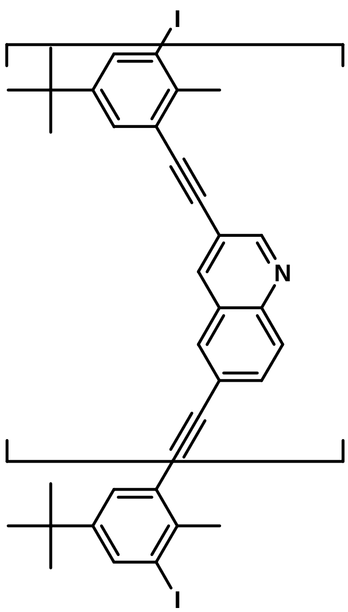

3,6-diethynylquinoline (0.500 g, 2.82 mmol) were reacted according to the general procedure to furnish a brown powder (729 mg, 86 %) which was slightly soluble in chloroform. IR (neat): υ 2954, 2865, 2208, 1588, 1538, 1494, 1453, 1393, 1363, 1255, 1215, 1132, 1002, 912, 878, 834, 757. ^{1}H NMR ($CDCl_3$): δ 9.09 (d, 1H), 8.28 (m, 1H), 8.09-8.01 (m, 2H), 7.84 (m, 2H), 7.61 (m, 2H), 2.89-2.43 (m, 4H), 1.54-1.30 (m, 12H). 13C NMR (CDCl3): δ 152.77, 150.77, 146.49, 140.26, 137.92, 137.61, 137.56, 132.97, 129.68, 127.36, 122.59, 118.37, 101.94, 92.78, 90.82, 53.28, 34.53, 25.74, 26.09. GPC (polystyrene standards): Pn = 11, PDI 1.69. λ_{max} (abs, CHCl3): 310, 368 nm. λ_{max} (em, CHCl3): 381 nm.

UV-Vis and Emission Spectroscopy Procedure. UV-visible spectra were recorded using a Jasco V-530 UV-Vis spectrophotometer. Fluorescence spectra were obtained using a Jasco FP-6500 spectrofluorimeter. Fluorescence and absorption emission measurements of the polymer samples were carried out in chloroform at a concentration relative to the repeat unit of the polymer (stock solution, SS). Polymers 8, 10, and 12 were excited at the wavelength of maximum absorption of the pristine polymers in chloroform.

Aggregation of Polymer 8. Polymer **8** was dissolved in chloroform at a concentration of 2.0 x 10^{-3} (SS). 5 mL of SS was placed in a cuvette and an absorption spectrum was taken. 1 mL of methanol was added to the cuvette, and a second absorption spectrum was taken. The cuvette mixture was poured back into solution A, and was repeated several times.

Fluorescence spectra: Titration of Polymers with Trifluoroacetic Acid. Polymer samples (10 mg of **8**, **10**, and **12**) were dissolved in chloroform (1 L). 50 mL of these solutions were subsequently diluted by additional chloroform (450 mL) to give the stock solution with 4.0 x 10^{-2} mM for polymer **8**, 5.0 x 10^{-2} mM for polymer **10**, and 2.0 x 10^{-2} mM for polymer **12**.

2.1 **Polymer 8**. 2.0 mL of SS (4.0 x 10^{-2} mM) of **8** was placed in a quartz cuvette, and a fluorescence spectrum was taken. Then, 50 μL of TFA was added, and a second fluorescence spectrum was taken and showed a bathochromic shift from 417 to 524 nm (Figure 2.5).

2.2 **Polymer 10**. 2.0 mL of SS (5.0 x 10^{-2} mM) of 10 was placed in a quartz cuvette and fluorescence spectrum was taken. Then, 50 μL of TFA was added and a second fluorescence spectrum was taken which showed a decrease in the intensity of the emission (Figure 1.7). 450 μL of additional TFA was added, and a third fluorescence spectrum was taken which showed no emission. SS was diluted to a concentration of 2.5 x10^{-3} mM, and addition of TFA gives the emission results shown in Figure 2.7.

2.3 **Polymer 12**. 2.0 mL of SS (2.0 x 10^{-2} mM) of 12 was placed in a quartz cuvette, and a fluorescence spectrum was taken. Then, 50 μL of TFA added, and a second fluorescence spectrum was taken and shows a bathochromic shift from 381 to 496 nm in its emission.

Metal-Induced Optical Shift in Absorption of the Polymers. Metal salt solutions were prepared in methanol at a concentration of 1.0 x 10^{-2} M. The following salts were used: $FeCl_2$ * $4(H_2O)$, $Al_2(SO_4)_3$, $AgPF_6$, $ZnCl_2$, $NiCl_2$, $PdCl_2$, $Mn(OAc)_2$, $FeCl_3$, $La(Otf)_3$, $PbCl_2$, and chloroform (1 L). These stock solutions contain 4.0 x 10^{-1} mM of polymer 3, 5.0 x 10^{-1} mM of polymer **6**, and

2.0×10^{-1} of polymer **8**. to obtain the spectra, 2 mL of the respective stock solutions were taken into a cuvette, and 0.1 mL of the metal solution in MeOH were added. To make sure that the effect originating from the additional methanol was negligible, a control experiment was performed in which 0.1 mL of methanol was added to the SS. This small amount of methanol did not cause aggregation and did not lead to a change in the absorption spectra of the polymers. Results of the addition of the metal salts to the polymers are shown in Table 2.2.

2.4. References

1. Bunz, U. H. F., *Chem. Rev.* **2000,** *100*, 1605.

2. Bangcuyo, C. G.; Bunz, U. H. F., *Macromolecules* **2001,** *34*, 7592.

3. Nanos, J. I.; Kampf, J. W.; Curtis, M. D.; Gonzalez, L.; Martin, D. C., *Chem. Mater.* **1995,** *7*, 2232.

4. Mao, S. S. H.; Liu, F. Q.; Tilley, T. D., *J. Am. Chem. Soc.* **1998,** *120*, 8245.

5. Lucht, B. L.; Mao, S. S. H.; Tilley, T. D., *J. Am. Chem. Soc.* **1998,** *120*, 4354.

6. Patil, A. O.; Heeger, A. J.; Wudl, F., *Chem. Rev.* **1988,** *88*, 183.

7. Reddinger, J. L.; Reynolds, J. R., *Adv. Polym. Sci* **1999,** *145*, 59.

8. Grem, G.; Leditzky, G.; Ullrich, B.; Leising, G., *Adv. Mater.* **1992,** *4*, 36.

9. Kraft, A.; Grimsdale, A. C.; Holmes, A. B., *Angew. Chem., Int. Ed. Engl.* **1998,** *37*, 402.

10. Lu, P.; Hong, H. P.; Cai, G. P.; Djurovich, P.; Weber, W. P.; Thompson, M. E., *J. Am. Chem. Soc.* **2000,** *122*, 7480.

11. McGehee, M. D.; Bergstedt, T.; Zhang, C.; Saab, A. P.; O'Regan, M. B.; Bazan, G. C.; Sradnov, V. I.; Heeger, A. J., *Adv. Mater.* **1999,** *11*, 1349.

12. Neher, D., *Adv. Mater.* **1995,** *7*, 691.

13. Zhang, X. J.; Shetty, A. S.; Jenekhe, S. A., *Macromolecules* **1999,** *32*, 7422.

14. Halls, J. M.; Arias, A. C.; MacKenzie, J. D.; Wu, W. S.; Inbasekaran, M.; Woo, P.; Friend, R. H., *Adv. Mater.* **2000,** *12*, 498.

15. Halls, J. M.; Walsh, C. A.; Greenham, N. C.; Marseglia, E. A.; Friend, R. H.; Moratti, S. V.; Holmes, A. B., *Nature* **1995,** *376*, 498.

16. Yu, G.; Gao, J.; Hummelen, J. C.; Wudl, F.; Heeger, A. J., *Science* **1995,** *270*, 1789.

17. Hide, F.; Diaz-Garcia, M. A.; Schwartz, B. J.; Heeger, A. J., *Acc. Chem. Res.* **1997,** *30*, 430.

18. See whole issue of Chem. Rev. (Washington, D.C.) 2000, 100(7)

19. Albert, K. J.; S., L. N.; Schauer, C. L.; Sotzing, G. A.; Stitzel, S. E.; Vaid, T. P.; Walt, D. R., *Chem. Rev. (Washington, D.C.)* **2000,** *100*, 2595.

20. Chentamarakshan, C. R.; Eldo, J.; Ajayagosh, A., *Macromolecules* **1999,** *32*, 5846.

21. Fu, D. K.; Xu, B.; Swager, T. M., *Tetrahedron* **1997,** *53*, 15487.

22. McQuade, D. T.; Pullen, A. E.; Swager, T. M., *Chem. Rev. (Washington, D.C.)* **2000,** *100*, 2537.

23. Swager, T. M., *Acc. Chem. Res.* **1998,** *31*, 201.

24. Hiller, M.; Kranz, C.; Huber, J.; Bauerle, P.; Schuhmann, W., *Adv. Mater.* **1996,** *8*, 219.

25. Al-Higari, M.; Birckner, E.; Heise, B. J.; Klemm, E., *J. Polym. Sci., Part A: Polym. Chem.* **1999,** *37*, 4442.

26. Baxter, P. N. W., *J. Org. Chem* **2000,** *65*, 1257.

27. Bouachrine, M.; Lere-Porte, J. P.; Moreau, J. J. E.; Serein-Spirau, F.; Torreilles, C., *J. Mater. Chem.* **2000,** *10*, 263.

28. Chen, L. X.; Jager, W. J. H.; Gosztola, D. J.; Niemczyk, M. P.; Wasielewski, M. R., *J. Phys. Chem. B* **2000,** *104*, 1950.

29. Chen, L. X.; Jager, W. J. H.; Niemczyk, M. P.; Wasielewski, M. R., *J. Phys. Chem. A* **1999,** *103*, 4341.

30. Chen, X. L.; Jenekhe, S. A., *Macromolecules* **1996,** *29*, 6189.

31. Chen, X. L.; Jenekhe, S. A., *Macromolecules* **2000,** *33*, 4610.

32. Edinger, A.; Ekeley, J. B., *J. Prakt. Chem.* **1902,** *174*, 209.

33. Egbe, D. A. M.; Klemm, E., *Makromol. Chem. Phys.* **1998,** *1999*, 2683.

34. Eichen, Y.; Nakhmanovich, G.; Gorelik, V.; Epshtein, O.; Poplawski, J. M.; Ehrenfreund, E., *J. Am. Chem. Soc.* **1998,** *120*, 10463.

35. Grummt, U. W.; Birckner, E.; Klemm, E.; Egbe, D. A. M.; Heise, B. J., *J. Phys. Org. Chem.* **2000,** *13*, 112.

36. Hayashi, H.; Yamamoto, T., *Macromolecules* **1998,** *31*, 6063.

37. Howitz, J.; Fraenkel, H.; Schroeder, E., *Leibigs Ann.* **1913,** *396*, 53.

38. Joshi, H. S.; Jamshidi, R.; Tor, Y., *Angew. Chem.* **1999,** *38*, 2722.

39. Kiamud-din, M.; Haque, M. E., *Pak. J. Sci. Ind. Res.* **1966,** *9*, 30.

40. Kumura, M.; Horai, T.; Hanabusa, K.; Shirai, H., *Adv. Mater.* **1998,** *10*, 459.

41. Ley, K. D.; Li, Y. T.; Johnson, J. V.; Powell, D. H.; Schanze, K. S., *Chem. Commun.* **1999**, 1749.

42. Ley, K. D.; Schanze, K. S., *Coord. Chem. Rev* **1998,** *171*, 287.

43. Ley, K. D.; Whittle, C. E.; Bartberger, M. D.; Schanze, K. S., *J. Am. Chem. Soc.* **1997,** *121*, 33423.

44. Mullekom, H. A. M.; Vekemans, J. A. J. M.; Meijer, E. W., *Chem. Eur. J.* **1998,** *4*, 1235.

45. Osaheni, J. A.; Jenekhe, S. A., *J. Am. Chem. Soc.* **1995,** *117*, 7389.

46. Pautzsch, T.; Rode, C.; Klemm, E., *J. Prakt. Chem.* **1999,** *341*, 548.

47. Prodi, L.; Bolletta, F.; Montalti, M.; Zaccheroni, N., *Coord. Chem. Rev.* **2000,** *205*, 59.

48. Reddinger, J. L.; Reynolds, J. R., *Chem. Mater.* **1998,** *10*, 1236.

49. Walters, K. A.; Ley, K. D.; Schanze, K. S., *Langmuir* **1999,** *15*, 5676.

50. Walters, K. A.; Schanze, K. S., *Synth. Met.* **1999,** *102*, 1585.

51. Wang, B.; Wasielewski, M. R., *J. Am. Chem. Soc.* **1997,** *119*, 12.

52. Wang, Q.; L., Y., *J. Am. Chem. Soc.* **2000,** *122*, 11806.

53. Wang, Q.; Wang, L.; Yu, L., *J. Am. Chem. Soc.* **1988,** *120*, 12860.

54. Willgerodt, c.; Arnold, E., *Chem. Ber.* **1901,** *34*, 3343.

55. Yamamoto, T.; Sugiyama, K.; Kushida, T.; Inoue, T.; Kanbara, T., *J. Am. Chem. Soc.* **1996,** *118*, 3930.

56. Yao, Y. X.; Zhang, Q. T.; Tour, J. M., *Macromolecules* **1998,** *31*, 8600.

57. Zhang, Q. T.; Tour, J. M., *J. Am. Chem. Soc.* **1997,** *119*, 9624.

58. Zotti, G.; Zecchin, S.; Schiavon, G.; Berlin, A.; Penso, M., *Chem. Mater.* **1999,** *11*, 3342.

59. Kloppenburg, L.; Jones, D.; Bunz, U. H. F., *Macromolecules* **1999,** *32*, 4194.

60. Halkyard, C. E.; Rampey, M. E.; Kloppenburg, L.; Studer-Martinez, S. L.; Bunz, U. H. F., *Macromolecules* **1998,** *31*, 8655.

61. Miteva, T.; Palmer, L.; Kloppenburg, L.; Neher, D.; Bunz, U. H. F., *Macromolecules* **2000,** *33*, 652.

62. Pschirer, N. G.; Bunz, U. H. F., *Macromolecules* **2000,** *33*, 3961.

63. Chambron, J. C.; Sauvage, J. P.; Amouyal, E.; Koffi, P., *New J. Chem.* **1985,** *9*, 527.

64. Cheng, Y.; Man, b.; Wudl, F., *J. Mater. Chem.* **1999,** *9*, 2183.

65. Nair, R. B.; Cullum, B. M.; Murphy, C. J., *J. Inorg, Chem.* **1997,** *30*, 962.

66. Nair, R. B.; Yeung, L. K.; Murphy, C. J., *J. Inorg, Chem.* **1999,** *38*, 2536.

CHAPTER 3

SYNTHESIS AND CHARACTERIZATION OF BENZOTHIADIAZOLE CONTAINING POLYARYLENEETHYNYLENES

3.1. Introduction

With the advent of the quinoline based copolymers (Chapter 2), we set our goal now towards the synthesis of the multi-pocketed quinoxaline based poly(*p*-aryleneethynylene)s. We took a look at the benzothiadiazole based poly(aryleneethynylene)s as a comparative polymer to the quinoxaline theorizing that the binding pocket would be as strong. These poly(aryleneethynylene)s[1] are an increasingly important class of stable, highly luminescent polymers with attractive optical,[1-6] electronic,[7-9] and sensory[10-12] properties. Until now, most of the attention has focused upon the dialkyl- and dialkoxy-PPEs, and only very few heteroaromatic poly(aryleneethynylene)s (PAE)s have been reported, notably in the groups of Yamamoto, Schanze, Pang, and Klemm.[13-18] These polymers incorporate pyridine,[13-16] thiophene,[17, 18] and bipyridine[19-21] units into PAEs. However, nothing is known about PAEs that contain larger and/or fused heterocyclic rings with two or more heteroatoms.

We herein describe the synthesis and electrochemical characterization of low-band gap PAE **19** featuring 2,1,3-benzothiadiazole units. From a retrosynthetic fashion from our target quinoxaline, we determined that the quinoxaline could be made from a benzothiadiazole (Scheme 3.1). It would also seem intuitive to create a polymer out of the benzothiadiazole due to the fact that the alkynes would be situated in a 4,7 arrangement unlike our comparative quinoline monomer (Chapter 2) where the alkynes were arranged in the 3,6 positions. Also, due to the electron deficient nature of the molecule, it would be a good candidate for the Heck-Cassar-Sonogashira-Hagihara (HCSH) coupling. The electron poor hetero-PAE **19** with its low lying LUMO, which according to PM3 calculations is 6.32 eV, should be of interest as a novel n-type semiconductor in which electron and not hole transport would be the predominant conduction process.

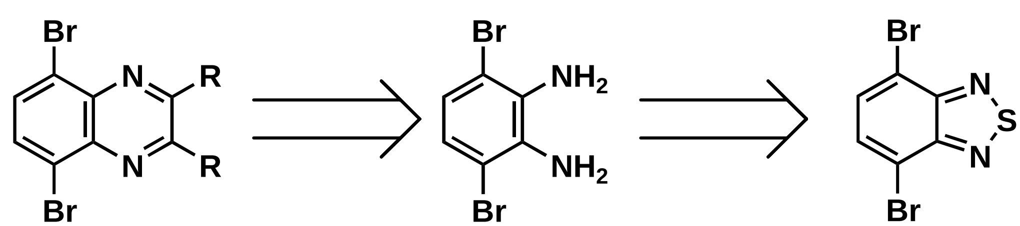

Scheme 3.1. Retrosynthetic view of quinoxaline starting from a benzothiadiazole.

3.2. Results and Discussion

Starting from the commercially available *o*-phenylenediamine, protection of the amines with thionyl chloride affords the 2,1,3-benzothiadiazole (Scheme 3.2). Bromination at 60 °C in acidic conditions, filtration of a brown solid, and multiple washing with aqueous sodium sulfite yields the 4,7-dibromo-2,1,3-benzothiadiazole **15** in 83 %. We have made multigram quantities of the dibromobenzothiadiazole with our largest batch being over 300 grams.

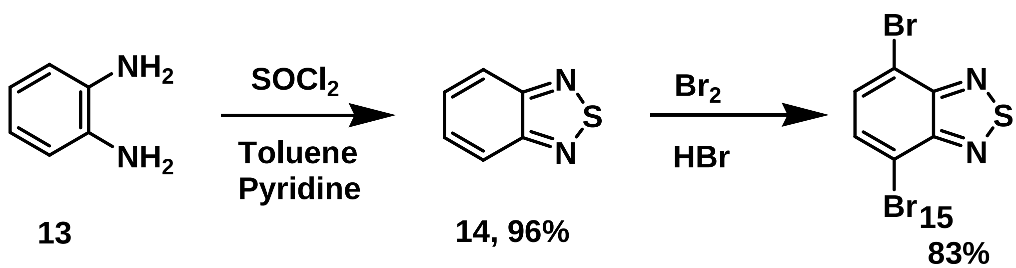

Scheme 3.2. Synthesis of 4,7-dibromo-2,1,3-benzothiadiazole **15** including yields. The dibromobenzothiadiazole **15** can be made by the hundreds of grams in one reaction.

However, coupling of 4,7-dibromo-2,1,3-benzothiadiazole to 1,4-diethynyl-2,5-bis(ethylhexyloxy)benzene under standard Pd catalysis at 80 °C in triethylamine was unsuccessful. The polymeric product was reddish in appearance and showed > 20% diyne defects according to ^{13}C NMR. Attempts to improve this approach by optimizing the reaction conditions failed. We anticipated that 4,7-diethynyl-2,1,3-benzothiadiazole **18** and a suitably substituted diiodobenzene would be better coupling partners in this polycondensation. Deciding that the 4,7-dibromo-2,1,3-benzothiadiazole was not very reactive under

HCSH coupling conditions, we directed our attention to synthesize the 4,7-diiodo derivative **16** instead (Scheme 3.3). 4,7-dibromobenzothiadiazole was placed in a 1000 ml flask with DMSO, CuI, and NaI, and was heated to 150 °C for 24 hours. This reaction allowed us to perform a halogen exchange on the ring by replacing the bromides with iodides in a 35 % yield. From there, we were able to couple trimethylsilylacetylene to the 4,7-diiodo-2,1,3-benzothiadiazole. Removal of the trimethylsilyl groups to furnish **2** was affected by potassium carbonate in methanol in an overall yield of 48% starting from **18** (Scheme 3.4).

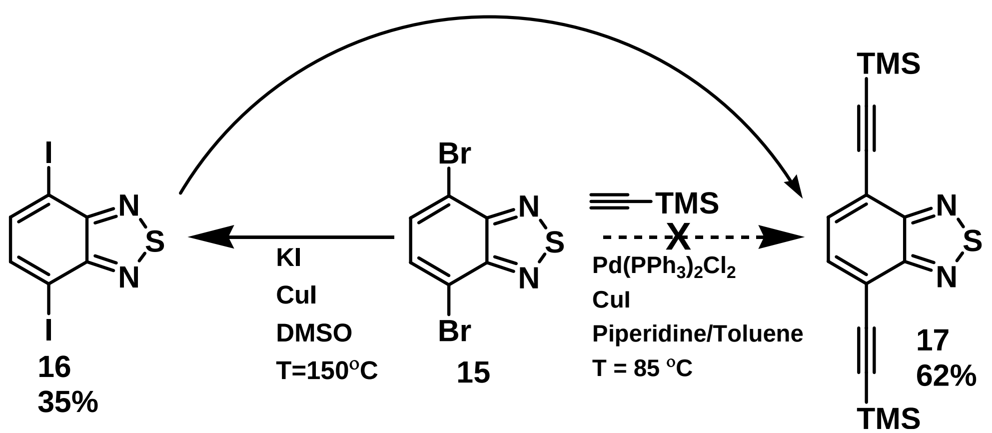

Scheme 3.3. The 4,7-dibromo-2,1,3 benzothiadiazole **15** was not reactive enough for the HCSH coupling. The transformation into the diiodide **16** facilitated the ease of the addition of the alkynes.

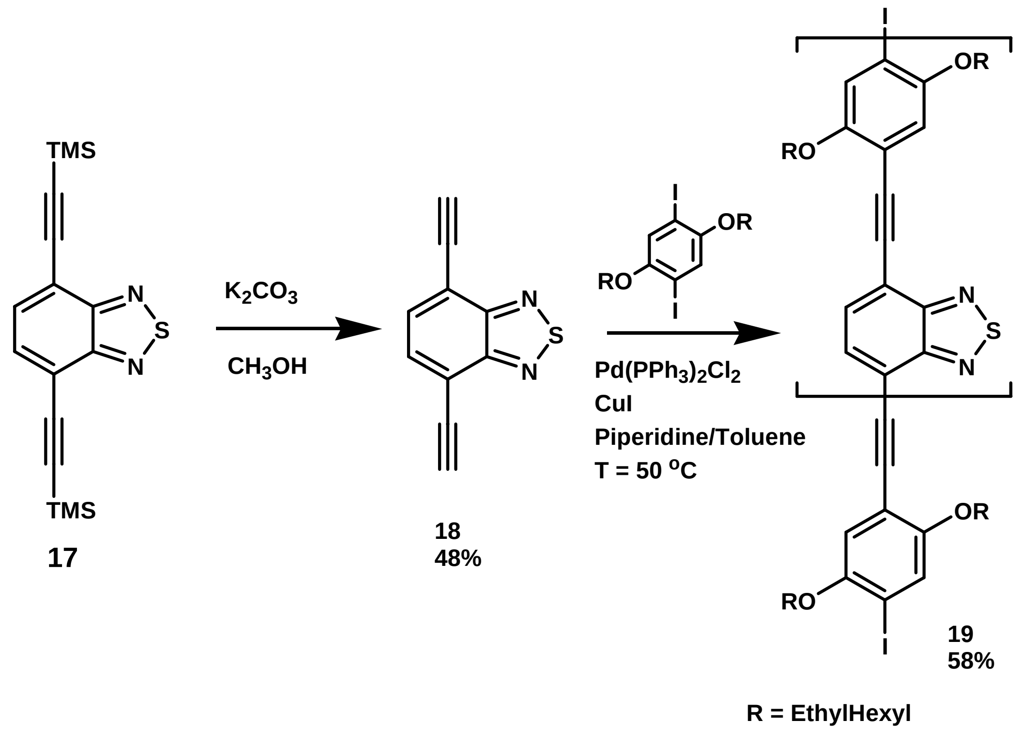

Scheme 3.4. Synthesis of the benzothiadiazole copolymer **19**.

Reaction of **18** with a diiodobenzene[6] was performed under standard Pd catalysis utilizing 5 mol % of $(Ph_3P)_2PdCl_2$ and CuI as catalyst at 85 °C for 48 h in a piperidine/toluene mixture. During the reaction, the solution turned dark red fluorescent and viscous. Aqueous workup, vacuum distillation of the solvents, and extraction of **19** with hexanes and methanol removed low molecular weight impurities and furnished **19** in a 58 % yield with a degree of polymerization (P_n) of 18 repeating units and polydispersity (M_w/M_n) of 2.78 according to GPC (polystyrene standards). The relatively low molecular weight of the polymer **19** and the low yield of the alkynylation of **15** suggest that the 2,1,3-benzothiadiazole ring may function as ligand for Pd(0). That would explain the moderate molecular weight and yield of **19**. The polymer was characterized by its NMR and IR data. Obtained films show some degree of lamellar order as evidenced by powder XRD (d = 1.54 nm). This d value represents the interlamellar distance between two polymer chains and corresponds approximately to the wingspan of the two extended (2-ethylhexyloxy) chains in **19**. In the range of 0.3 – 0.4 nm there is a broad diffraction feature suggesting the presence of ample pie-pie stacking with the overall order in **19** being low.[1]

A solution of **19** in chloroform appears orange and displays orange-red fluorescence with a maximum emission at 562 nm (Figure 3.2). In the solid state, **19** is nonfluorescent. Very thin films appear translucent red with a λ_{max} = 508, 553 nm (2.24 eV) compared to the yellow films of dialkyl-PPE λ_{max} = 439 nm (2.92 eV).[2, 3] The most eye catching property of any thick film of **19** is its golden-green metallic luster visible in Figure 2.1. The appearance of **4** is unusual for a PAE.

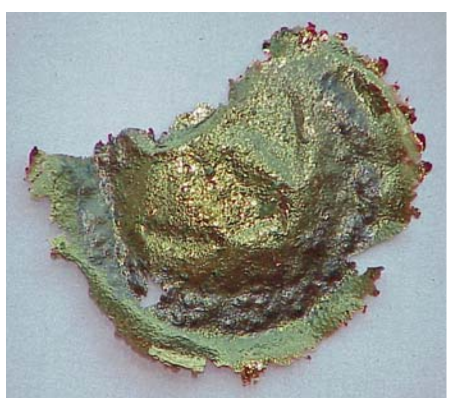

Figure 3.1. Thin drop-cast film of **19**. The material appears orange in solution, red in thin translucent films, and displays a golden-green luster in the solid state.

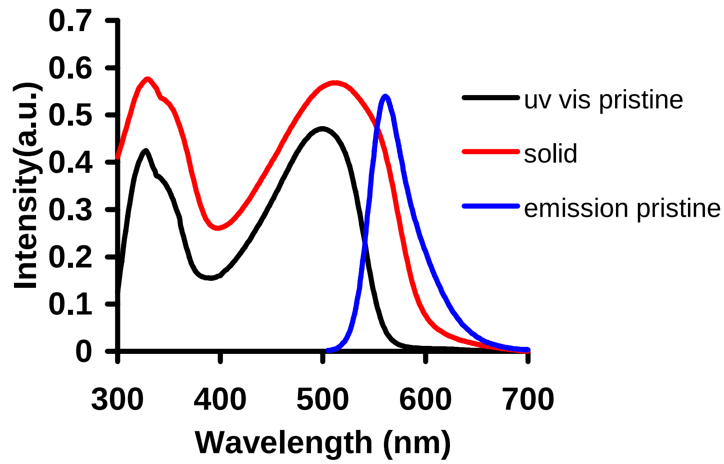

Figure 3.2. UV-Vis spectrum of polymer **19** in chloroform (λ_{max} = 498 nm) and in the solid state (λ_{max} = 508 nm with a shoulder at λ_{max} = 553 nm (2.24 eV)). On the right side is shown the emission spectrum of **4** in chloroform solution with λ_{max} of emission = 562 nm. In the solid, the polymer **19** is nonfluorescent.

Normally, these materials are powdery-yellow and nonlustrous. To explain this unusual behavior at least qualitatively, we performed a series of PM3 semiempirical calculations on oligomers **20-22** (Table 2.1). In comparison to **21** (calculated band gap 7.3 eV), the HOMO of **20** is almost unchanged. However, the LUMO is decreased by approximately 1 eV to give a calculated HOMO-LUMO gap of 6.32 eV. In **22**, the decrease of the band gap (6.9 eV) in comparison to **21** is due to a rise in the HOMO. These values (PM3) are meaningful in comparison of the different oligomers and greatly overestimate the absolute band gap due to the omission of interchain, solid-state, and configuration interactions. We further extract from the PM3 calculations that the HOMO of **4** is delocalized, while its LUMO, LUMO +1 and LUMO +2, are localized on the heteroaromatic rings.

We know that from the optical data of the polymers in thin films the band gap decreases by 0.58 eV when going from PPEs to **19**. The (optical) band gap of **19** is almost as low as that of the poly(alkylthiophene)s (1.9 – 2.0 eV), making it an n-dopable low band gap polymer. Cyclic voltammetry displayed a reversible reduction of **19** with an $E_{1/2}$ of –1.42 V vs *Ag/Ag*+. It is accompanied by a color change from red to black. The electrochemical band gap for **19** is 2.34 eV. Both optical and electrochemical band gaps are in excellent agreement with the electrochemical band gap being slightly larger.

Table 3.1. Comparison of PM3 Band-Gap Calculations of Several Conjugated Oligomers

Structure	Homo PM3 (eV)	LUMO PM3 (eV)	Band Gap Calc. (eV)
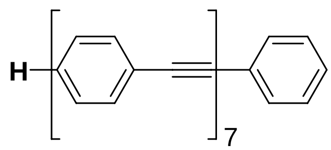 20	-8.46	-1.18	7.28
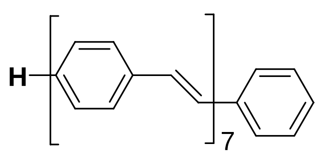 21	-8.08	-1.21	6.87
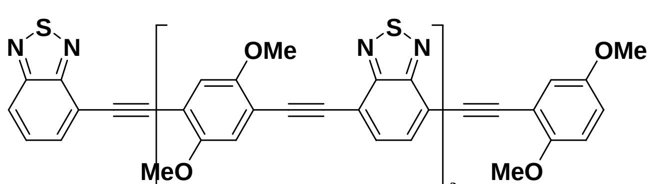 22	-8.42	-2.10	6.32

Nanostructuring of Polymer 19

In conjunction with Dr. Sherine O'bare, formally from Cathy Murphy's group at the University of South Carolina, we decided to try to structure the copolymer **19** by attaching it onto gold nanoparticles. The mode of attachment was theorized was to be a bond between the sulfur of the thiadiazole ring and the gold surface. We theorized that we could do it with these heterocyclic polyaryleneethynylenes with the discreet advantage of not only characterization of the polymer beforehand, but also with a facile ease of the coating process. From there, we would dissolve the gold nanoparticle, and then form a novel hollow PAE tube that would be fluorescence.

The polymer **19** was diluted in cetyltetrabutylammonium bromide (CTAB), a surfactant, and water. The polymer was only slightly soluble in CTAB and needed to be sonicated for 1 hr to be completely dissolved. It was then mixed into a solution of gold nanoparticles suspended in ethanol. The suspension was then vigorously stirred for 16 hours at ambient temperature. The resultant suspension was centrifuged, the liquid decanted, and the particles dispersed into water.

To see whether to polymer coated the gold nanoparticles, we decided to look at them through SEM. The initials solutions (10 μL of a 0.25 M solution) that were used were too concentrated as evident by SEM, however, we could see that that our original premise was viable. The particle coatings were too thick and the gold could not even been seen due to the thickness. After diluting the polymer down to a concentration of 10 μL of a 0.025 M solution, we could see that the polymer was coating the gold at a reasonable thickness. UV-Vis and fluorescence data were used to supplement our information that the polymer was supported onto the gold substrates. There was a slight shift in the absorption maxima from

523 nm to 519 nm. Our emission studies also show that the gold coated polymer emitted at λ_{max} at 569 nm.

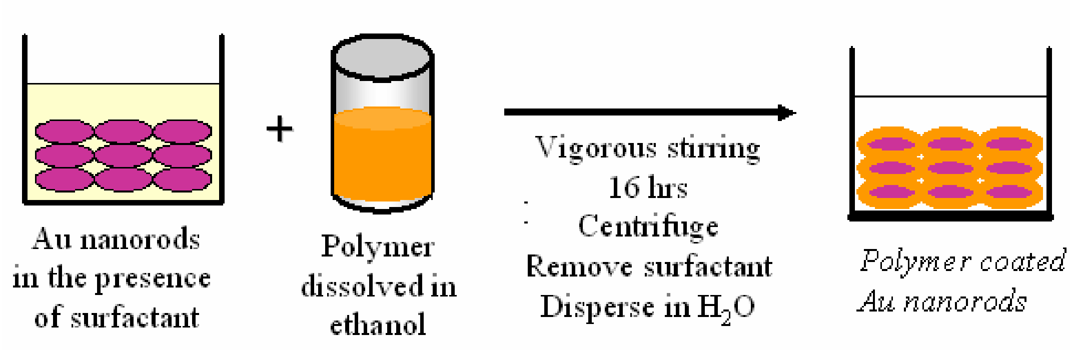

Figure 3.3. Cartoon depiction on the coating of the gold nanoparticles used in the fabrication of the hollow PAE tubes.

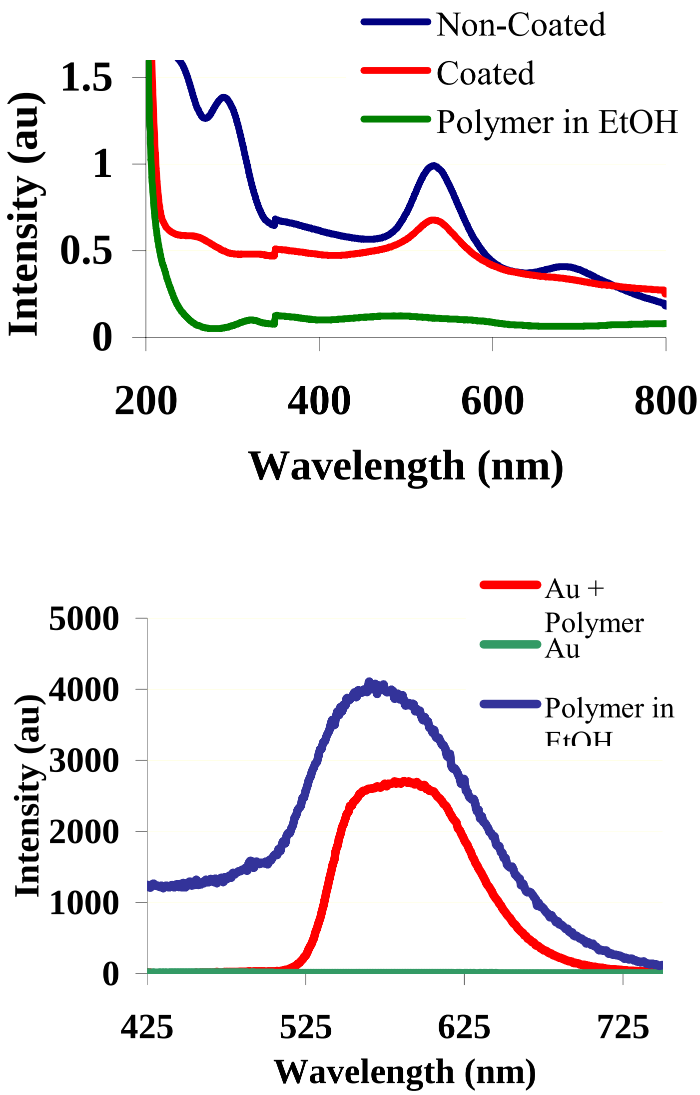

Figure 3.4. The absorption spectra (top) shows that that the polymer was coating the gold with the absorption λ_{max} = 569 nm. The fluorescence graph (bottom) shows a λ_{max} = 598 nm which can assume that the polymer is coated on the gold nanoparticles.

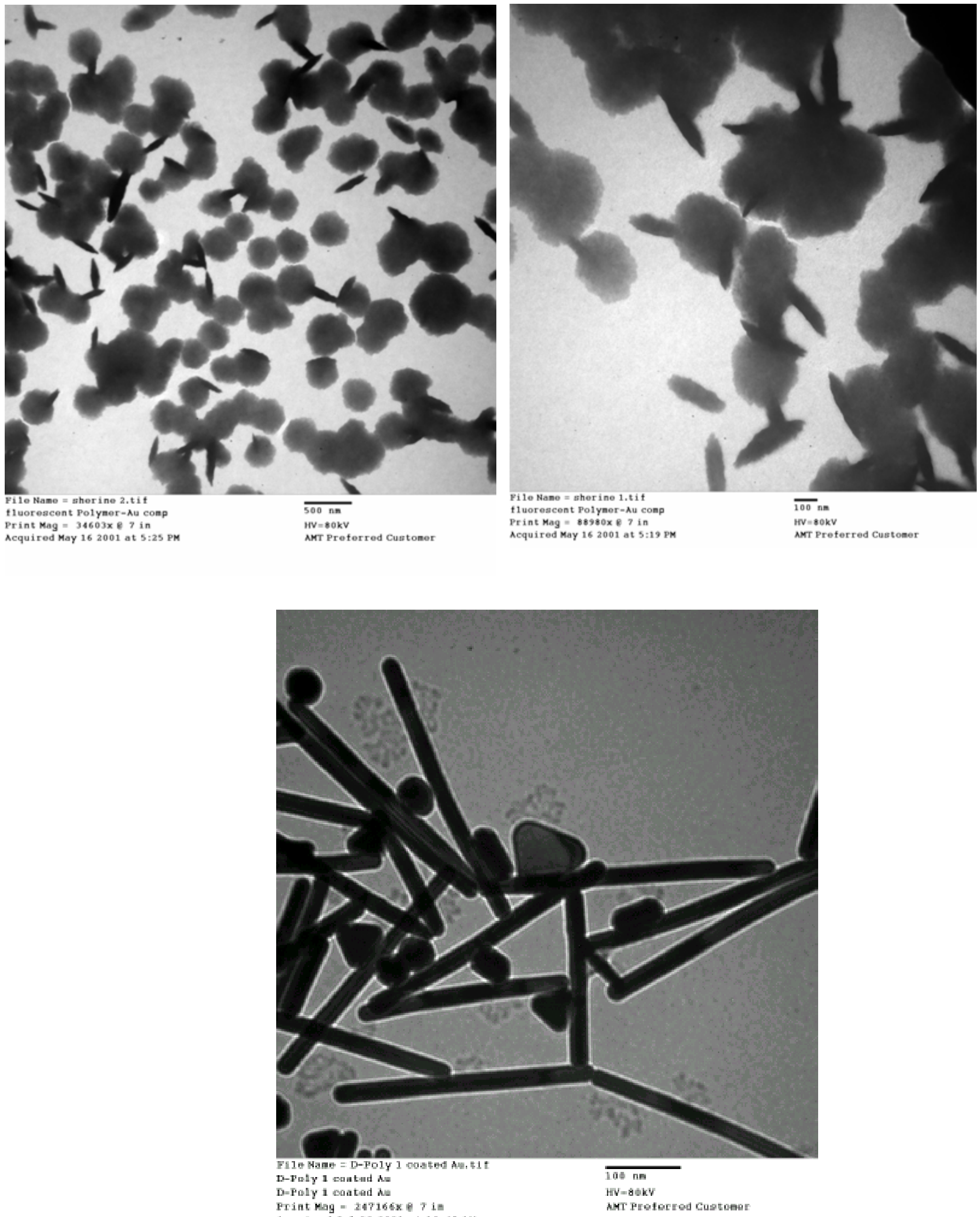

Figure 3.5. The top two figures display the polymer solution becoming too concentrated and the inability to see the gold nanoparticles that are encased. The bottom photo clearly shows the gold nanoparticles along with a thin white outline that is the PAE coating the outer edge. The concentration used was 10 µL from a 0.025 M solution.

Our next step was to dissolve the gold particles with a strong base to see if we could form the hollow PAE tubes. The dissolution of the gold nanoparticles was performed by immersing the particles in sodium cyanide. The same procedure that is detail above was repeated to isolate the particles. By SEM, we found out that the hollow tubes were not stable enough by themselves to withhold their structure. After the dissolution of the gold nanoparticle, the PAE would collapse onto itself as shown in Figure 3.6. Thus, we determined that these PAEs would not make suitable materials for hollow carbon tubes.

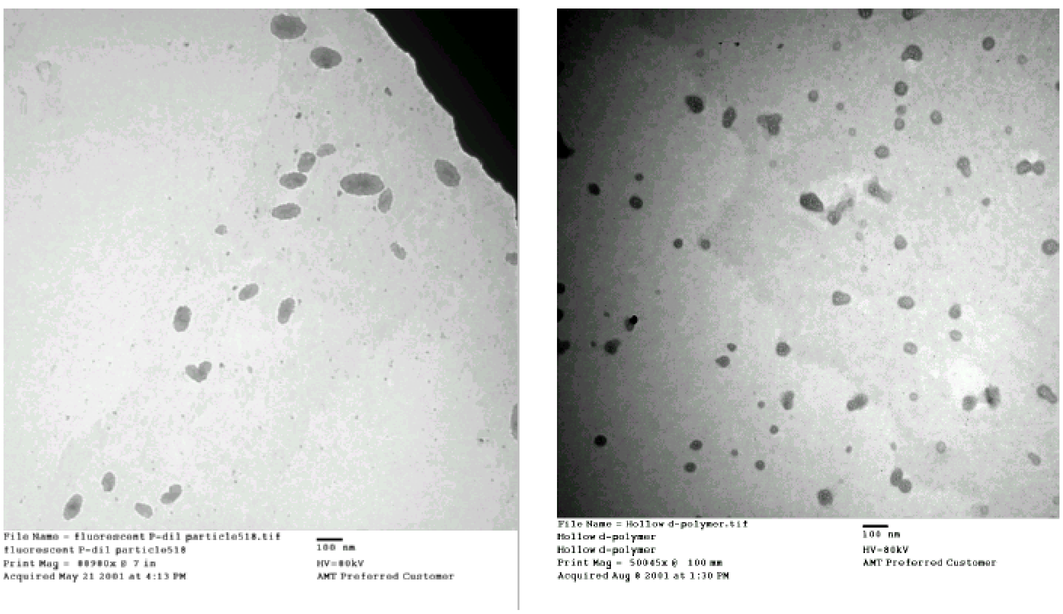

Figure 3.6. The collapsing of tubes from copolymer **19** and formation of aggregates after the dissolution of the gold nanoparticles by a strong base, sodium cyanide. These aggregates form on the range of 100-200 nm.

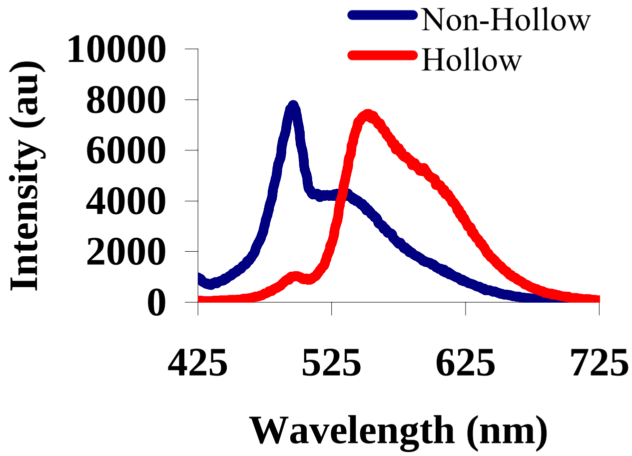

Figure 3.7. The emission spectrum shows the non-hollow tube (blue) and hollow tube (red) respectively. The bathochromic shift (λ_{max} = 517 nm to 560 nm) from the hollow tube along with the SEM pictures correlate to the formation of aggregates.

Conclusion

We have synthesized a low band gap heterocyclic poly(aryleneethynylene) that shows both a low lying LUMO and HOMO. This polymer is reversibly reduced and has a green-golden luster in the solid state. It may be interesting as a n-semiconductor in organic device applications. We have also shown that these materials could be of use in nanostructuring through the use of gold or another strongly binding substrate. In the future, we hope to achieve a self standing hollow fluorescent tube.

3.3. Experimental

4,7-Bis(trimethylsilyl)ethynyl-2,1,3-benzothiadiazole 17. Under inert conditions, **1**[22-25] (4.46 g, 11.5 mmol), $Pd(PPh_3)_2Cl_2$ (554 mg, 0.575 mmol), CuI (100 mg, 0.529 mmol), toluene (5 mL), and piperidine (20 mL) were combined. Trimethylsilylacetylene (2.45 g, 24.9 mmol) was added drop-wise to the stirred solution. After 16 h at ambient temperature the reaction mixture was poured into dichloromethane (50 mL) and water. The organic layer was washed twice with water (75 mL), 25% NH_4OH (100 mL), and water (100 mL), dried over magnesium sulfate, and stripped of solvent. Purification by crystallization from methanol at -78 °C gives green-yellow crystals (2.12 g, 55%). ^{1}H NMR ($CDCl_3$): δ 6.80 (s, 2H), 0.00 (s, 9H). ^{13}C NMR ($CDCl_3$): δ 154.19, 133.12, 117.24, 103.61, 99.96, 0.13. IR (cm^{-1}): υ 3306.7, 3051.1, 2962.3, 2900.5, 2853.5, 2247.0, 2152.9, 1944.6, 1875.7, 1683.6, 1559.8, 1537.8, 1490.1, 1411.1, 1357.0, 1338.9, 1248.6, 1027.6, 909.7, 888.9, 759.7.

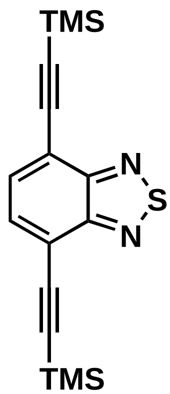

4,7-Diethynyl-2,1,3-benzothiadiazole (18). To a 250 mL round-bottom flask, 4,7-bis(trimethylsilyl)ethynyl-2,1,3-benzothiadiazole (2.00 g, 6.08 mmol), potassium carbonate (approximately 2.5 g), methanol (125 mL), and water (1 mL) were added and stirred overnight at room temperature. The solution was poured into dichloromethane (50 mL) and water (100 mL). Aqueous workup and crystallization from methanol at -78 °C furnished a green-yellow crystalline material (0.971 g, 86%). ^{1}H NMR

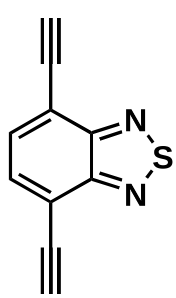

($CDCl_3$): δ 7.74 (s, 2H), 3.66 (s, 2H). ^{13}C NMR ($CDCl_3$): δ 154.63, 132.67, 117.45, 102.24, 100.25. IR (cm^{-1}): υ 2943.0, 2890.7, 2864.4, 2724.8, 2249.1, 2152.7, 1882.8, 1641.8, 1559.3, 1488.7, 1462.0, 1383.5, 1365.3, 1338.0, 1261.2, 1169.0, 1072.3, 995.8, 916.5, 845.6.

Preparation of 2,1,3-Benzothiadiazole-*b*-alkyne-*b*- 2,5-bis(2-ethylhexyloxy)benzene Copolymer (19). Under inert conditions, **18** (0.310 g, 1.68 mmol), 2,5-bis(ethylhexyloxy)-1,4-diiodobenzene[6] (0.908 g, 1.54 mmol), $Pd(PPh_3)_2Cl_2$ (74.0 mg, 0.077 mmol), CuI (15.0 mg, 0.077 mmol), dichloromethane (5 mL), and piperidine (15 mL) were added and heated to 85 °C for 48 h. Dilution with chloroform (100 mL), washing with water (2 x 100 mL), 25% NH_4OH (100 mL), and water (100 mL), and drying with $MgSO_4$ are followed by removal of solvent under vacuum. The resulting solid was thoroughly washed with hexanes (until clear) followed by extensive washings with methanol (until clear) to furnish a red-flaky solid with green-metallic luster that was well-soluble in chloroform and dichloromethane (0.412 g, 58%). ^{1}H NMR ($CDCl_3$): δ 7.77 (bs, 2H), 7.16 (bs, 2H), 3.97 (bs, 2H), 1.80-0.78 (bm, 15H). ^{13}C NMR ($CDCl_3$): δ 154.31, 154.23, 132.37, 117.35, 116.55, 114.00, 94.47, 91.28, 72.14, 39.69, 30.65, 29.26, 24.38, 23.99, 23.19, 14.19, 11.40. IR (cm^{-1}): υ 3009.7, 2958.7, 2929.2, 2872.6, 2858.3, 2361.0, 2339.8, 2204.6, 1683.7, 1616.2, 1506.9,

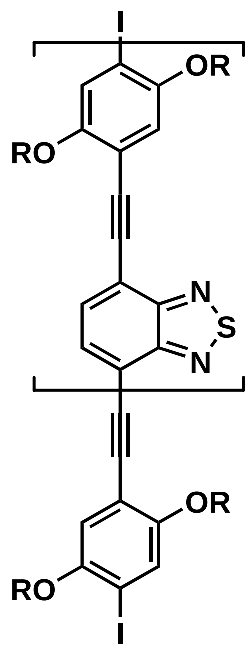

1464.7, 1416.7, 1381.0, 1342.9, 1277.0, 1215.5, 1157.4, 1115.6, 1032.6, 893.0, 844.8, 756.1. GPC (polystyrene): *P*n 19, *M*w/*M*n) 2.78.

Preparation of 2,1,3-Benzothiadiazole-*b*-alkyne-*b*-2,5-bis(2-ethylhexyloxy)benzene Gold Nanoparticles coatings and their Hollow tubule derivatives. The polymer x was taken and dissolved into CTAB at a concentration of 0.025 M according to the Pn value and the repeat unit molecular weight. The solution was sonicated for 1 hour at room temperature to allow the polymer to completely dissolve. 10 μL of the solution was added to a suspension of the gold nanoparticles in ethanol. This suspension was stirred vigorously for 16 hours after which it was centrifuged then decanted of surfactant. The resultant solid was then dispersed into water. The samples were then placed in a scanning electron microscope (Hitachi 2500 Delta), and the pictures were obtained digitally.

3.4. References

1. Bunz, U. H. F., *Chem. Rev.* **2000,** *100*, 1605.

2. Halkyard, C. E.; Rampey, M. E.; Kloppenburg, L.; Studer-Martinez, S. L.; Bunz, U. H. F., *Macromolecules* **1998,** *31*, 8655.

3. Pschirer, N. G.; Bunz, U. H. F., *Macromolecules* **2000,** *33*, 3961.

4. Pschirer, N. G.; Vaughn, M. E.; Dong, Y. B.; ZurLoye, H. C.; Bunz, U. H. F., *Chem. Commun.* **2000**, 85.

5. Evans, U.; Soyemi, O.; Doescher, M. S.; Bunz, U. H. F.; Kloppenburg, L.; Myrick, M. L., *Analyst* **2001**, 508.

6. Kloppenburg, L.; Jones, D.; Bunz, U. H. F., *Macromolecules* **1999,** *32*, 4194.
7. Montali, A.; Smith, P.; Weder, C., *Synth. Met.* **1998,** *97*, 123.

8. Schmitz, C.; Posch, P.; Thelakkat, M.; Schmidt, H. W.; Montali, A.; Feldman, K.; Smith, P.; Weder, C., *Adv. Func. Mater.* **2001,** *11*, 41.

9. Weder, C.; Sarwa, C.; Montali, A.; Bastiaansen, G.; Smith, P., *Science* **1998,** *279*, 835.

10. Yang, J. S.; Swager, T. J., *J. Am. Chem. Soc.* **1998,** *120*, 11864.

11. Zhou, Q.; Swager, T. M., *J. Am. Chem. Soc.* **1995,** *117*, 12593.

12. Swager, T. M., *Acc. Chem. Res.* **1998,** *31*, 201.

13. Li, Y. T.; Whittle, C. E.; Walters, K. A.; Ley, K. D.; Schanze, K. S., *Pure Appl. Chem* **2001,** *73*, 497.

14. Ley, K. D.; Li, Y. T.; Johnson, J. V.; Powell, D. H.; Schanze, K. S., *Chem. Commun.* **1999**, 1749.

15. Ley, K. D.; Schanze, K. S., *Coord. Chem. Rev* **1998,** *171*, 287.

16. Ley, K. D.; Whittle, C. E.; Bartberger, M. D.; Schanze, K. S., *J. Am. Chem. Soc.* **1997,** *121*, 33423.

17. Yamamoto, T., *Bull. Chem. Soc. Jpn.* **1999,** *72*, 621.

18. Hayashi, H.; Yamamoto, T., *Macromolecules* **1998,** *31*, 6063.

19. Li, J.; Pang, Y., *Macromolecules* **1998,** *31*, 5740.

20. Egbe, D. A. M.; Klemm, E., *Makromol. Chem. Phys.* **1998,** *1999*, 2683.

21. Grummt, U. W.; Birckner, E.; Klemm, E.; Egbe, D. A. M.; Heise, B. J., *J. Phys. Org. Chem.* **2000,** *13*, 112.

22. Pesin, V. G.; Khaletskii, A. M.; Chzi-chzhun, C., *J. Gen. Chem.* **1957,** *27*, 1643.

23. Khaletskii, A. M.; Pesin, V. G.; Chzi-chzhun, C., *Acad. Sci. (USSR)* **1956,** *106*, 31.

24. Pilgram, K.; Zupan, M.; Skiles, R., *J. Heterocycl. Chem.* **1970,** *7*, 629.

25. Tsuba, Y.; Suzuki, T.; Miyashi, T., *J. Org. Chem* **1992,** *57*, 6749.

CHAPTER 4

SYNTHESIS AND CHARACTERIZATION OF QUINOXALINE CONTAINING POLYARYLENEETHYNYLENES

4.1. Introduction

After the completion of the benzothiadiazole containing copolymers, we set our sights on our initial goal of creating the quinoxaline based polymers. Citing back to the introduction, the benzothiadiazole plays an integral role in the synthesis of the quinoxaline monomers because it can be formed in one condensation step where the driving force of the reaction is the formation of the aromatic pyrazine ring. The other participating molecule in this condensation reaction is a diketone, where various R groups could be attached. These pendant side chains can act as either a solubilizing group for the monomer or it can enhance the sensing abilities of the polymer by adding more recognitions sites to the molecule. This is an attractive and diverse technique because of the large availability of commercial diketones or their relative ease of synthesis through the use of an alkyne. The production of these quinoxaline based PAEs allowed us to determined the viability of the proposed goal of the "self assembling ladder polymers".

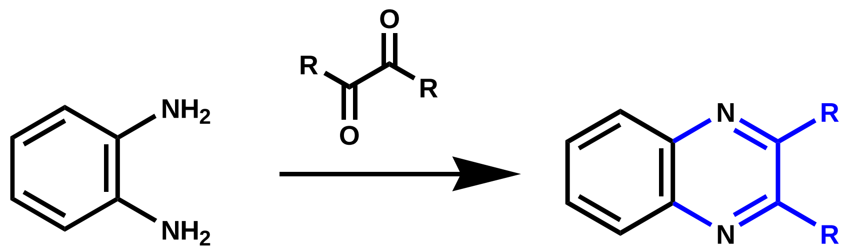

Scheme 4.1. The formation of the quinoxaline molecule is driven by the aromaticity of the pyrazine fused ring depicted in blue.

These poly(aryleneethynylene)s (PAE)[1-5] are a class of conjugated polymers in which aryl groups are interspersed by alkyne units. Their high stability and photophysical properties make PAEs attractive. PAEs have found interest as semiconductors, polarizers, and sensory materials.[6-9] While the parent dialkyl/dialkoxysubstituted poly(*p*-phenyleneethynylene)s (PPE) are well-known and thoroughly investigated, heterocyclic PAEs[10-14] have been less explored despite the expectation of these materials to behave differently. Jenekhe, Schanze, Yamamoto, Klemm, and our group have started to explore the field of hetero-PAEs as interesting emitting and *n*-type semiconducting materials.[15-21] Within this chapter we will report the synthesis, ionochromic effect, and electrochemistry of the first quinoxaline-containing PAEs, **28** and **31**.

4.2. Results and Discussion

Starting from 4,7-dibromo-2,1,3-benzothiadiazole[22] using a reductive method with sodium borohydride in methanol at ambient temperatures, we were able to prepare the 1,4-dibromo-2,3-diaminobenzene in an 10-59 % yield (Scheme 4.2). These molecules furnished the quinoxalines **25** and **29** in high yields by condensation with benzil or acenaphthenequinone. These reactions were generally performed in refluxing ethanol for 12 hours. A catalytic amount of acid, usually H_2SO_4 or HCl, could be employed to increase efficiency.

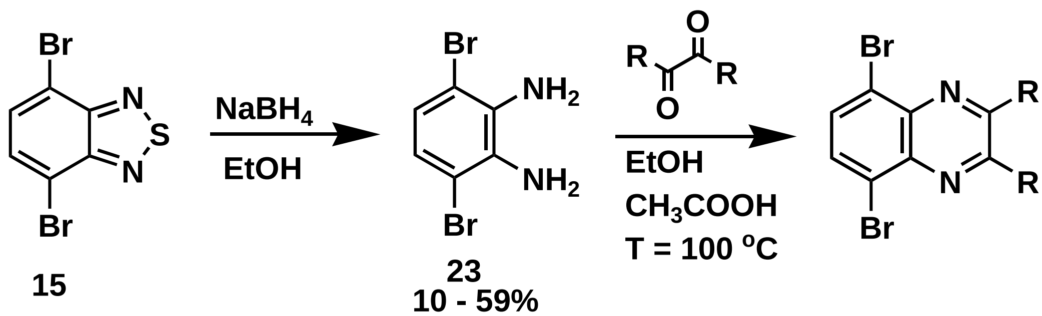

Scheme 4.2. Reaction scheme in the formation of the quinoxalines starting from 4,7-dibromo-2,1,3-benzothiadiazole.

Depending on which pendant side chains we wanted to obtain, it could be easily accessible through modification of the diketone that we would choose to use (Scheme 4.3). We were able to obtain our diketones from two available sources: (1) the diketones that were commercially available and (2) oxidation of a bisphenyl ethynes. The bisphenyl ethynes proved of synthetic use in that they were able to construct symmetrical diones that contain conjugated ring systems. We were able to construct many diketones through the use of our oxidation technique, but were unable to incorporate most of these into polymers because of the extremely low yields, sometimes less that 2 %, or the fact that most of these monomers would possess some unknown impurity (generally between 5-7 %) that was difficult to be removed by purification (Figure 4.1). Those impurities would interfere with the polycondensation process often yielding low molecular weith polymers. With these thoughts in mind, we decided to continue to the polymer process through the use of the commercially available diketones in benzil and acenapthylquinone. However, this turns out to be problematic for our "pseudo" ladder polymer in that the quinoxaline homopolymer became insoluble and unprocessible, thus suffering the same drawbacks as the traditional ladder polymers.

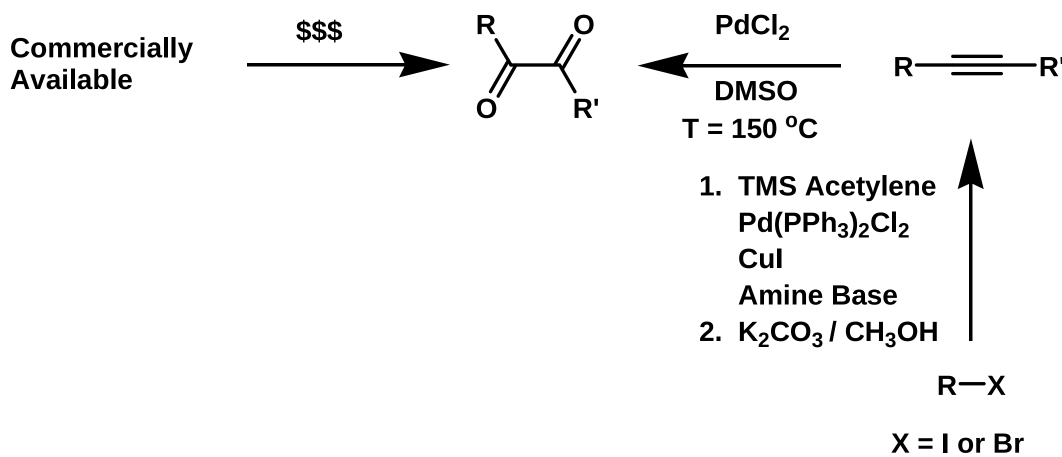

Scheme 4.3. The diketones were either available through commercial sources or could be obtained by the oxidation of an alkyne.

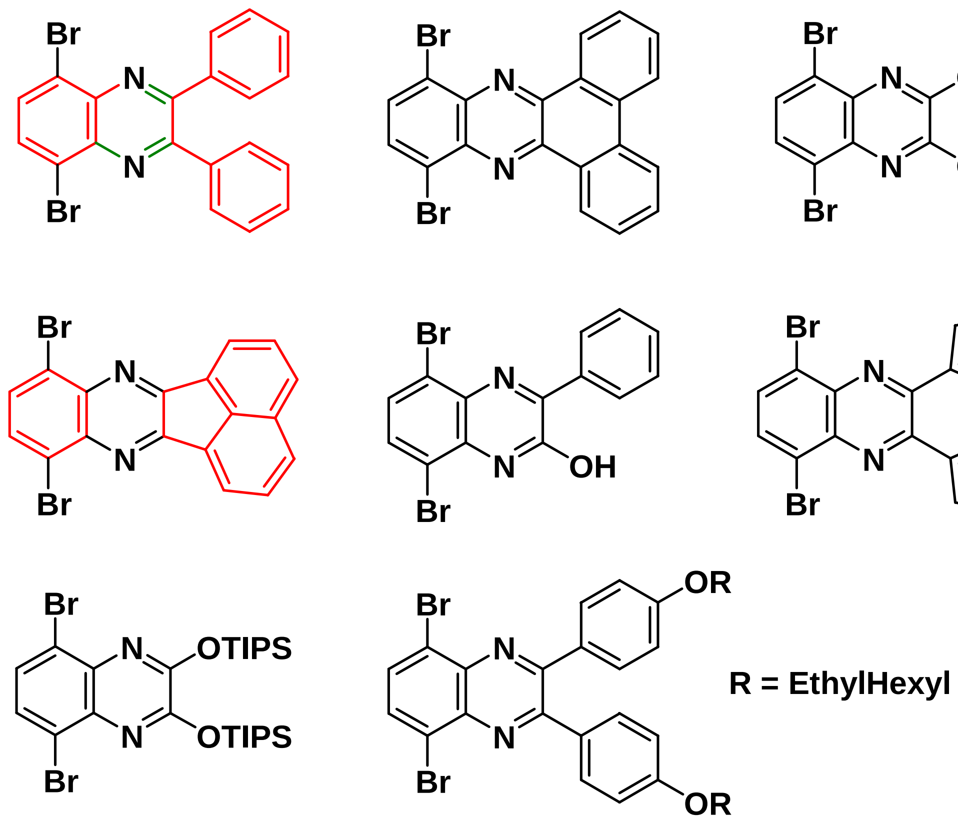

Figure 4.1. Pictorial summary or library of the quinoxalines synthesized by the condensation reaction. The molecules that are represented in red are the ones that we have carried through to the polymer process.

First attempts to alkynylate **25** utilizing $(Ph_3P)_2PdCl_2$ and CuI in triethylamine failed. The addition of THF as a cosolvent to increase the efficiency of the reaction, as described by Krause,[23] allowed the coupling of trimethylsilylacetylene to **25** in excellent yields (Scheme 4.4). The monomer **26** was isolated as colorless but highly fluorescent material. After removal of the TMS groups by K_2CO_3, we were able to obtain the diethynylquinoxaline in an overall yield of 86%. Transfer of this protocol to **29** furnished **30** in an 83% overall yield. With the two monomers in hand, we performed Pd catalyzed couplings of **27** and **31** respectively to 2,5-bis- (2¢-ethylhexyloxy)-1,4-

diiodobenzene. Utilizing standard coupling conditions (5 mol % $(Ph_3P)_2PdCl_2$, 5 mol % CuI in piperidine), **27** furnished the desired PAE **28** in 95 % isolated yield (aqueous workup, precipitation into methanol, Scheme 4.5) and a degree of polymerization (P_n) of 110 repeating units according to gel permeation chromatography. In the case of **31**, we coupled the soluble bis(trimethylsilyl)-substituted monomer to the diiodide. Monomer **30** was insoluble in most organic solvents and sparingly soluble in chloroform. We decided it would be best to deprotect the molecule in situ during a HCSH reaction.

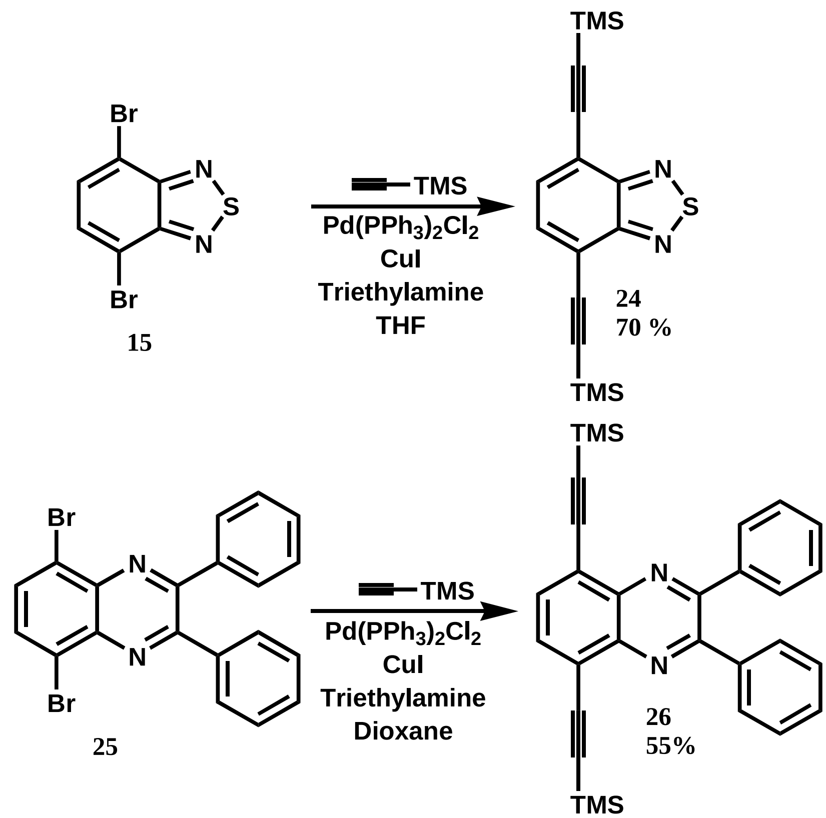

Scheme 4.4. The scheme above shows that the HCSH coupling reaction could be enhanced with polar additives such as THF or Dioxane. We were able to reproduce the reaction on the nonreactive dibromobenzothiadiazole. We were able to obtain 70 % yields with the benzothiadiazoles, and in the case of the quinoxalines 55 % yields were obtained.

Module **29** was deprotected in situ (KOH in ethanol), coupled, and gave the sparingly soluble polymer **31** (1-2 mg in 10 mL of chloroform) in an 86% isolated yield and a P_n of 36. While **28** dissolved easily in organic media such as chloroform and dichloromethane, the acenaphthalene substituted derivative **31** was considerably less soluble. Consequently, we were only able to obtain the solution phase ^{1}H and ^{13}C NMR spectra of **28** and a solution-phase ^{1}H NMR spectrum of **31**. All of the collected spectroscopic data are in agreement with the proposed polymeric structure. X-ray powder diffraction shows both polymers to be amorphous, with no distinct ordering present.

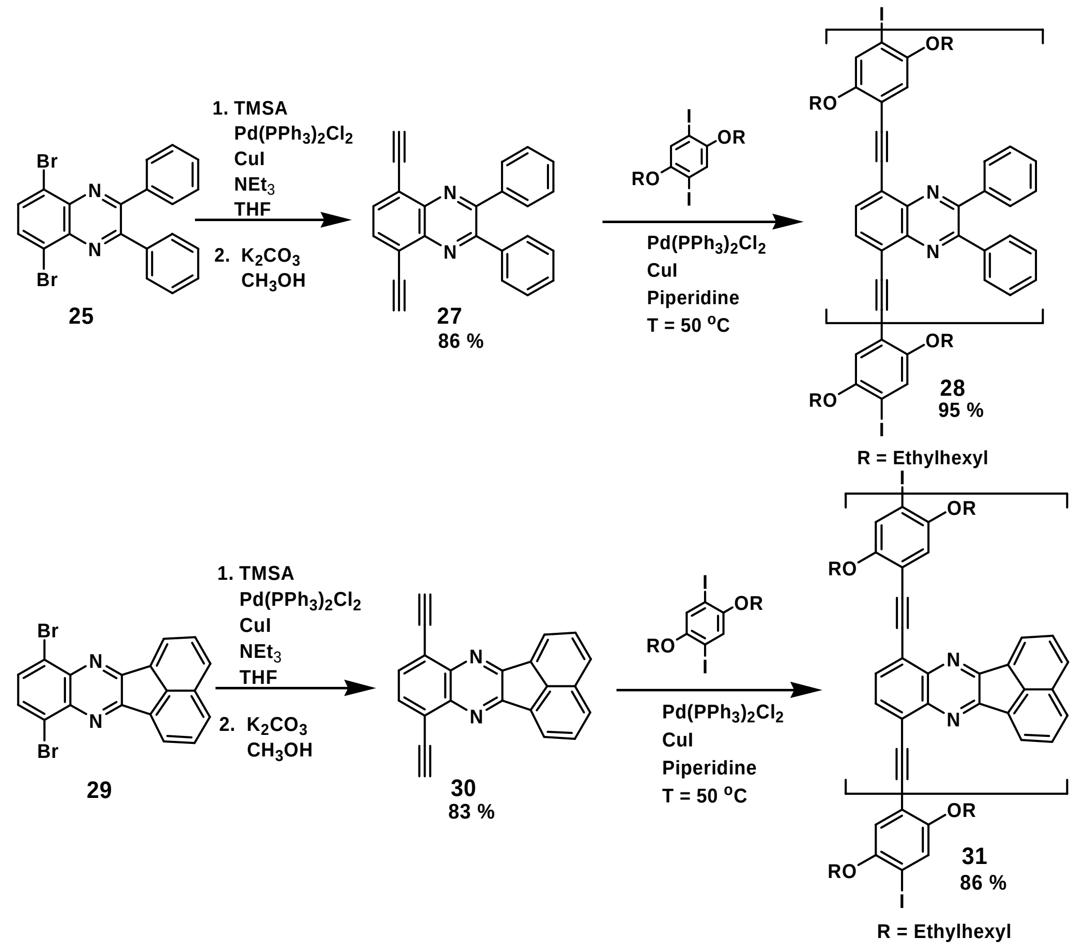

Scheme 4.5. Synthesis of the diphenylquinoxaline based PAE **28** and the acenaphthylquinoxaline based PAE **31**. Both of the monomers have used the polar additive THF to increase yields of the monomers.

In thin films, both polymers appear reddish translucent, while thick preparations are golden-green and lustrous. The polymers' appearances resemble that of benzothiadiazole-based PAEs **19**.[15, 20, 21] The polymers **28** and **31** show a λ_{max} of absorption in chloroform at 462 (**28**) and 474 nm (**31**). The small differences in absorption are probably due to the increased size of the conjugated heterocyclic unit in **31**. Polymer **28** was spun cast onto a quartz slide. Its UV-Vis spectrum (Figure 4.2, top, λ_{max} = 534 nm) is different from that in solution. The observed bathochromic shift (62 nm) is considerable, and probably due to planarization of the chains in the solid state. Aggregation and interchain interactions of the charge-transfer type will likewise play a role here. This aggregation behavior is distinctive and similar to that observed for the PPEs as well as for the poly(fluorenyleneethynylene)s.[24-26] The optical behavior of **28** in thin films can be effectively simulated by addition of methanol to a solution of the polymer in chloroform (Figure 4.2).

Addition of a solution of lithium trifluorosulfonate in acetone does not have an effect on the absorption spectrum. However, silver(I) salts and trifluoroacetic acid (TFA) have a distinct influence of the absorption spectrum of **28** (Figure 4.3). In both cases, the primary absorption peak disappears and a sloping but featureless shoulder appears. For TFA this band extends well into the 700+ nm range. Dilute solutions of **31** show a similar behavior as their absorption goes asymptotically to zero at wavelengths above 700 nm upon addition of TFA or Ag^+. It is noticeable that thin films of **28** show a bathochromic shift in absorption when exposed to a solution of $AgNO_3$ in methanol (534 nm to 560 nm), but are essentially unchanged when exposed to fumes of HCl or trifluoroacetic acid. The reason for this surprising behavior is the great hydrophobicity of the polymers **28** and **31** mediated through the ethylhexyl side chains.

The emission peaks of the polymers **28** and **31** in dilute chloroform solution are almost indiscernible from each other with an emission maximum at 538 nm for **28** and 540 nm for **31**. Addition of a small amount of TFA or of Ag^+

ions quenches their fluorescence. Addition of methanol to the polymer **28** does change its emission, and a slight red shift from 540 to 550 nm is recorded.

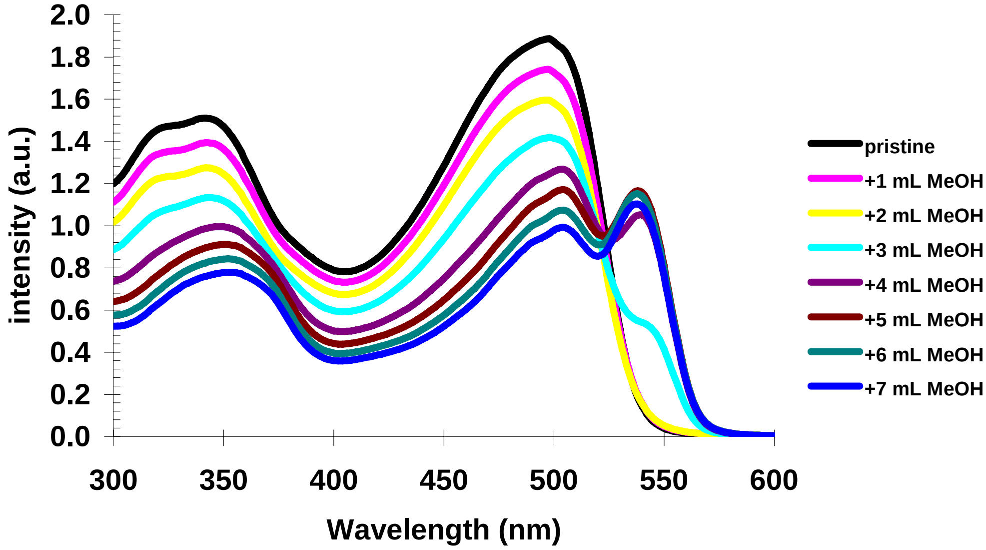

Figure 4.2. Solution UV-Vis spectra (λ_{max} = 460 nm, chloroform), and aggregation UV-Vis spectra of PAE **28** upon addition of methanol vs thin film UV-Vis (λ_{max} = 534 nm) spectrum of **28**.

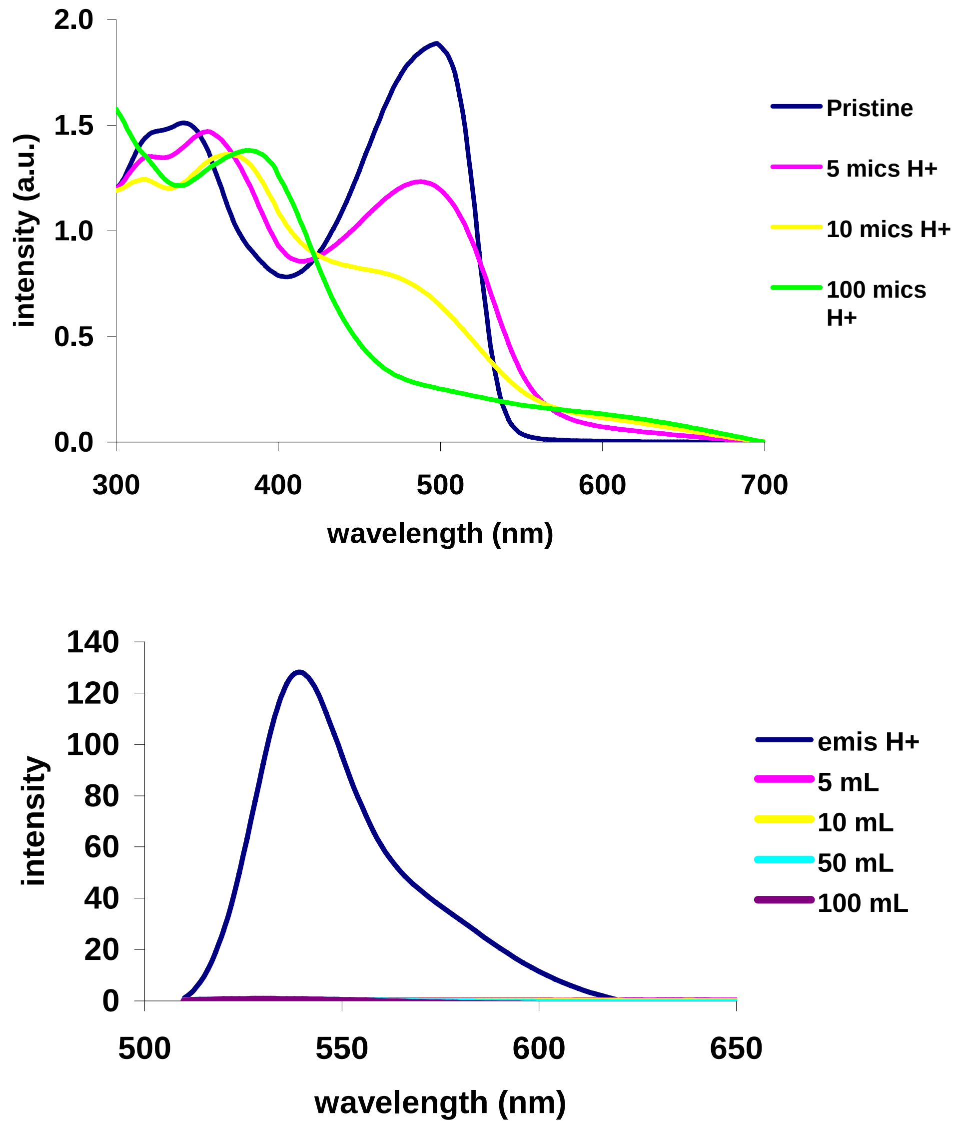

Figure 4.3. Top: Addition of trifluoroacetic acid to polymer **28** (10 mg L^{-1}). Bottom: Solution of PAE **28** and its emissions with the addition of trifluoroacetic acid (10 mg L^{-1}).

Table 4.1. Comparison of PM3 Band Gap Calculations of Several Conjugated Oligomers

Structure	HOMO PM3 (eV)	LUMO PM3 (eV)	Band Gap calc. (eV)
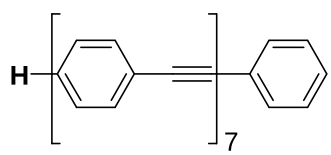 **20**	-8.64	-1.18	7.28
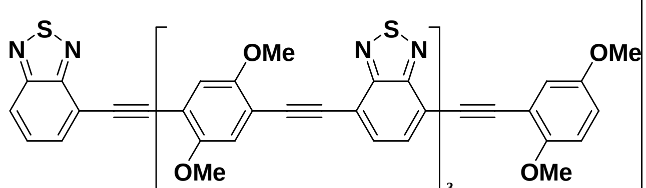 **22**	-8.42	-2.10	6.32
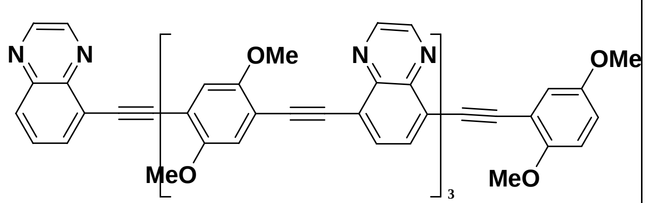 **32**	-8.22	-1.47	6.75

The golden luster and presence of the electron withdrawing quinoxaline units in **28** and **31** suggests that these polymers are electronically different from the PPEs. Quantum chemical calculations reveal that the HOMO-LUMO gap (Hartree-Fock, 6-31G**, implemented as Spartan Pro, Wavefunction Inc., on Windows 2000) of diethynylbenzothiadiazole (HOMO) -8.45 eV, LUMO) 0.69 eV) is lower than that of diethynylquinoxaline (HOMO) -8.11 eV, LUMO) 1.31 eV). The polymer **28** is more electron rich than **19** as indicated by both the ab initio calculation of the monomer and the semiempirical PM3 (Spartan Pro) calculations of model octamers (Table 4.1). The quinoxaline building block seems thus less electron accepting than the benzothiadiazole unit. However, the PM3 results are qualitative and should not be over-interpreted, but the trend seen in Table 3.1 is mirrored in the cyclic voltammograms of the polymer **28** and the benzothiadiazole-containing polymer **19**.[15] We performed the CV of thin films of **28** that was spin cast onto an indium tin oxide slide.[27] While **19** is reduced at -1.42 V,[15] reversible reduction of **28** occurs at -1.54 V (at -1.66 V reoxidation) under change of color from red to green, giving testimony to the higher lying LUMO of **28**. However, a second clean reduction of **28** is observed at -1.99 V suggesting that the polymer chains can be higher charged. It is reasonable to assume that in the first step only every second repeating unit is charged in **28** and that in a second reduction step the remaining quinoxaline modules are reversibly reduced.

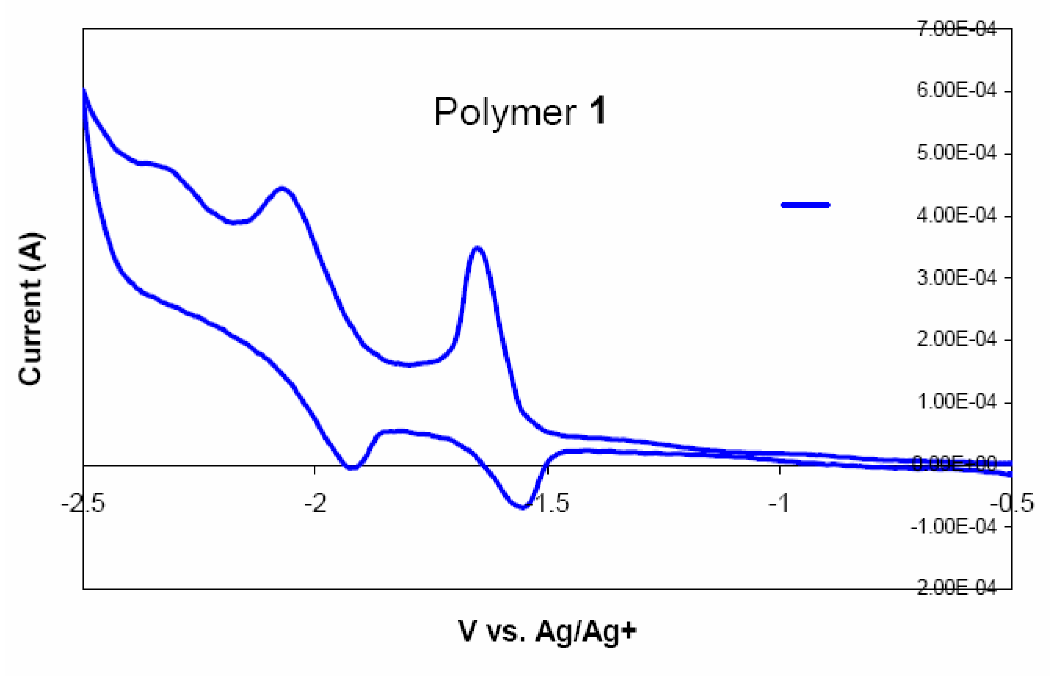

Figure 4.4. Cyclic voltammogram of the polymer **28.** Peak potentials: Reduction - 1.54, -1.91 V; re-oxidation -2.08, -1.66 V vs. AgCl/Ag couple.

Conclusion

In conclusion, we described the synthesis, characterization, aggregation, and ionochromicity of the novel quinoxaline-containing PAEs **28** and **31**. These materials are interesting *n*-semiconductors and highly effective sensory materials for Ag^+ and H^+ ions in solution. These materials as well have interesting solid state properties that are similar in our case to the benzothiadiazole containing PAEs. However, the production of the quinoxaline homopolymer is problematic. Without sufficient solubilizing groups on the aromatic core, the polymer is very insoluble and unprocessible. Current research within this topic will try to resolve these remaining issues, so that our original premise would become viable. Having creating the quinoxaline copolymers, we hope to use them in metal sensing applications, and also hope to study its potential use in solid state applications.

4.3. Experimental

Reagents solvents and catalysts were of commercial grade and used as obtained. ^{1}H- and ^{13}C-NMR spectra were recorded in $CDCl_3$ on a Bruker AM 300 or a Varian Mercury 400 spectrometer. The mass spectra were measured on a VG 70SQ. IR spectra were obtained using a Perkin Elmer FTIR 1600 on NaCl plates. Gel Permeation Chromatography: Molecular weight determinations were performed using a Waters Styragel HMW 6E (7.8 mm i.d. × 300 mm) GPC column (20 µm particles/10 µm frits) eluted with $CHCl_3$ at ambient temperature (flow rate of 1 mL/min). Molecular weight results were based on 10 polystyrene standards (M_w = 3 900 000, 1 980 000, 996 000, 629 000, 210 000, 70 600, 28 600, 10 900, 3000, and 1300) purchased from Waters (type SM-105). P_n was determined by dividing M_n resulting from the GPC by 100. Dibromo-2,1,3-benzothiadiazole,[1] 3,6-dibromo-*ortho*-phenylenediamine,[2] 5,8-dibromo-2,3-diphenylquinoxaline,[3] 5,8-dibromo-acenapthylquinoxaline, and the other quinoxalines were made according to literature procedures.

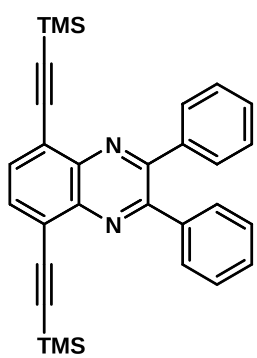

Preparation of 5,8-bis(trimethylsilylethynyl)-2,3-diphenylquinoxaline. To a flame dried 50 mL Schlenk flask, 5,8-dibromo-2,3-diphenylquinoxaline (0.586 g, 1.33 mmol), $Pd(PPh_3)_2Cl_2$ (46.7 mg, 0.066 mmol), CuI (52.3 mg, 0.275 mmol), THF (5 mL) and triethylamine (10 mL) were added under a slow stream of nitrogen. Trimethylsilylacetylene (0.270 g, 2.75

mmol) was added via syringe, and the reaction was stirred overnight at 80°C. The reaction was poured into a mixture of dichloromethane (100 mL) and water (150 mL). The organic layer was washed three times with water (100 mL) followed by 10 % NH_4OH (150 mL). The aqueous layer was washed three times with dichloromethane (30 mL), and the organic layers were combined. The organic layer was dried over anhydrous sodium sulfate, and the solvent was evaporated to give a brown powder. Purification by column chromatography with eluent hexanes/dichloromethane (80/20) furnished colorless crystals (0.601 g, 95 %). MP: 230 ^{o}C (decomp.). ^{1}H-NMR ($CDCl_3$): 7.79 (s, 2H), 7.71-7.68 (m, 4H), 7.34-7.31 (m, 6H), 0.323 (s, 18H). ^{13}CNMR ($CDCl_3$): δ 152.90, 138.65, 133.07, 130.24, 129.30, 128.12, 123.39, 103.39, 101.21, 0.00. IR (neat): ν 3056, 2958, 2896, 2147, 1559, 1466, 1443, 1378, 1336, 1247, 1214, 1155, 1095, 1062, 1026, 840, 757 cm^{-1}. MS ($C_{30}H_{30}N_2Si_2$): m/z 474.

Preparation of 5,8-diethynyl-2,3-diphenylquinoxaline. To a 100 mL round

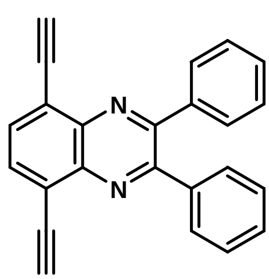

bottom flask, 5,8-bis(trimethylsilylethynyl)-2,3-diphenylquinoxaline (0.670 g, 1.41 mmol) was added to a solution of methanol (50 mL) and potassium carbonate (5.00 g, 36.2 mmol) and stirred overnight at room temperature. The solution was poured into a mixture of dichloromethane (50 mL) and water (100 mL). The organic layer was washed three times with water (75 mL). The aqueous layer was washed three times with dichloromethane (30 mL) and dried over sodium sulfate. The solvent was evaporated to give a yellow powder (0.396 g, 90 %). MP: 183 ^{o}C (decomp.). ^{1}H-NMR ($CDCl_3$): δ 7.88 (s, 2H), 7.63-7.60 (m, 4H), 7.37-7.28 (m, 6H), 3.61 (s, 2H). ^{13}CNMR ($CDCl_3$): δ 153.83, 141.19, 138.56, 133.88, 130.22, 129.30, 128.25, 123.04, 85.35, 79.95. IR (neat): ν 3275, 3240, 2961, 2960, 2848, 2351, 2100, 1433, 1378, 1338, 1259, 1222, 1091, 1053, 1029, 922, 846, 775 cm^{-1}. MS ($C_{24}H_{14}N_2$): m/z 330.

Preparation of Polymer 28. To a flame dried 50 mL Schlenk flask, 5,8-

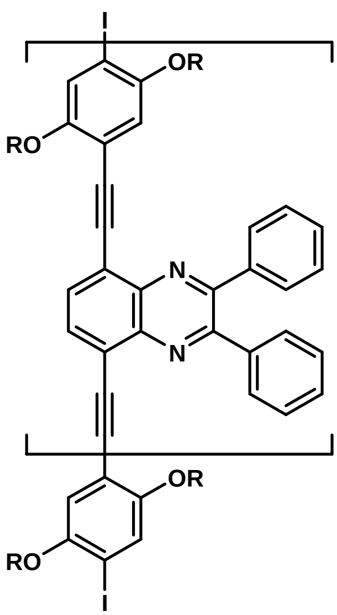

diethynyl- 2,3-diphenylquinoxaline (0.210 g, 0.636 mmol), 1,4-diiodo-2,5-bis(2-ethylhexyloxy)benzene (0.339 g, 0.578 mmol), $Pd(PPh_3)_2Cl_2$ (100 mg, 0.142 mmol), CuI (50.0 mg, 0.260 mmol), and toluene (6m L) were added under a slow stream of nitrogen. Piperidine (6 mL) was added to the reaction via syringe. The reaction mixture was stirred and kept at 30°C for 24 h. The solution was poured into a mixture of chloroform (75 mL) and water (100 mL). The organic layer was washed three times with water (100 mL) followed by 50% NH_4OH (150 mL). The aqueous layer was washed twice with chloroform (20 mL), and the organic layers were combined. To the resultant organic layer, methanol (400 mL) was added to precipitate the polymer. Suction filtration produced a dark red polymer with a green metallic luster (0.400 g, 96%). ^{1}H-

NMR ($CDCl_3$): δ 7.96 (bs, 2H), 7.78-7.76 (bm, 4H), 7.40-7.28 (bm, 6H), 4.00 (bm, 4H), 1.86-0.89 (bm, 30H). ^{13}C-NMR ($CDCl_3$): δ 154.06, 153.13, 141.07, 138.97, 132.80, 128.08, 128.01, 127.97, 127.73, 127.49, 117.37, 94.91, 92.43, 72.09, 39.59, 30.71, 29.16, 24.02, 23.11, 14.07, 11.26. IR (neat): ν 2953, 2920, 2856, 2354, 2327, 1818, 1669, 1632, 1601, 1485, 1444, 1415, 1382, 1276, 1220, 1034 cm^{-1}. GPC (polystyrene standards): P_n 110, M_w/M_n = 3.03. λ_{max} (abs, $CHCl_3$): 324, 454 nm. λ_{max} (em, $CHCl_3$): 540 nm.

Preparation of 5,8-bis(trimethylsilylethynyl)acenapthylquinoxaline. To a

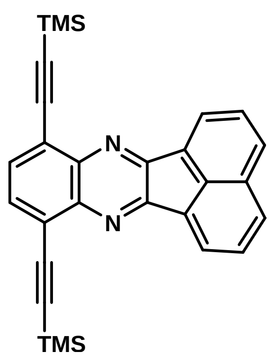

flame dried 50 mL Schlenk flask, 5,8-dibromo-acenapthylquinoxaline (0.990 g, 2.40 mmol), $Pd(PPh_3)_2Cl_2$ (100 mg, 0.142 mmol), CuI (100 mg, 0.521 mmol), triphenylphosphine (150 mg, 5.71 mmol), and triethylamine (20 mL) were added under a slow stream of nitrogen. Trimethylsilylacetylene (0.610 g, 6.21 mmol) was added via syringe, and the reaction was stirred overnight at 80°C. Then, the reaction was poured into a mixture of dichloromethane (100 mL) and water (150 mL). The organic layer was washed three times with water (100 mL) followed by 10 % NH_4OH (150 mL). The aqueous layer was washed three times with dichloromethane (30 mL), and the organic layers were combined. The organic layer was dried over anhydrous sodium sulfate, and the solvent was evaporated to give a light brown powder. Purification by column chromatography with eluent hexanes/dichloromethane (80/20) furnished colorless crystals (0.882 g, 83 %). MP: 243 ^{o}C (decomp.). ^{1}H-NMR ($CDCl_3$): δ 8.17 (s, 2H), 8.44 (d, 2H), 8.12 (d, 2H), 7.85 (t, 2H), 0.40 (s, 18H). ^{13}CNMR ($CDCl_3$): δ 154.58, 141.71, 137.05, 132.99, 131.54, 129.96, 129.87, 128.62, 124.00, 122.71, 103.27, 101.74, 0.04. IR (neat): ν 3053, 2993, 2958, 2897, 2153, 1614, 1568, 1486, 1423, 1357, 1246, 1216, 1174, 1125, 1034, 841, 770 cm^{-1}. MS ($C_{28}H_{26}N_2Si_2$): m/z 446.

Preparation of Polymer 31. To a flame dried 50 mL Schlenk flask, 5,8-bis(trimethylsilylethynyl)acenapthylquinoxaline (0.250 g, 0.559 mmol), 1,4-diiodo-2,5-bis(2'-ethylhexyloxy)benzene (0.330 g, 0.562 mmol), $(PPh_3)_2Pd\ Cl_2$ (50.0 mg, 0.071 mmol), CuI (50.0 mg, 0.260 mmol), and tetrahydrofuran (5mL) were added under a slow stream of nitrogen. A saturated ethanol/KOH solution (1 mL) was also added. Piperidine (7 mL) was introduced to the reaction via syringe. The reaction was stirred and held at 30°C for 48 h. The solution was poured into a mixture of chloroform (75 mL) and water (100 mL). The organic layer was washed three times with water (100 mL) followed by 50% NH_4OH (150 mL). The aqueous layer was washed twice with chloroform (20 mL), and the organic layers were combined. To the resultant organic layer, methanol (400 mL) was added to precipitate the polymer. Suction filtration

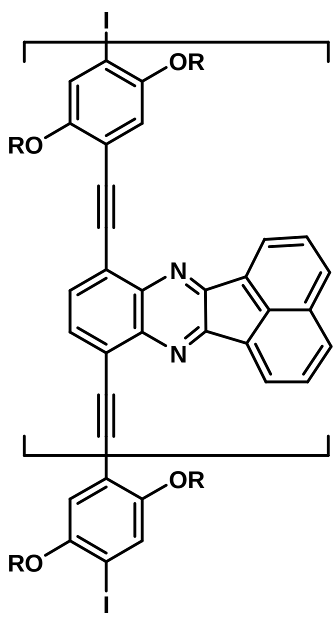

produced an orange polymer (0.305 g, 86%). ^{1}H-NMR ($CDCl_3$): δ 8.60 (s, 2H), 8.18 (s, 2H), 8.01 (s, 2H) 7.90 (s, 2H), 7.41 (s, 2 H), 4.15 (s, 4H), 1.56, 1.25, 0.88 (3 bm, 30H). ^{13}C-NMR (CP-MAS): δ 152.48, 129.92, 92.69, 70.65, 45.61, 38.62, 28.23, 22.11, 12.11. IR (neat): ν 2957, 2916, 2848, 2356, 2280, 1558, 1456, 1438, 1412, 1375, 1275, 1217, 1115, 1031, 826, 773 cm^{-1}. GPC (polystyrene): P_n 37, M_w/M_n 1.44. λ_{max} (abs, $CHCl_3$): 274, 326, 476 nm. λ_{max} (em, $CHCl_3$): 540 nm.

Electrochemical Characterization and Cyclic Voltammetry of Polymer 28. The experimental instrumentation for the electrochemical measurements have been described elsewhere.[5] A thin film of the polymer 3 was spun cast from chloroform (10 mg/mL) and the formed film on the ITO slide was immersed into a dichloromethane solution with a platinum counter electrode. The measurement was performed with 0.1 M tetrabutylammonium perchlorate supporting electrolyte. The polymer-coated electrode was utilized as working electrode in a standard 3-electrode electrochemical setup. The potential was measured against a platinum wire pseudo-reference electrode. The AgCl/Ag couple was used as a standard for the reduction.

4.4. References

1. Bunz, U. H. F., *Chem. Rev.* **2000,** *100*, 1605.

2. Bunz, U. H. F., *Acc. Chem. Res.* **2001,** *34*, 998.

3. Moore, J. S., *Acc. Chem. Res.* **1997,** *30*, 402.

4. Giesa, R., *J. Macromol. Chem. Phys.* **1996,** *36*, 631.

5. Giesa, R.; Schulz, R. C., *J. Macromol. Chem. Phys.* **1990,** *191*, 857.

6. Pschirer, N. G.; Miteva, T.; Evans, U.; Roberts, R. S.; Marshall, A. R.; Neher, D.; Myrick, M. L.; Bunz, U. H. F., *Chem. Mater.* **2001,** *13*, 2691.

7. Schmitz, C.; Posch, P.; Thelakkat, M.; Schmidt, H. W.; Montali, A.; Feldman, K.; Smith, P.; Weder, C., *Adv. Func. Mater.* **2001,** *11*, 41.

8. Weder, C.; Sarwa, C.; Montali, A.; Bastiaansen, G.; Smith, P., *Science* **1998,** *279*, 835.

9. Yang, J. S.; Swager, T. J., *J. Am. Chem. Soc.* **1998,** *120*, 11864.

10. Yamamoto, T., *Bull. Chem. Soc. Jpn.* **1999,** *72*, 621.

11. Yamamoto, T.; Honda, K.; Ooba, N.; Tomaru, S., *Macromolecules* **1998,** *31*, 7.

12. Li, J.; Pang, Y., *Macromolecules* **1997,** *30*, 7487.

13. Al-Higari, M.; Birckner, E.; Heise, B. J.; Klemm, E., *J. Polym. Sci., Part A: Polym. Chem.* **1999,** *37*, 4442.

14. Ley, K. D.; Whittle, C. E.; Bartberger, M. D.; Schanze, K. S., *J. Am. Chem. Soc.* **1997,** *121*, 33423.

15. Bangcuyo, C. G.; Bunz, U. H. F., *Macromolecules* **2001,** *34*, 7592.

16. Bangcuyo, C. G.; Rampey-Vaughn, M. E.; Quan, L. T.; Angel, S. M.; Smith, M. D.; Bunz, U. H. F., *Macromolecules* **2002,** *35*, 1563.

17. Jegou, G.; Jenekhe, S. A., *Macromolecules* **2001,** *34*, 7926.

18. Monkman, A. P.; Palsson, L. O.; Higgins, R. W. T.; Wang, C.; Bryce, M. R.; Batsanov, A. S.; Howard, J. A. K., *J. Am. Chem. Soc.* **2002,** *124*, 6049.

19. Nurulla, I.; Tanimoto, A.; Shiraishi, K.; Sasaki, S.; Yamamoto, T., *Polymer* **2002,** *43*, 1287.

20. Ley, K. D.; Li, Y. T.; Johnson, J. V.; Powell, D. H.; Schanze, K. S., *Chem. Commun.* **1999**, 1749.

21. Morikita, T.; Yamaguchi, I.; Yamamoto, T., *Adv. Mater.* **2001,** *13*, 1862.

22. Yamamoto, T.; Kanbara, T.; Ooba, N., *Chem. Lett.* **1994**, 1709.

23. Thorand, S.; Krause, N., *J. Org. Chem* **1998,** *63*, 8551.

24. Halkyard, C. E.; Rampey, M. E.; Kloppenburg, L.; Studer-Martinez, S. L.; Bunz, U. H. F., *Macromolecules* **1998,** *31*, 8655.

25. Miteva, T.; Palmer, L.; Kloppenburg, L.; Neher, D.; Bunz, U. H. F., *Macromolecules* **2000,** *33*, 652.

26. Pschirer, N. G.; Bunz, U. H. F., *Macromolecules* **2000,** *33*, 3961.

27. Cyclic voltammetry was performed in thin films with AgCl/Ag as a standard reference.

CHAPTER 5

NANOSTRUCTURING OF POLY(ARYLENEETHYNYLENE)S: FORMATION OF NANOTOWERS, NANOWIRES, AND NANOTUBULES BY TEMPLATED SELF-ASSEMBLY

5.1. Introduction

Within this chapter we report novel, nanoscale polyaryleneethynylene (PAE) morphologies that are created by a solution molding process utilizing nanostructured anodiscs (Whatman filter disks, alumina wafers). As seen in a previous chapter, we tried to fabricate polymeric architecture by use of gold nanoparticles and benzothiadiazole containing PAEs. This is a different and scaled down approach to self assembled nanostructures. If we are able to create novel nanostructures, then it would be of great use due to the fact that this technique is very inexpensive, quick, and done with by solution phase dropcasting the polymer rather than the conventional technique used.

Depending upon the molecular structure of the utilized PAE, different self assembled nanostructures are formed during templating. Nanostructuring of conjugated polymers is an important process that modifies their electronic and electron transport properties.[1-13] Nanostructuring plays a crucial role in device applications, for example in the fabrication of photovoltaic cells, where self-assembly of an interpenetrating network of a conjugated polymer and an *n*-

semiconductor is the critical factor for success.[14-17] Nanostructuring is of interest in photonic band gap materials[18, 19] and fabrication of heterojunction devices in which two different conjugated polymers have to interact intimately to increase their interface.[14-17] In many cases, conjugated polymers show self-assembly into nanoscopic structures; however, their self-assembly modes are difficult to control and not always predictable.[20-24] Thus, it is of interest to develop processes that furnish conjugated polymers with an engineered nanoshape. A potent and elegant solution for this problem was developed by Martin for organic, inorganic, and metallic nanostructures utilizing templating procedures.[8-13] This approach utilizes filter anodiscs that are commercially available, are inexpensive, and display pores of defined size and diameter. The material of choice is deposited into these pores, and the anodisc is dissolved in dilute base or acid to give nanotubes of excellent quality. While metallic and insulator nanostructures have been made by this method, only very few examples of conjugated polymers have been structured by this method.[8-13] Polyaniline, polythiophene, and polypyrrole are examples of polymers that form electrochemically *in* the preformed pores of the filter disk.[8-13] However, there is a large number of conjugated polymers available that do *not* form by electropolymerization. As a result, these materials have to be nanostructured in a different way. In this paper, we describe the fabrication of semiconducting nanotowers, nanowires, and nanotubules by solution phase self-assembly of poly(aryleneethynylene)s **33-37,** in which we will refer these polymers to the respective numbers in this chapter only.[25-33]

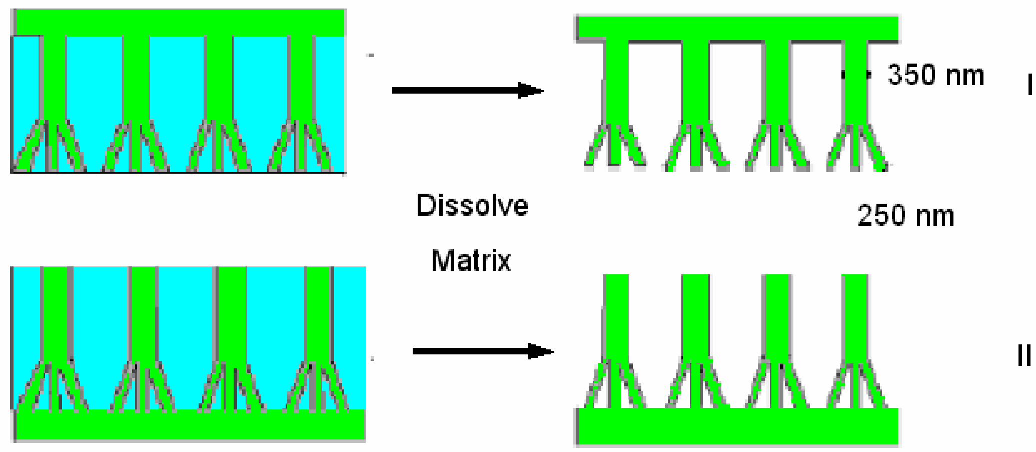

Figure 5.1. Schematic of the formation of PAE nanotowers and nontubules. Depending on which side the polymer was casted upon, 2 different configurations could be achieved. The larger pores are estimated by SEM to be approximately 350 nm while the branches measure to be 250 nm.

5.2. Results and Discussion

In the first experiment, a dilute solution of polymer **33** was drop cast (Figure 1, geometry II, Figure 5.1) onto a Whatman filter anodisc[34] and allowed to dry. Subsequent dissolution of the alumina mask led to products that had formed nanotubes of poor quality (by SEM). Utilizing dilute solutions of **33** led to fragile nanostructures that were washed away when dissolving the anodisc. In subsequent experiments, we utilized more concentrated solutions (10 mg/mL, see experimental). These solutions were utilized mostly in geometry II, and gave more robust products that were examined by SEM.

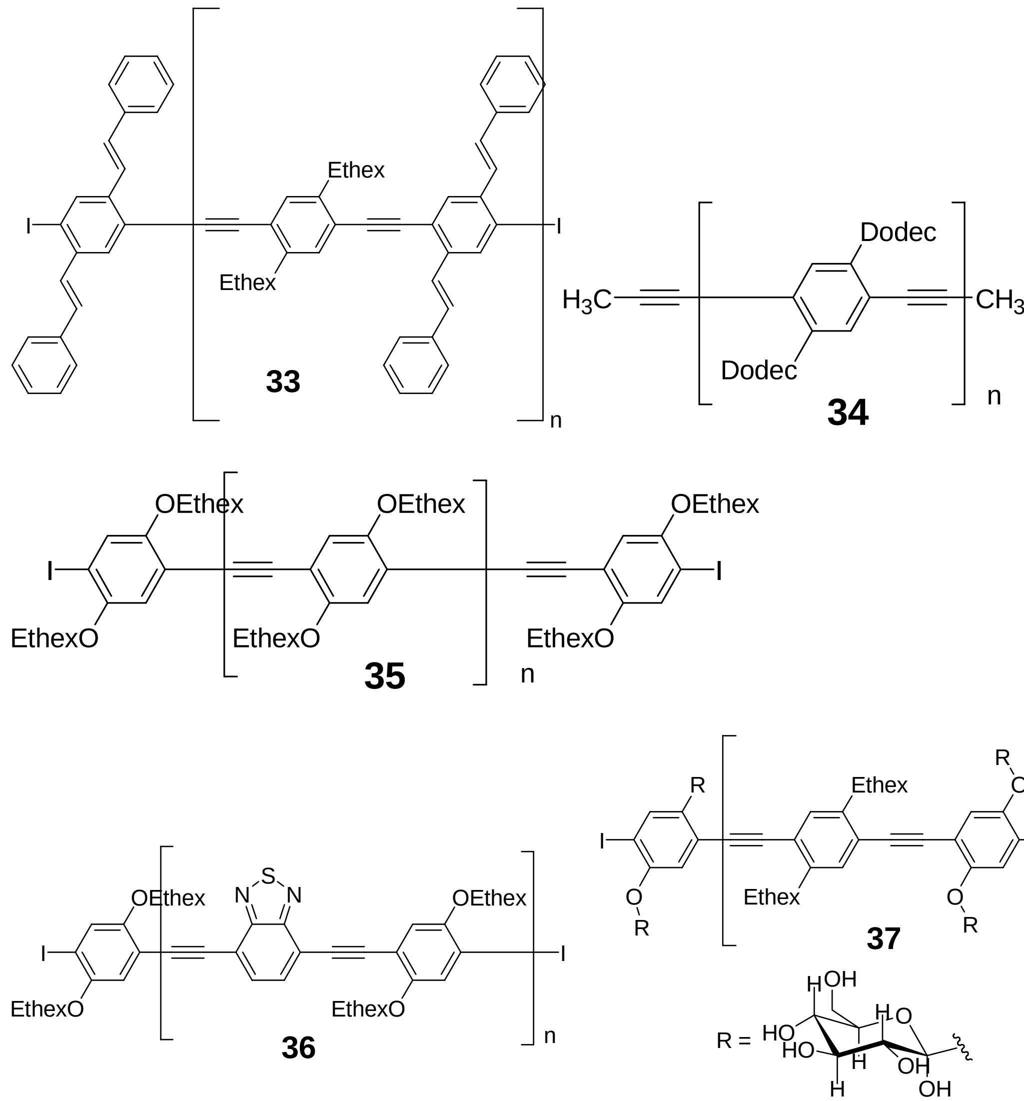

Figure 5.2. List of polymers used in the manufacturing of the templated assisted nanostructuring. The polarity of the polymers seem to have an effect on the structures that were created.

Polymer **33** forms both filled and hollow nanotubes with an aspect ratio of approximately 32 (Figure 5.3). The width of the tubes ranges from 300 to 350 nm, which is in good agreement with the specifications of the filter pores. The length of the tubes ranges from 2 to 10 μm. The aspect ratio is quite low (7-32). Even though the length of the channels in the Whatman filters is 60 μm, the pores of the disk are only slightly penetrated by the viscous polymer solution. Annealing of the anodisc/polymer hybrid structure did not lead to better penetration of the polymer into the inorganic pores. Similarly, dimensioned nanostructures were observed after dissolution of the anodisc. We wanted to explore the influence of PAE structure on the process of the nanowire formation. As a consequence, we investigated PAEs **34-37.** The heterocyclic polymer **36** (Figure 5.4) formed well-developed wires that seemed to penetrate the pores almost completely. The dimension of these wirelike structures is 350 nm x 30 μm, and the aspect ratio of these solid wires is approximately 90. The wires are well developed over the entire area of the film. Visible is the splicing of the template that is preserved in the top part of the wires. This splicing leads to a cauliflower-like topology that is typical for a geometry II (Figure 5.1) preparation. The heterocyclic polymer **36**, an excellent film-former, is almost ideal for the generation of tubules and wires of great length. The more polar, sugar-substituted, and methanol soluble PPE **37** forms a different nanoscale morphology altogether.

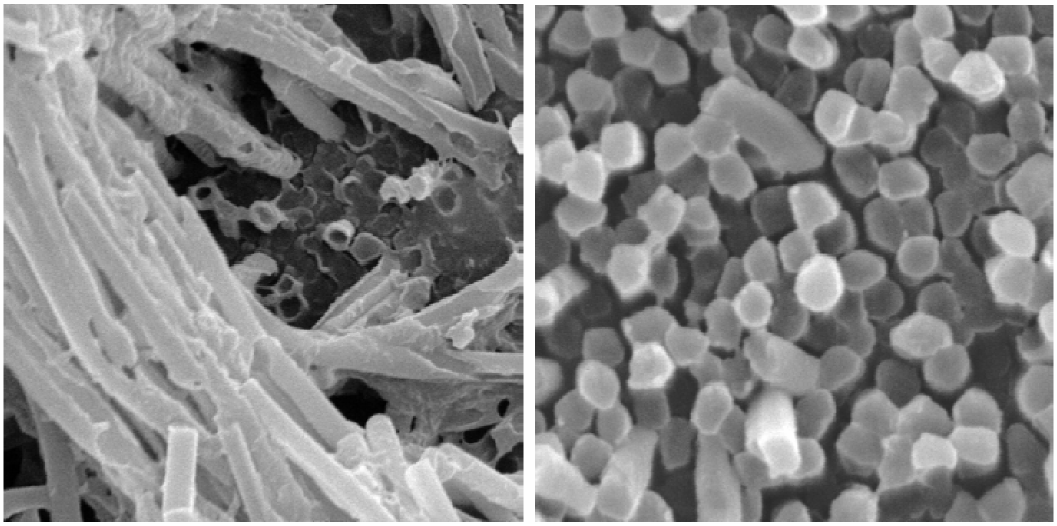

Figure 5.3. Polymer **33**. Picture dimensions are 6x6 μm (left) and 4.5 x 4.5 μm (right). Drop-cast films. On the left picture the junction of hollow and solid tubules is shown. The right picture shows a perfect fill of the mesopores.

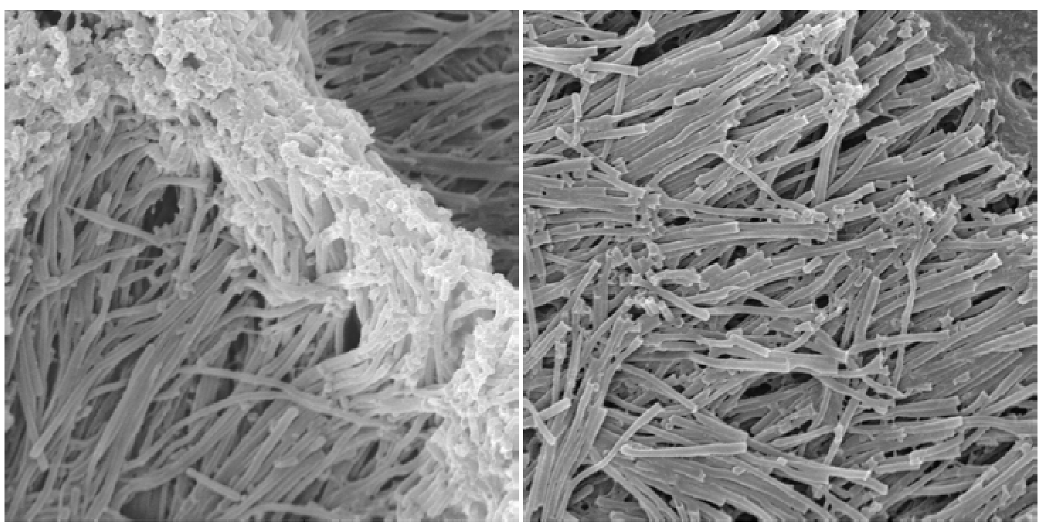

Figure 5.4. Polymer **36**. Picture dimensions are 18 x 18 μm in both cases. Well visible is the wire-like characteristic of the polymer preparation. The aspect ratio of the wires is in excess of 50. Especially remarkable is that the nanostructures are almost defect-free. On the left side the cauliflower geometry of the top is visible. This geometry mirrors the geometry of the utilized Whatman mask.

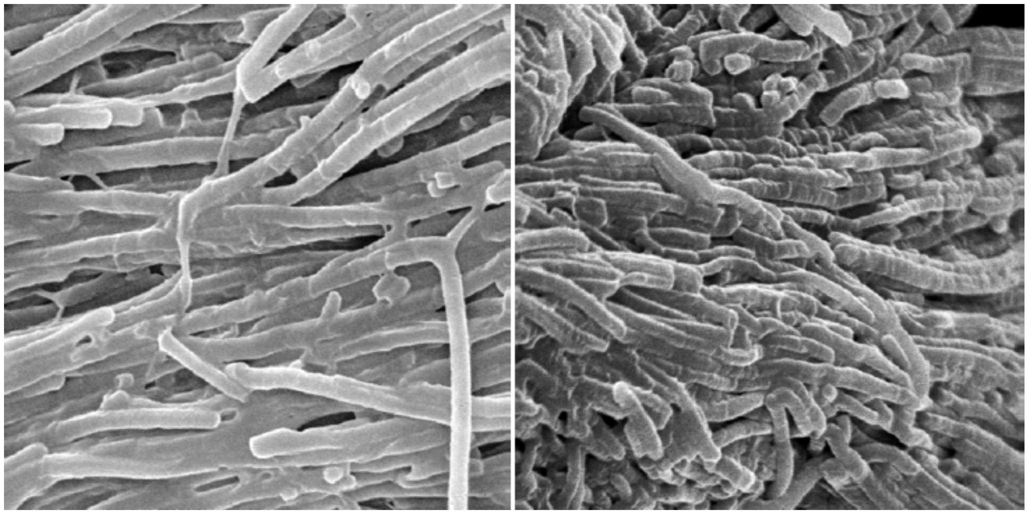

Figure 5.5. PPE **35**. The picture dimensions are 9 x 9 μm (left) and 6x6 μm (right). Particularly interesting is the horizontal striation of 140 nm in these blunted wires. The aspect ratio of 3 is approx. 30.

For **37**, short "macaroni" tubules are formed (Figure 5.6). Their outer diameter is 330 nm, while the diameter of the "eye" is 210 nm. The tubules are 2 μm long, and their aspect ratio is only slightly above 6. Concentrated solutions give isolable macaroni structures, while dilute solutions give materials that fragment upon dissolution of the anodisc. In the case of **37,** the hollowness of the tubes is visible via defects that lead to some holes in the walls of the tubes. The highly hydrophobic didodecyl-PPE **34** forms short nanotubes that show the cauliflower geometry of the spliced matrix (Figure 5.6).

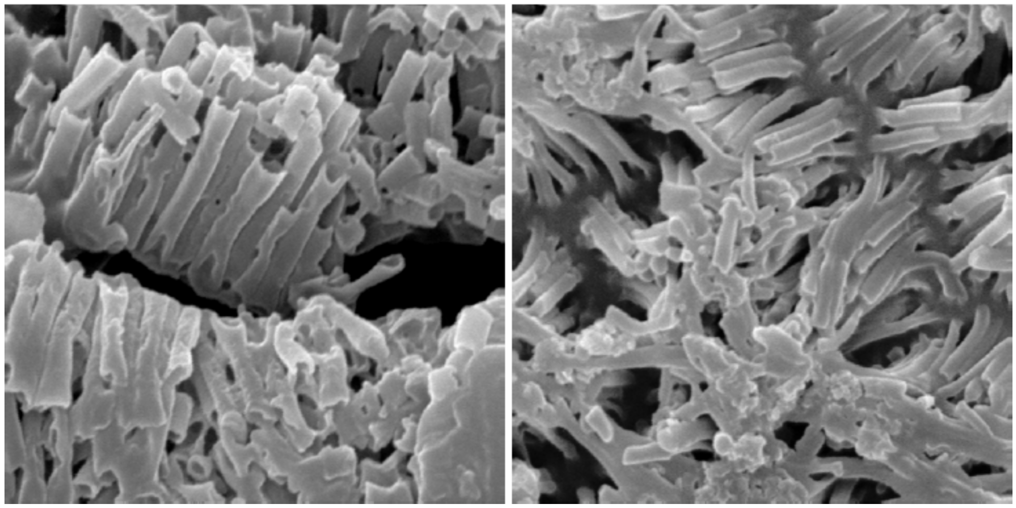

Figure 5.6. Sugar-PPE **37** forms thick macaroni-type structures. The thickness of the wall in these tubes is 60 nm and the picture dimensions are 6 x 6 μm. On the right-hand a picture of the cauliflower geometry of the didodecyl-PPE **34.** The picture dimensions are 9 x 9 μm. The splitting into the narrow base-wires is well visible and represents the topology of the Whatman filter anodisc.

We examined as well a moderately polar PPE, bisethylhexyloxy- PPE **35**. This PPE furnished long, well developed wire-type structures that seem to be solid, completely filled, 200-300 nm thick, and up to 43 μm long. Aspect ratios of 140-215 result. These materials seem to penetrate the membrane almost completely. Additionally, these tubules show (Figure 5.5) horizontal striations that are slightly irregular but have an average width of 140 nm. In all of the examined cases, we obtain nanostructures which are covered by the bulk material in the form of a thin film on the bottom. An interesting observation is that the formation of the nanostructures is not visibly correlated with the molecular weights[35] of the examined PAEs.

Conclusion

In conclusion, we have extended Martin's nanostructuring process to PAE's, and shown that these can be viable materials for nanostructuring. Up to now, conjugated polymers have been *formed* inside the pores of anodiscs by electrolytic processes. We have demonstrated that PAE's can be *cast* into the mesopores of anodiscs to give free-standing, high aspect ratio nanostructures of excellent quality after the removal of the template with aqueous base. This aspect gives us an advantage for these main reasons: (1) the structure of the polymer in use is well defined, (2) P_n and PDI are all determined for the polymer, (3) the relatively quick and inexpensive ease of dropcasting the polymer, and (4) the reproducibility of the experiment. The nanostructuring of conjugated materials may lead to advancement in semiconductor applications by increasing the surface area of the polymer under consideration. At the moment, we are attempting to process the nanostructures into thin films of homogeneous thickness by spin casting, and our future work in this area will focus on the construction of photovoltaic and light emitting devices in collaboration with electrical engineers as well as the develop of thin film transistors.

Table 5.1. Properties of Nanostructures Formed by Poly(aryleneethynylene)s **33-37** Utilizing Whatman Filter Anodiscs .

Polymer	**33**		**34**	**35**	**36**		**37**
Geometry	I	II	II	II	I	II	I
Observed structure	T_u	T_u, T_o	T_o	T_o	T_o	T_u, T_o	T_u
Length (μm)	2.5	9.5	7	43	30	T_o 12 T_u 3	2.1
Width (nm)	DI 250 Do 350	300	300	200 – 300	350	DI 270 Do 340	DI 210 DO 330
Aspect ratio	7	> 32	23	Up to 140	86	T_o 34 T_u 8.6	6.4
Pn PDI	55 2.8		512 3.8	316 24	19 2.8		75 2.2

The utilized filters have pore width of 340 nm, Anodisc 47, 0.2 μm

T_u = Tubules; T_o = Towers

5.3. Experimental

Synthesis of the polymers **33-37** has been described.[28-33] Solutions of the polymers were prepared in chloroform or THF by heating and sonicating the respective polymer to ensure that the polymers dissolved. Dilute solutions were approximately 1 mg polymer/mL solvent and concentrated solutions were 10-15 mg polymer/mL solvent. Films were drop-cast from chloroform onto the commercially available anodiscs[34] (Whatman Anodisc 47; 0.2 μm pore size); approximately 0.5 mL of the solution were utilized per film. After allowing the solvent to evaporate for 1 h, the discs were affixed onto a stationary phase (3M clear packing tape), and placed in a 1 mol/L NaOH solution for 1 h to allow the template to dissolve completely. The films were rinsed three times with deionized water, and dried briefly in a vacuum oven at 90-100 ^{o}C. The samples were cut into small portions (pie pieces, 1 cm length) to fit as many as possible samples on the sample holder. The samples were placed into a sputterer (Denton Vacuum Inc., Desk II), and 0.4 nm of Au was sputtered onto the films. The samples were then placed in a scanning electron microscope (Hitachi 2500 Delta), and the pictures were obtained digitally.

5.4. References

1. Landfester, K.; Montenegro, R.; Scherf, U.; Guntner, R.; Asawapirom, U.; Patil, S.; Neher, D.; Kietzke, T., *Adv. Mater.* **2002,** *14*, 651.

2. Kulbaba, K.; Cheng, A.; Bartole, A.; Greenberg, S.; Resendes, R.; Coombs, N.; Safa-Sefat, A.; Greedan, J. E.; Stover, H. D. H.; Ozin, G. A.; Manners, I., *J. Am. Chem. Soc.* **2002,** *124*, 12522.

3. Raez, J.; Manners, I.; Winnik, M. A., *J. Am. Chem. Soc.* **2002,** *124*, 10381.

4. Grimsdale, A. C.; Bauer, R.; Weil, T.; Tehebotareva, N.; Wu, J. S.; Watson, M., *Synthesis* **2002**, 1229.

5. Wiesler, U. M.; Weil, T.; Mullen, K., *Top. Curr. Chem.* **2001,** *121*, 1.

6. Morgenroth, F.; Kubel, C.; Mullen, K., *J. Mater. Chem.* **1997,** *7*, 1207.

7. Moon, J. H.; Swager, T. M., *Macromolecules* **2002,** *35*, 6086.

8. Sapp, S. A.; Mitchell, D. T.; Martin, C. R., *Chem. Mater.* **1999,** *11*, 1183.

9. Cepak, V. M.; Hulteen, J. C.; G., C.; Jirage, K. B.; Lakshmi, B. B.; Fisher, E. R.; Martin, C. R.; Yoneyama, H., *Chem. Mater.* **1997,** *7*, 1065.

10. Martin, C. R., *Acc. Chem. Res.* **1995,** *28*, 61.

11. Martin, C. R., *Chem. Mater.* **1996,** *8*, 1739.

12. Cai, Z. H.; Martin, C. R., *J. Am. Chem. Soc.* **1989,** *111*, 4138.

13. Kros, A.; Van Hovell, W. F. M.; Sommerdijk, N. A. J. M.; Nolte, R. J. M., *Adv. Mater.* **2001,** *13*, 1555.

14. Wudl, F., *Mater. Chem.* **2002**, 1959.

15. Yu, G.; Gao, J.; Hummelen, J. C.; Wudl, F.; Heeger, A. J., *Science* **1995,** *270*, 1789.

16. Friend, R. H., *Phys. Scr.* **1996,** *T66*, 9.

17. Granstrom, M.; Petritsch, K.; Arias, A. C.; Lux, A.; Andersson, M. R.; Friend, R. H., *Nature* **1998,** *395*, 257.

18. Muller, M.; Zentel, R.; Maka, T.; Romanov, S. G.; Torres, C. M. S., *Adv. Mater.* **2000,** *12*, 1499.

19. Deutsch, M.; Vlasov, Y. A.; Norris, D. J., *Adv. Mater.* **2000,** *12*, 1176.

20. Samori, P.; Francke, V.; Mangel, T.; Mullen, K.; Rabe, J. P., *Opt. Mater.* **1998,** *9*, 390.

21. Samori, P.; Francke, V.; Mullen, K.; Rabe, J. P., *Chem. Eur. J.* **1999,** *5*, 2312.

22. Samori, P.; Severin, N.; Mullen, K.; Rabe, J. P., *Adv. Mater.* **2000,** *12*, 579.

23. Perahia, D.; Traiphol, R.; Bunz, U. H. F., *Macromolecules* **2001,** *34*, 151.

24. Altmann, M.; Bunz, U. H. F., *Angew. Chem.* **1995,** *34*, 569.

25. Bunz, U. H. F., *Chem. Rev.* **2000,** *100*, 1605.

26. Bunz, U. H. F., *Acc. Chem. Res.* **2001,** *34*, 998.

27. Kloppenburg, L.; Jones, D.; Bunz, U. H. F., *J. Am. Chem. Soc.* **1998,** *120*, 7973.

28. Kloppenburg, L.; Jones, D.; Bunz, U. H. F., *Macromolecules* **1999,** *32*, 4194.

29. Erdogan, B.; Wilson, J. N.; Bunz, U. H. F., *Macromolecules* **2002,** *35*, 7863.

30. Wilson, J. N.; Waybright, S. M.; McAlpine, K.; Bunz, U. H. F., *Macromolecules* **2002,** *35*, 3799.

31. Wilson, J. N.; Windscheif, P. M.; Evans, U.; Myrick, M. L.; Bunz, U. H. F., *Macromolecules* **2002,** *35*, 8681.

32. Bangcuyo, C. G.; Evans, U.; Myrick, M. L.; Bunz, U. H. F., *Macromolecules* **2001,** *34*, 7592.

33. Halkyard, C. E.; Rampey, M. E.; Kloppenburg, L.; Studer-Martinez, S. L.; Bunz, U. H. F., *Macromolecules* **1998,** *31*, 8655.

34. Whatman Claims a pore size of 0.2 μm. Our observations of blank discs revealed that only one side displayed pores of 0.2 μm. The opposite side of clearly displays pores of greater size (0.3 - 0.35 μm), but they are less numerous. Obviously, a fusion of channels must take place during the anodization process, which is in fact revealed by the observed geometries of the polymer structures.

35. Ricks, H.; Choudry, U. H.; Marshall, A. J.; Bunz, U. H. F., *Macromolecules* **2003,** *36*, 1424.

CHAPTER 6

PERALKYNYLATED BENZOTHIADIAZOLES AND ITS *O*-PHENYLENEDIAMINE DERIVATIVE

6.1. Introduction

With the completion of the quinoxaline containing copolymers, we decided to take a molecular approach to alkynes and create some “carbon rich” materials. ‘Carbon rich’ defines an exciting class of symmetrical and aesthetically pleasing compounds. Most, but not all of these carbon rich compounds contain multiple alkyne units. A specific class of carbon rich compounds is that of the peralkynylated annulenes and peralkynylated aromatic hydrocarbons (Figure 6.1). A prime example of this subclass is hexaethynylbenzene described by Vollhardt in 1986.[1-3] Other representatives are the peralkynylated thiophenes[4] and some of their cyclooligomers,[5] the peralkynylated dehydroannulenes,[6-9] the peralkynylcyclopentadienyl radicals,[10] as well as the tetraethynylcyclobutadiene complexes[11, 12] and peralkynylcymantrenes.[13, 14]

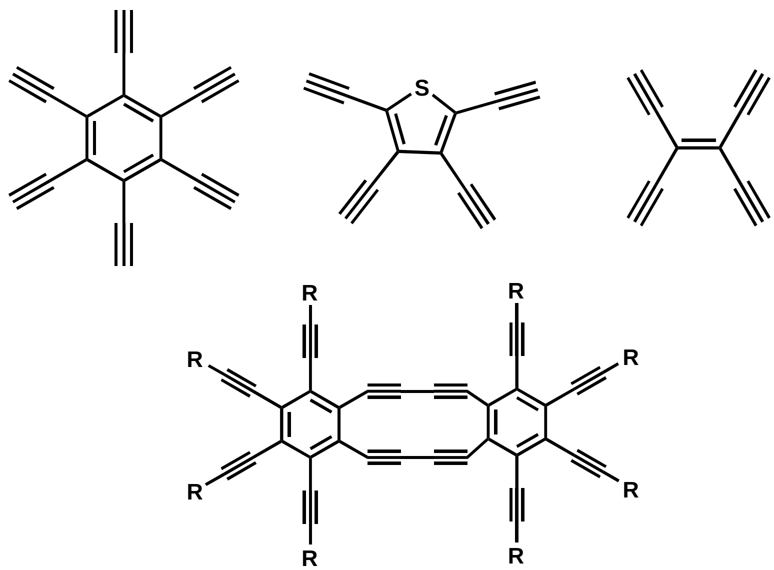

Figure 6.1. Some examples of known carbon rich molecules.

With the exception of the thiophene case, peralkynylated heterocycles are sparse. Pentaethynylpyridine, tetraethylnylpyrazine, and similar molecules have never been made, perhaps because their precursors, the perhalogenated heterocycles, are difficult to come by. An exception to this rule is tetrabromobenzo[2,1,3]thiadiazole (**38**) that can be obtained by direct bromination of benzothiadiazole with Iron powder as a catalyst[15] (Scheme 6.1). Within this chapter, we will discuss the synthesis of the peralkynylated benzothiadiazoles and its optical properties as well as the peralkynylated *o*-phenylenediamine derivative.

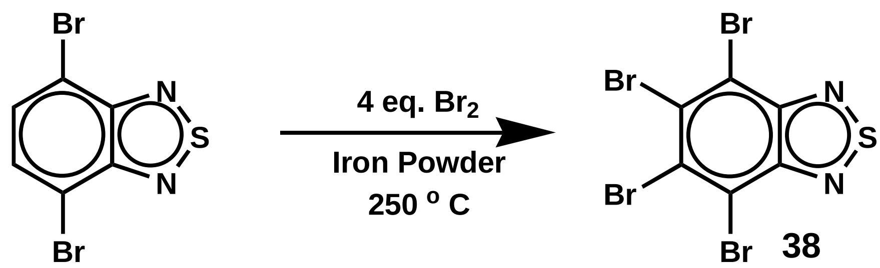

38

43%

Scheme 6.1. The synthesis of the tetrabromobenzothiadiazole **38** can be used to synthesize multigram quantities. The reaction is extremely exothermic and can retain its temperature > 275 oC for hours.

6.2. Results and Discussion

The tetrahalide **38** was available in 10 g-quantities, stable, and sufficiently soluble to perform further chemistry. We decided to use the dibromobenzothiadiazole because of its availability in large gram quantities, and we would have to put less work into the reaction since two bromides already occupy the ring. This reaction involves the addition of molecular bromine in molten dibromobenzothiadiazole with a catalytic amount of Iron powder at temperatures above 250 ^{o}C. One must take caution while performing this reaction since it is extremely exothermic and sustain its temperature above 275 ^{o}C for several hours.

Reaction of the tetrabromide **38** with terminal alkynes under Heck–Cassar–Sonogashira– Hagihara conditions[16] led to the smooth formation of the desired tetraethynylbenzothiadiazoles **39** in 41–91% yields (Scheme 6.2). These reactions were performed in a pressure tube under inert atmosphere at 120 ^{o}C for 16 hours. Isolated alkynes **39** are yellow crystalline with the exception of the phenyl substituted **39d**, which is an orange solid. Taking the tetra(trimethylsilylethynyl)benzothiadiazoles, we tried to remove the aliphatic periphery and wanted to obtain the "naked" tetraethynylbenzothiadiazole. However, after deprotection and isolation, the product was a black color that was undeterminable by NMR. The "naked" alkynylbenzothiadiazole was not investigated further.

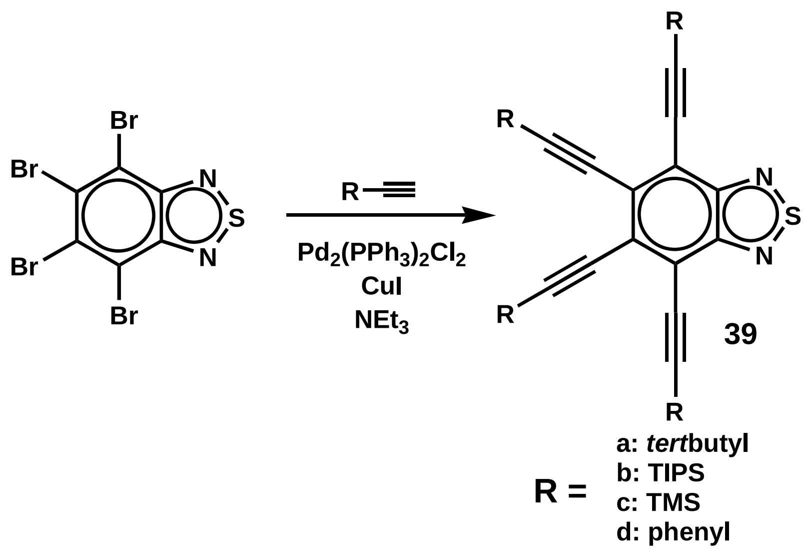

Scheme 6.2. Synthesis, yields, and substituent key for the tetrakisalkynylatedbenzothiadiazoles.

The arenes **39a–c** are greenish fluorescent in the solid state and strongly blue (**39c**) to yellowish orange (**39d**) fluorescent in solution. Figure 6.2 and 6.3 shows the absorption and emission spectra of **39**. The UV-Vis spectra of **39a–c** are similar to each other and show a λ_{max} at 422– 428 nm. The tetraethynyl **39d** shows a bathochromically shifted λ_{max} at 462 nm giving testimony to the enhanced conjugation of the central chromophore into the phenylacetylene substituents. In emission, the differences are more pronounced (Figure 6.3) and **39d** experiences a 72 nm red shift in emission when compared to **39c**. But even in the cases of **39a–c** where the absorption spectra are almost superimposable, the emission maxima range from 473–496 nm. Addition of trifluoroacetic acid led to an almost complete quenching of the fluorescence. In thin solid films, the fluorescence is slightly blue shifted when compared to solution. This effect is particularly pronounced in the case of **39d** where aggregate formation[17, 18] leads to blue shifted emission in the solid state. Interestingly enough, the absorption spectra of **39** in the solid state are similar to those in solution.

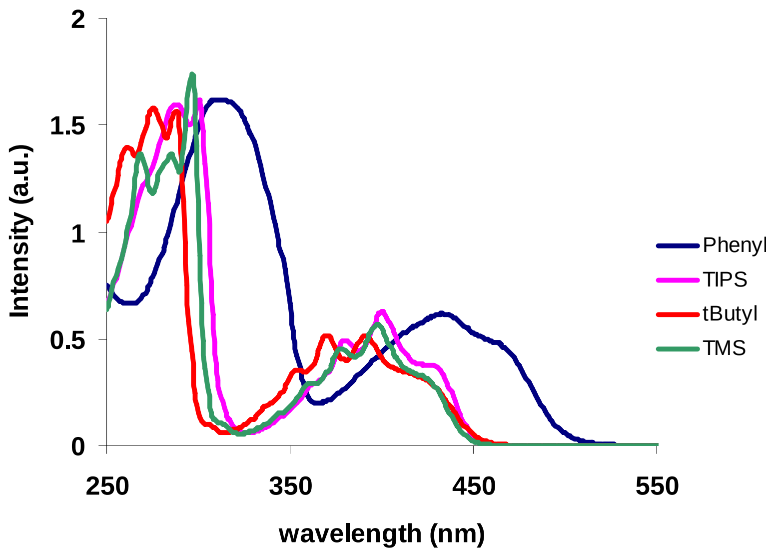

Figure 6.2. UV-Vis spectra of **39a**, **39**, and **39d** in $CHCl_3$ solution

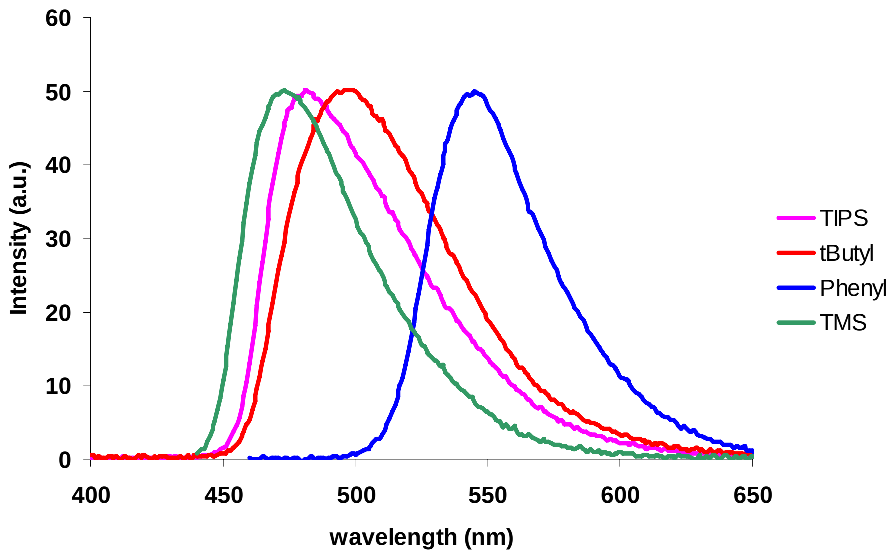

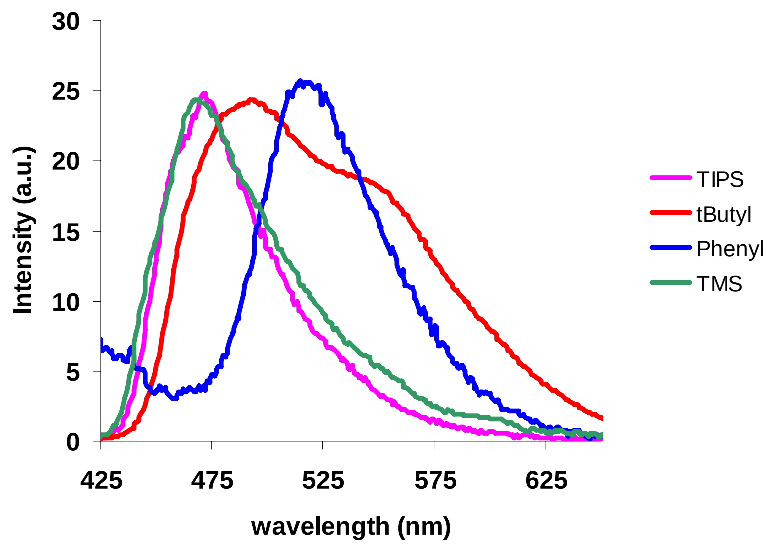

Figure 6.3. Top: Emission spectra of **39a–d** in $CHCl_3$ solution. Bottom: Emission spectra of **39a**, **39c**, and **39d** in thin films.

The ^{1}H and ^{13}C NMR spectra of **39** are simple due to the high symmetry. The ^{13}C NMR spectrum of **39a** is discussed here. At δ = 153.5, 129.1, and 118.6 ppm the resonances for the benzothiadiazole nucleus are recorded, while the four alkyne resonances appear at δ = 110.2, 109.34, 77.23, and 75.02 ppm. The *tert*-butyl groups show resonances at δ = 31.16, 31.12, 28.83, and 28.76 ppm. The peaks with the highest intensity (δ = 31.16, 31.12 ppm) can be attributed to the methyl resonances. Due to the esthetic appeal of the peralkynylated perimeter, we performed a crystal structure analysis of the derivative **39a** which crystallizes from CH_2Cl_2–MeOH solution. A suitable specimen could be obtained. Figure 6.3 shows an ORTEP of **39a**. The aromatic core is planar and the six carbon atoms C-25, C-25, C-5, C-2, C-7, and C-8 are collinear, while the two inner alkynes are somewhat bent (Figure 6.3). According to quantum chemical calculations the slight bent of **39a** is due to a crystal packing effect and not an innate structural property of **39a**.[19]

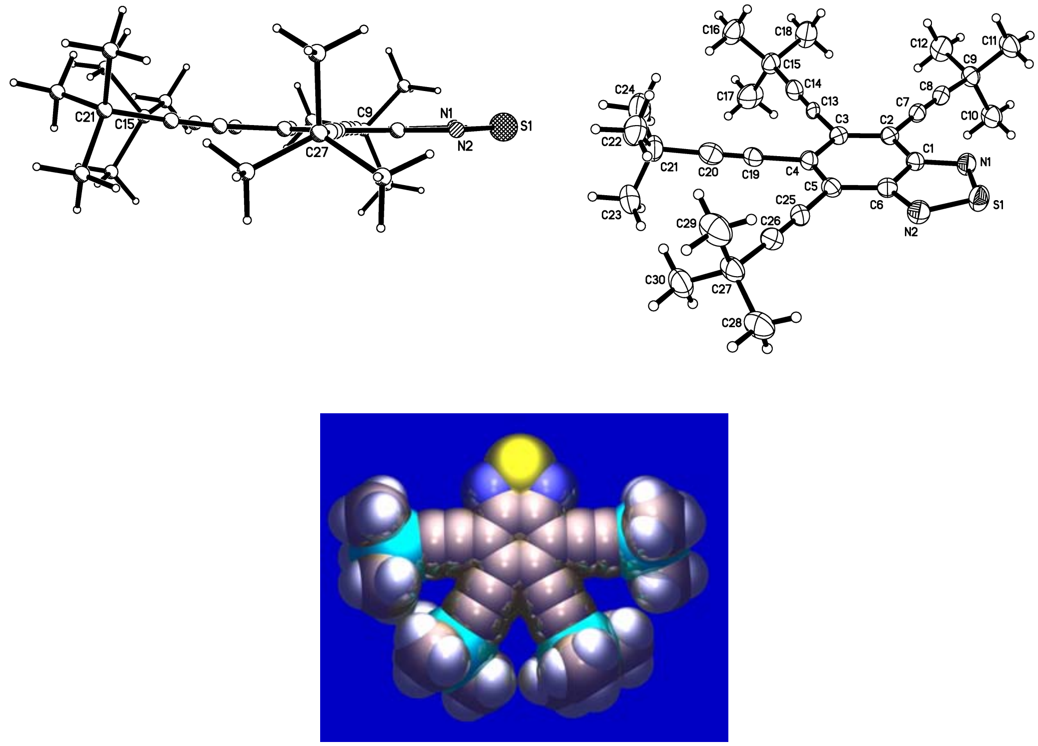

Figure 6.4. a) ORTEP of **39a**. Bond lengths and bond angles of **39a** are in excellent agreement with literature described values for other peralkynylated perimeters. b) Side view of a molecule of **39c** in the solid state. The sulfur atom is pointed to the right. The molecule is almost flat and only the two inner alkyne legs are slightly outward bent. Bottom: Space filling model of the tetraalkynylatedbenzothiadiazole.

We took the synthesis a step further and produced the peralkynylated phenylenediamine derivative **40** of the tetraalkynylbenzothiadiazole **39**. The phenylenediamine has become a versatile building block in which we used to build larger peralkynylated core molecules shown in the next chapter. The formation of the peralkynylated phenylenediamine derivatives **40** were achieved by reduction with lithium aluminum hydride in dry THF at ambient temperatures.

The tetra(trimethylsilylethynyl)benzothiadiazoles were an unsuitable molecule in this endeavor due to the fact that the TMS groups were sensitive to the reduction reaction. As a result, we decided to use the benzothiadiazoles whose alkynylated outer periphery included the *tert*-butyl groups and the TIPS groups (Scheme 6.3).

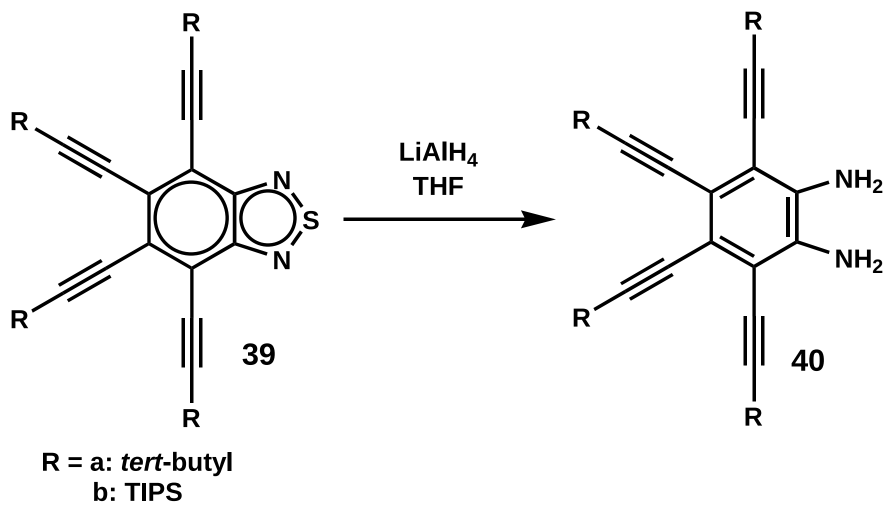

Scheme 6.3. Reduction of the benzothiadiazoles with LiAlH4 yields the o-phenylenediamine in quantitative yields.

The tetraalkynyl-o-phenylenediamine **40** can be stable for extended periods of time in air and ambient temperature but will slowly oxidize into a brownish-black color. This is due to the fact that the free amines form a carbonate salt with atmospheric carbon dioxide and water. Reduction of the benzothiadiazoles **39** produced a red crystalline solid in near quantitative yields. We were able to grow a suitable specimen for crystal structure analysis by co-crystallizing the phenylenediamine with hexafluorobenzene and slow evaporation from CH_2Cl_2 (Figure 6.5). The phenylenediamine crystallized well with hexafluorobenzene because of its inherent electron rich core forms a donor acceptor type relationship with the electron deficient hexafluorobenzene. Consequently, we try to produce the “naked” tetraalkynylphenylenediamine, however, it suffered drawbacks similar to the ones observed in the benzothiadiazoles. The product was a black oil and was undeterminable by NMR.

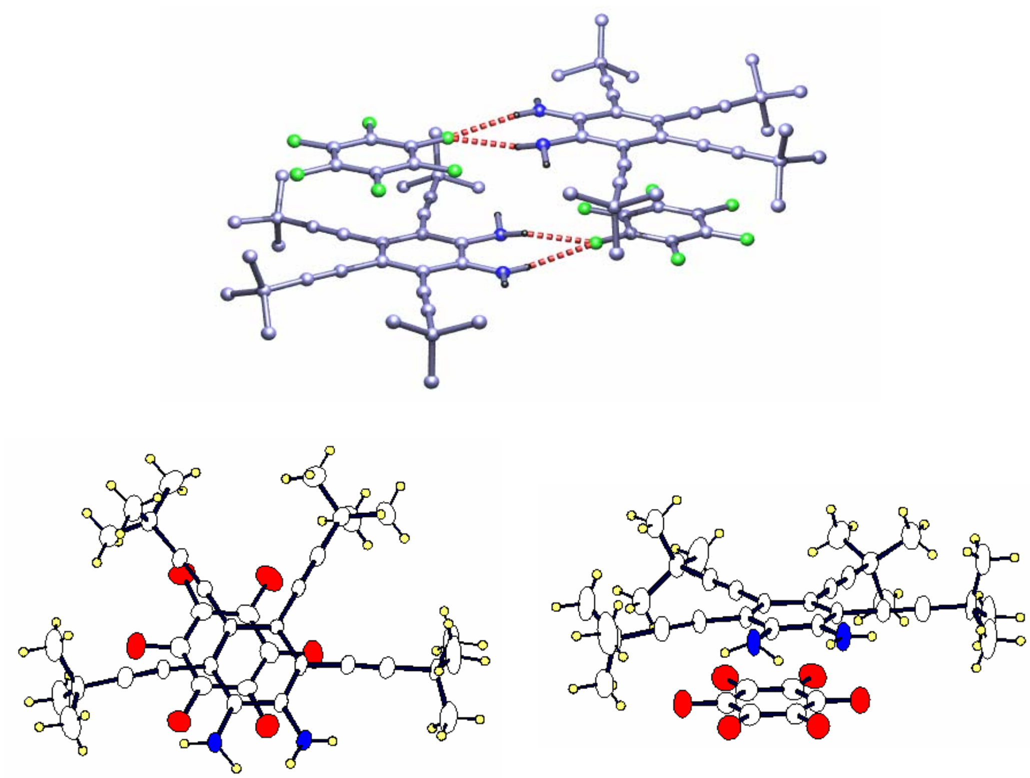

Figure 6.5. Crystal structure of the tetraalkynyl-o-phenylenediamine **40a** co-crystallized with hexafluorobenzene. We can see in the top picture that there is some hydrogen bonding between two hydrogens from the diamine and a fluoride atom.

Conclusion

In conclusion, we have demonstrated the synthesis of a series of peralkynylated benzothiadiazoles **39a-d** in a one step method starting from the easily available tetrabromobenzothiadiazole **38**. This synthesis mimics Vollhardt's and Whitesides' original approach for the synthesis of peralkynylated p-perimeters. These modules are interesting precursors for the synthesis of tetraalkynylphenylenediamines and their bis-diazonium salts. The synthesis of the phenylenediamine also proved viable and easily accessible by reducing the corresponding benzothiadiazoles with LiAlH4. In the future, we hope to investigate the phase behavior of **39a–d** and their complexation chemistry with transition metals. The efficient and well-tunable solid-state emission of **39** makes them potentially useful as *n*-semiconductors in thin film transistors, photovoltaic cells, and light emitting diodes.

6.3. Experimental

General Preparation to the Tetraalkynylated Benzothiadiazoles 39. To a flame dried 250 mL pressure tube, 3,4,5,6-tetrabromo[2,1,3]benzothiadiazoles **38**, $Pd(PPh_3)_2Cl_2$ (1 mol%), CuI (1 mol%), and Et_3N (30 mL) were added and purged with N_2 for 1 min. Acetylene (6 mol equiv) was carefully added via syringe, and the reaction was stirred overnight at 120 °C. The reaction was poured into a mixture of CH_2Cl_2 (100 mL) and water (100 mL). The organic layer was washed with water (3 · 100 mL) followed by 10% NH_4OH (75 mL). The aqueous layer was washed with CH_2Cl_2 (3 · 50 mL), and the organic layers were combined. The organic layer was dried over anhydrous Na_2SO_4, and the solvent was evaporated.

3,4,5,6-tetra(*tert*-butylethynyl)-2,1,3-benzothiadiazole 39a. Prepared from

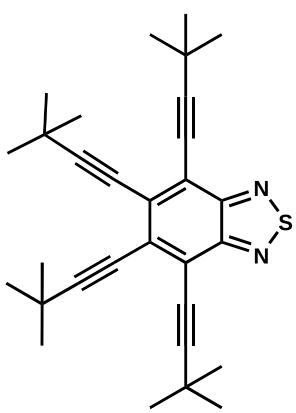

compound **38** (8.13 g, 17.99 mmol). Purification by column chromatography with hexanes–CH_2Cl_2 (1:1) followed by crystallization in MeOH–CH_2Cl_2 furnished yellow crystals (7.48 g, 91%); MP: 157 °C. IR (neat): ν 2968, 2925, 2896, 2866, 2358, 2341, 2219, 1541, 1502, 1458, 1388, 1361, 1319, 1294, 1269, 1249, 1203, 1145, 1103, 1029, 879, 829. ^{1}H NMR ($CDCl_3$): δ = 1.42 (s, 18 H), 1.40 (s, 18 H). ^{13}C NMR ($CDCl_3$): δ = 153.50, 129.08, 118.59, 110.19, 109.34, 77.23, 75.02, 31.16, 31.12, 28.83, 28.76. MS ($C_{30}H_{36}N_2S$): m/z = 456. UV-Vis (absorption, $CHCl_3$): λ_{max} = 425, 391, 370, 354, 288, 275, 261 nm. UV-Vis (absorption, thin film): λ_{max}

= 422, 390, 353, 285, 273, 259 nm. UV-Vis (emission, $CHCl_3$): λ_{max} = 496 nm. UV-Vis (emission, thin film): λ_{max} = 480, 540 nm.

3,4,5,6-tetra(triisopropylsilylethynyl)-2,1,3-benzothiadiazole 39b. Prepared

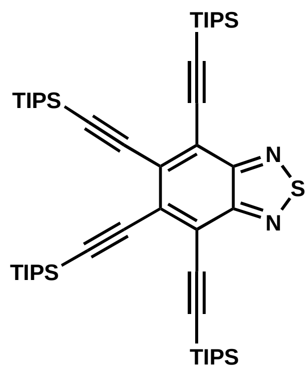

from compound **38** (5.00 g, 11.1 mmol). Purification by column chromatography with hexanes–CH_2Cl_2 (7:3) followed by crystallization in EtOH furnished yellow crystals (5.00 g, 53%); MP: 232–235 °C. IR (neat): ν = 2943, 2889, 2864, 2758, 2715, 2148, 1533, 1490, 1461, 1452, 1382, 1365, 1352, 1311, 1276, 1234, 1161, 1072, 1018, 997, 972, 919, 883, 840. ^{1}H NMR ($CDCl_3$): δ = 1.17–1.13 (m, 84 H). ^{13}C NMR ($CDCl_3$): δ = 154.45, 127.42, 120.56, 106.83, 104.17, 102.67, 101.62, 19.03, 18.87, 11.99, 11.64. MS ($C_{50}H_{84}N_2SSi_4$): *m/z* = 856. UV-Vis (absorption, CHCl3): λ_{max} = 428, 100, 380, 358, 301, 289 nm. UV-Vis (absorption, thin film): λ_{max} = 429, 401, 381, 362, 288, 271 nm. UV-Vis (emission, $CHCl_3$): λ_{max} = 482 nm. UV-Vis (emission, thin film): λ_{max} = 470 nm.

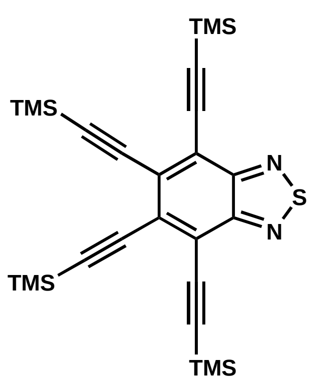

3,4,5,6-tetra(trimethylsilylethynyl)-2,1,3-benzothiadiazole 39c. Prepared from compound **38** (1.07 g, 2.36 mmol). Purification by column chromatography with hexanes–CH_2Cl_2 (13:7) followed by crystallization in MeOH–CH_2Cl_2 furnished yellow crystals (0.490 g, 40%); MP: 133 °C. IR (neat): ν = 2958, 2898, 2358, 2339, 2156, 1456, 1355, 1278, 1247, 975, 842. ^{1}H NMR ($CDCl_3$): δ = 0.32 (s, 9 H), 0.30 (s, 9 H). ^{13}C NMR ($CDCl_3$): δ = 153.17, 129.13, 119.41, 108.60, 107.57, 100.76, 98.90, 0.12, 0.09. MS ($C_{26}H_{36}N_2SSi_4$): m/z = 520. UV-Vis (absorption, $CHCl_3$): λ_{max} = 422, 398, 378, 296, 285, 269 nm. UV-Vis (absorption, thin film): λ_{max} = 422, 397, 377, 359, 295, 282, 267 nm. UV-Vis (emission, CHCl3): λ_{max} 472 nm. UV-Vis (emission, thin film): λ_{max} = 469 nm

3,4,5,6-tetra(phenylethynyl)-2,1,3-benzothiadiazole 39d. Prepared from

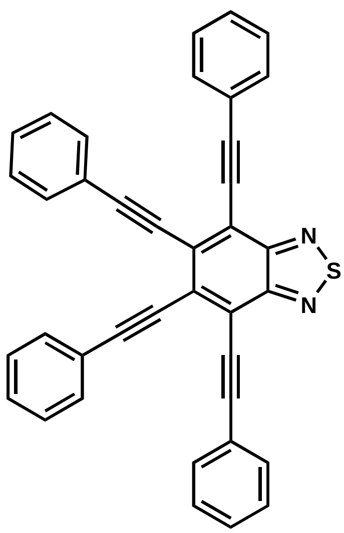

compound **38** (0.513 g, 1.14 mmol). Purification by column chromatography with hexanes–CH_2Cl_2 (13:7) furnished orange crystals (0.249 g, 41%). MP: 212 °C. IR (neat): ν = 3049, 2927, 862, 2208, 1953, 1890, 1814, 1755, 1598, 1494, 1442, 1390, 1317, 1186, 1070, 1024, 966, 916, 879, 840. ^{1}H NMR ($CDCl_3$): δ = 7.71 (s, 4 H), 7.66–7.65 (m, 8 H), 7.26–7.25 (m, 8 H). ^{13}C NMR ($CDCl_3$): δ = 153.29, 131.99, 131.81, 1219.15, 129.09, 128.97, 128.41, 128.35, 122.73, 122.55, 118.69, 102.03, 101.33, 87.18, 85.19. UV-Vis (absorption, $CHCl_3$): λ_{max} = 462, 433, 310 nm. UV-Vis (absorption, thin film): λ_{max} = 445, 422, 350, 321 nm. UV-Vis (emission, $CHCl_3$): λ_{max} = 547nm. UV-Vis (emission, thin film): λ_{max} = 519 nm.

General Procedure for the Tetraalkynylated o-Phenylenediamines 40. A flame dried 250 mL round bottom schlenk flask was charged with the corresponding 3,4,5,6-tetraalkynylated[2,1,3]benzothiadiazoles **39**. Dry THF (150 mL) was added to the flask. While slowly running nitrogen over the stirring solution, LiAlH4 (4 equivalents) was added portion-wise over a period of 30 minutes. The reaction was allowed to stir at room temperature for 4 hrs. The reaction was poured into a 10 % solution of aqueous NH_4Cl, and extracted with diethyl ether (3 x 100 mL). The organic layer was dried over anhydrous Na_2SO_4, and the solvent was evaporated.

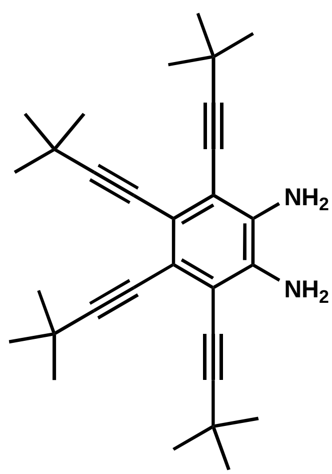

3,4,5,6-tetra(*tert*-butylethynyl)-o-phenylenediamine 40a. Prepared from compound **39a** (1.00 g, 2.18 mmol). No further purification is needed after workup as outlined in general procedure produces a red solid (0.760 g, 81 %). MP: 167 °C (dec.). ^{1}H NMR ($CDCl_3$): δ = 3.34 (bs, 4 H), 1.42 (s, 18 H), 1.40 (s, 18 H). ^{13}C NMR ($CDCl_3$): δ = 136.89, 119.38, 113.01, 109.50, 108.97, 77.37, 75.46, 31.25, 31.02, 28.76, 28.52.

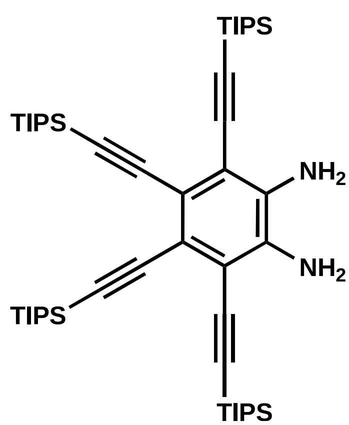

3,4,5,6-tetra(triisopropylsilylethynyl)-2,1,3-benzothiadiazole 40b. Prepared from compound **39b** (1.00 g, 1.16 mmol). No further purification is needed after workup as outlined in general procedure furnishes a red solid (0.706 g, 73 %). MP: 185 °C (dec.). ^{1}H NMR ($CDCl_3$): δ = 3.22 (bs, 4H), 1.17–

1.13 (m, 84 H). ^{13}C NMR ($CDCl_3$): δ = 136.45, 118.97, 112.69, 106.98, 104.47, 102.25, 101.48, 19.14, 18.72, 12.16, 11.42.

6.4. References

1. Diercks, R.; Armstrong, J. C.; Boese, R.; Vollhardt, K. P. C., *Angew. Chem., Int. Ed. Engl.* **1986**, *25*, 268.

2. Boese, R.; Green, J. R.; Mittendorf, J.; Mohler, D. L.; Vollhardt, K. P. C., *Angew. Chem., Int. Ed. Engl.* **1992**, *31*, 1643.

3. Tovar, J. D.; Nux, N.; Jarrosson, T.; Khan, S. I.; Rubin, Y., *J. Org. Chem* **1997**, *62*, 3432.

4. Neenan, T. X.; Whitesides, G. M., *J. Org. Chem* **1988**, *53*, 2489.

5. Zhang, D. M.; Tessier, C. A.; Youngs, W. J., *Chem. Mater.* **1999**, *11*, 3050.

6. Diederich, F., *Nature (London)* **1994**, *369*, 199.

7. Anthony, J.; Knobler, C. B.; Diederich, F., *Angew. Chem., Int. Ed. Engl.* **1993**, *32*, 406.

8. Diederich, F., *Chem. Commun.* **2001**, 219.

9. Diederich, F.; Rubin, Y., *Angew. Chem., Int. Ed. Engl.* **1992**, *31*, 1101.

10. Jux, N.; Holczer, K.; Rubin, Y., *Angew. Chem., Int. Ed. Engl.* **1996**, *35*, 1986.

11. Bunz, U. H. F., *Top. Curr. Chem.* **1999**, *201*, 131.

12. Bunz, U. H. F.; Rubin, Y.; Tobe, Y., *Chem. Soc. Rev.* **1999**, *28*, 107.

13. Bunz, U. H. F.; Enkelmann, V., *Organometallics* **1994**, *13*, 3823.

14. Bunz, U. H. F.; Enkelmann, V.; Rader, J., *Organometallics* **1993**, *12*, 4756.

15. Bublitz, D. E., *J. Heterocycl. Chem.* **1972**, *9*, 539.

16. Bunz, U. H. F., *Chem. Rev.* **2000**, *100*, 1605.

17. Koren, A. B.; Curtis, M. D.; Francis, A. H.; Kampf, J. W., *J. Am. Chem. Soc.* **2003**, *125*, 5040.

18. Koren, A. B.; Curtis, M. D.; Kampf, J. W., *Chem. Mater.* **2000**, *12*, 1519.

19. Molecular geometries were determined by AM1 and B3LYP utilizing the 6-31G** basis set. The calculations were carried out with Spartan '04 on a windows XP platform.

CHAPTER 7

PRECURSORS TO THE PERALKYNYLATED HETEROCYCLIC FUSED RING SYSTEMS

7.1. Introduction

To follow up on both the synthesis of the tetraalkynylated benzothiadiazoles and the quinoxaline based PAEs, we decided to broaden our synthetic approach to encompass the production of peralkynylated quinoxalines and other larger structures of heteroacenes. These peralkynylated acenes are a structurally fascinating and aesthetically pleasing class of "carbon rich" compounds.[1-13] These acenes, such as pentacene, are important for electronic applications that are used in photovoltaic cells and thin film transistors.[14-18] Pentacene shows excellent charge mobility in the crystalline state and it is easily processible and stable.[19-21] Higher acenes are theorized to possess similar properties, yet they de-aromatize and are very sensitive materials.[22, 23] However, Anthony has shown that the dialkynyl pentacenes contain interesting solid state electronic properties and are very stable.[24-34]

Peralkynylated acenes are relatively unknown. This phenomenon can be explained by use of molecular modeling. The alkynes that are in close proximity to each other create steric problems. These steric problems lead to significant distortion of the molecular core which is a similar to that observed for octaphenylnaphthalene by Pascal.[33-35] Thus, the conventional HCSH palladium catalyzed coupling would not work well because of steric repulsion.[36-38] Even if the peralkynylated adducts would form, the triple bonds would perform Bergman-like[39-45] reactions due to the relative proximity to each other. We have decided that staggering the alkynes with a nitrogen spacer in between rings would help to alleviate some of the steric strain. However, peralkynylated heteroacenes, with the exception of 2,4,6-triethynyl-1,3,5-triazine, remain unknown to date.[46-48] Within this chapter, we will discuss the synthesis of peralkynylated large heterocyclic fused ring systems and the fabrication of unsymmetrical heteroacenes.

7.2. Results and Discussion

Starting from the known Scheme 6.2, reaction with 3,3-dimethylbutyne in the presence of a palladium catalyst and copper iodide (HCSH conditions) produced the tetratheynylbenzothiadiazole **39** in excellent yield and purity as discussed in chapter 6. Different alkynes can be coupled to the tetrabromide to furnish certain derivatives. However, we decided to mainly use *tert*-butyl acetylenes. The reason why we have decided to use a *tert*-butyl end group was two fold: (1) the chemical stability of the *tert*-butyl group to the reductant, in our case $LiAlH_4$, ensured that we did not produce the “naked alkyne” and (2) the *tert*-butyl group meant the product would become crystalline, and the growth of single crystal specimens would be easier as opposed to a triisopropylsilyl group (TIPS). Reduction of the tetraalkynylbenzothiadiazole **39a,b** with lithium aluminum hydride gives the novel red tetraethynyl-o-phenylenediamine **40** in quantitative yields (Scheme 6.3). This o-phenylenediamine is stable for extended periods of time in air and at room temperatures but will slowly oxidize into a brownish black color. This diamine is a versatile and excellent precursor to peralkynylated heterocycles that we envisioned to create.

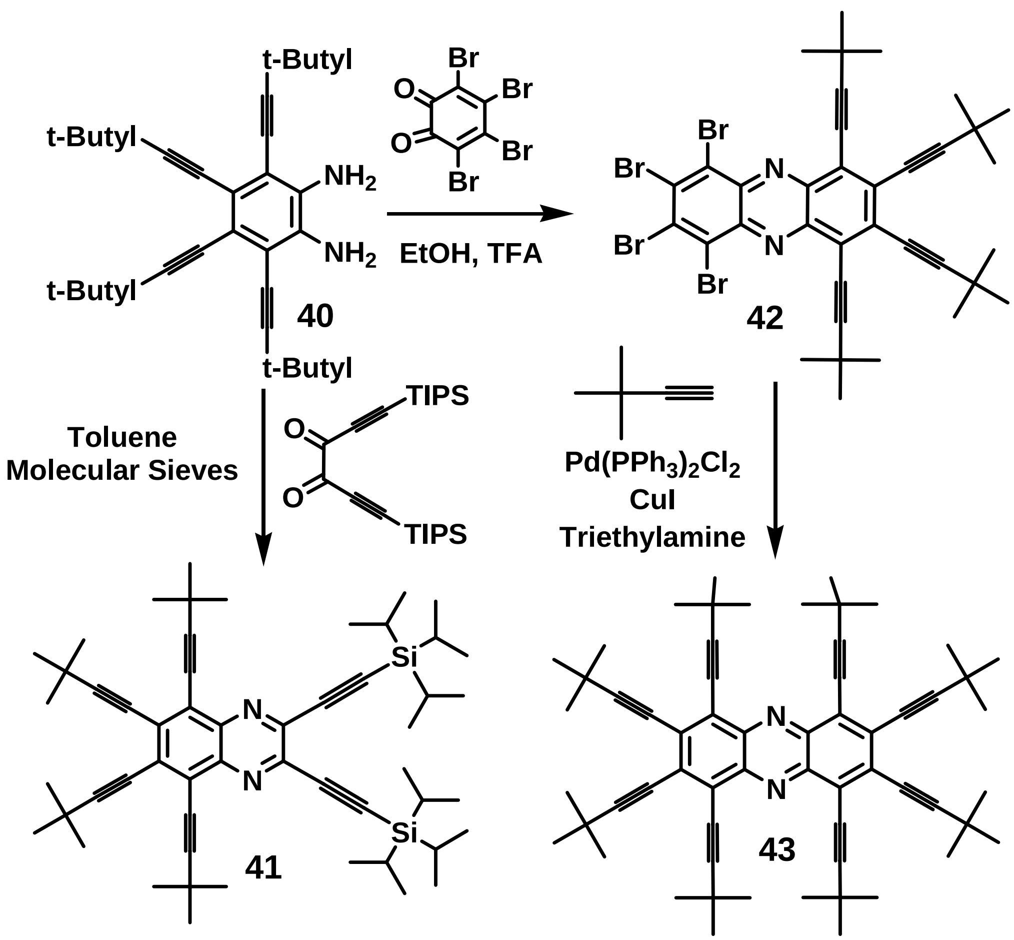

Scheme 7.1. Synthesis of the hexa-alkynylquinoxaline **41** (left) and octaalkynylphenazine **43** (right).

A condensation reaction with the use of molecular sieves in toluene at 80 ^{o}C of the tetralkynyl-o-phenylenediamine **40** with a diketone forms the hexa(alkynylated)quinoxaline **41** in good yields as stable yellow crystals (Scheme 7.1). The force that drives these reactions is the formation of the aromatic six-membered ring system. Even with **41** symmetry and NMR data showing that its unequivocal, we were unable to obtain a suitable specimen for crystal structure analysis of the quinoxaline due to the fact that the crystals were highly twinned.

We could also take a different approach and increase the core size by one pyrazine ring. This would be achieved by condensing o-bromanil with the starting o-phenylenediamine at 78 ^{o}C in ethanol (Scheme 6.1). It is noteworthy to add that a catalytic amount of acid was added to the ethanolic mixtures to increase the yields. The tetrabromophenazine precursor **42** subsequently underwent a HCSH coupling with *tert*-butylacetylene to furnish the octaalkynylphenazine **43** in a 23 % yield. Coupling the tetrabromophenazine **42** is facile because the molecule is electron deficient. The electron accepting nature of the molecule helps to facilitate the HCSH reaction.

We were able to obtain a suitable specimen for crystal structure analysis of the octaalkynylphenazine **43**. The *tert*-butyl substituents are surrounding the aromatic core, and the removal of the peri-hydrogens leads to a situation in which all of the substituents are well accommodated.

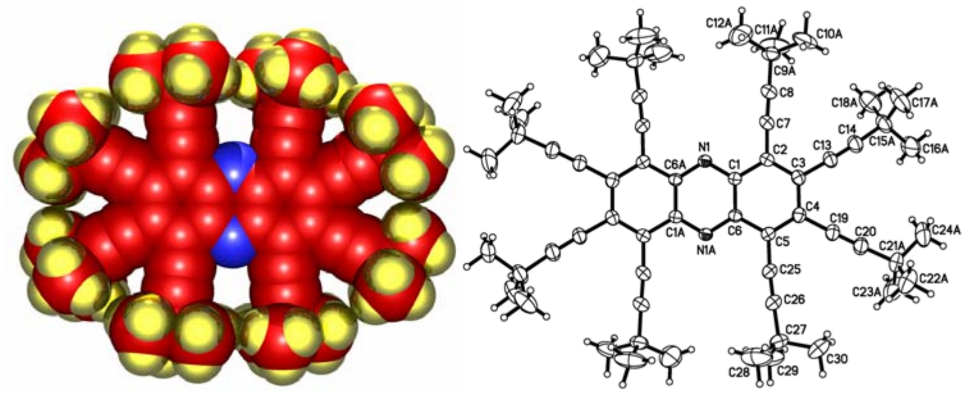

Figure 7.1. Crystal structure of the octaethynylphenazine **43** with *tert*-butyl substituents.

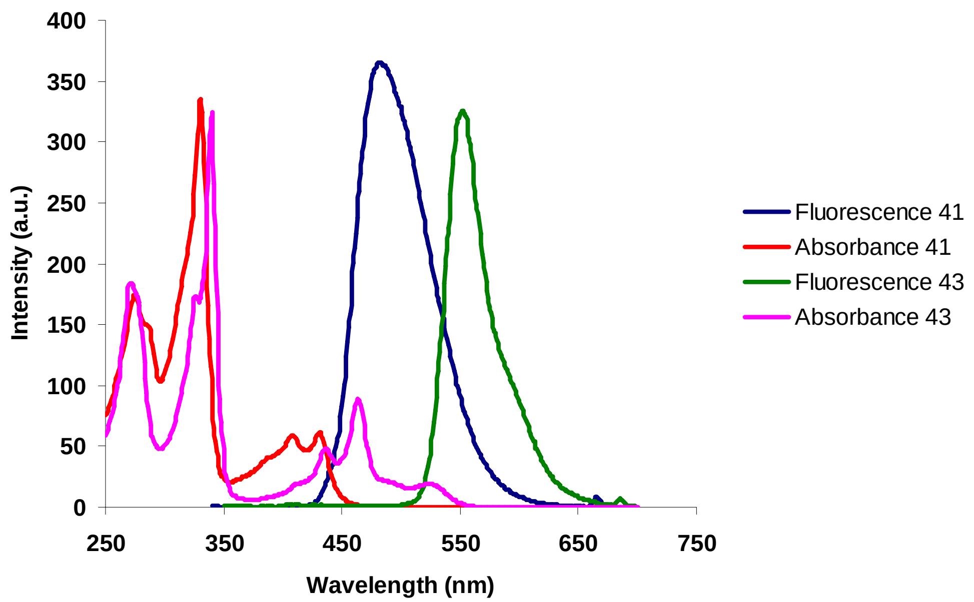

Figure 7.2. The UV-Vis and fluorescence spectra of **41** and **43** in chloroform. Going from the quinoxaline **41** to the phenazine **43** leads to a significant bathochromic shift in both absorption and emission.

By introducing the alkynes into compounds **41** and **43**, it will lead to a significant decrease in the band gap. Compared to the acenes, **41** and **43** with a analogous number of fused rings display a lower lying HOMOs and LUMOs which is a consequence of the electron withdrawing character of the incorporated nitrogens in the core and the alkyne substituents. The band gaps of **41** and **43** are predicted to be smaller than those of the corresponding acenes due to the chromophoric properties of the alkyne groups. However, the lower lying HOMOs should stabilize **41** and **43** with respect to oxidation compared to the respective acenes of similar size.

We wanted to extend the conjugation of the molecule not through the alkynes but through the core. It was decided that we could make symmetrical heteroacenes by a tetraaminobenzoquinone **49**.[49] Taking the commercially available p-chloranil **44**, our first attempts were to add amines on the ring by substitution with sodium azide failed. We took a different approach and performed a Gabriel reaction on the chloranil. This reaction involved a substitution reaction of the halogens by potassium phthalamide followed by a solvolysis with hydrazine (Scheme 7.2). We were able to place the phthalamides onto the chloranil in a quantitative yield (**45**). Our next step of hydrazinolysis was achieved to form the tetraaminobenzoquinone **46** in a 78 % yield. In the ^{13}C NMR spectrum of **46** shows two signals, d = 178.6 and 121.2 ppm, which is in excellent agreement with our structure. Treating the tetraaminobenzoquinone **46** with N-thionylaniline furnishes the dark red bis(thiadiazole)benzoquinone **48** in 50 % yield. We are currently working on the addition of TMS acetylide onto the quinone with a subsequent reduction would yield the alkynylated bis(benzothiadiazole) derivative **48**.[27-30] The tetraamine **49** would become a versatile building block for many peralkynylated molecules as well as a viable monomer for PAE synthesis. The alkynylated bis(benzothiadiazoles) **48** would be an attractive molecule as well to use in the formation of PPEs based on previous chapter work.

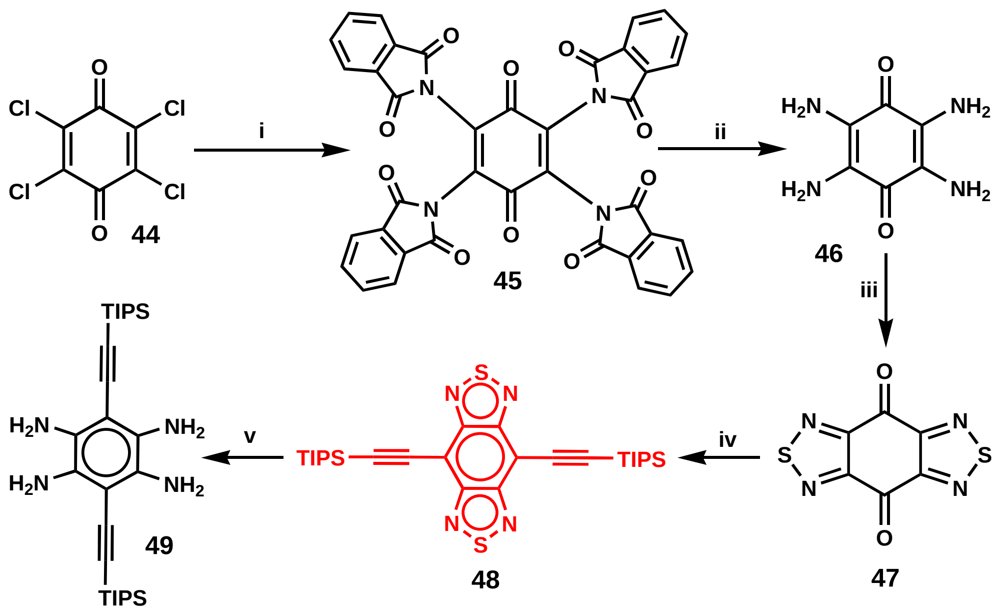

Scheme 7.2. Synthesis of the tetraamino-diethynylbenzene **49**. The molecule in read is the farthest that we have completed on this synthesis. (i) potassium phthalamide/ dry DMF/ 16 hrs; (ii) Hydrazine hydrate 51%/ H_2O/ 2hrs; (iii) thionyl chloride/ pyridine/ toluene/ reflux 12 hours; (iv) TMS acetylide/ dry THF followed by $SnCl_2$/ acetone/ acetic acid; (v) $LiAlH_4$/ dry THF.

We now diverted our attention to the 6,7-Bis-[(triisopropylsilanyl)-ethynyl]-4,9-bis-trimethylsilanylethynyl-2-thia-1,3-diaza-cyclopenta[b]naphthalene **60** (Scheme 7.3). This is a versatile molecule in that it would allow us to deprotect the thiadiazole portion, and let us create an unsymmetrical building block. This molecule contains 4 nitrogens in the fused ring system along with a sulfur. This molecule could be made starting from commercially available

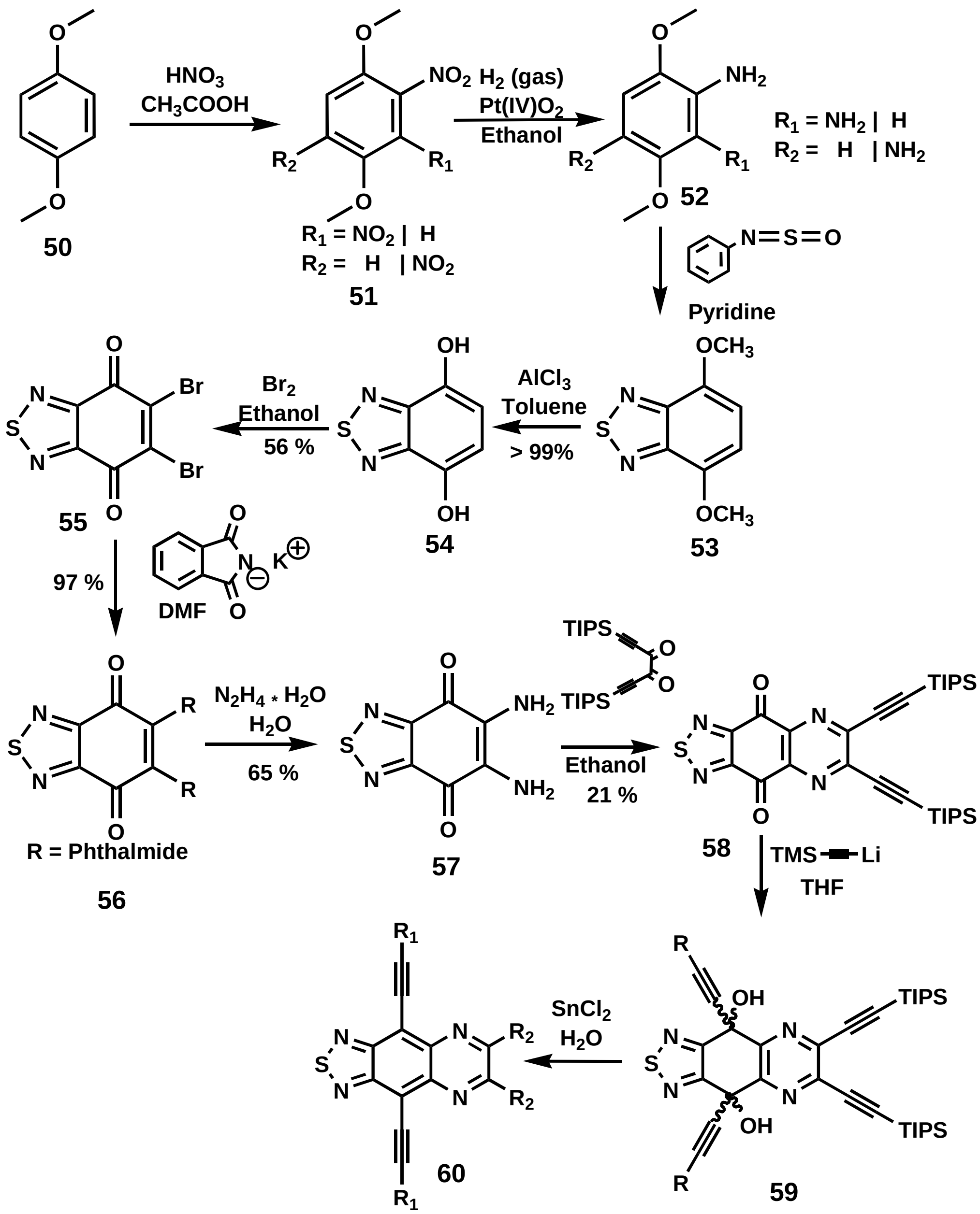

Scheme 7.3. Schematic for the step-wise synthesis of **60**.

1,4-dimethoxybenzene **50** in a linear eight step synthesis. 1,4-dimethoxybenzene **50** is nitrated with nitric acid/acetic acid mixture and heated to 60 oC for 8 hrs. This reaction produces a isomeric yellow solid in which the nitro groups are substituted in both the ortho and the para positions. From there, the dinitro-dimethoxybenzene **51** is hydrogenated in a Parr apparatus at 2 bar of hydrogen pressure with platinum dioxide as a catalyst.[50] This reaction also produces both the ortho and para substituted phenylenediamines **52**. In our next reaction, we can now separate the isomers and produce the desired products. Reaction of the isomeric mixture of the phenylenediamine **52** with N-thionylaniline furnishes the dimethoxybenzothidiazole **53** in 68 % yield.[51] Removal of the methyl groups happens via aluminum trichloride to give the benzothiadiazole-diol **54** in almost quantitative yield. Subsequent bromination of the diol leads to the oxidized and halogenated adduct **55**. A substitution reaction of the bromines with potassium phthalamide in dry DMF gives the phthalamido derivative **56**. Hydrazinolysis removes the phthalamides and the free amines are formed **57** as violet black solids.[52] Reaction of the diamine **57** with a diketone gives the thiadiazole-quinoxaline derivative **58** in 21 % yield. We have very recently reacted the thiadiazole quinoxaline **58** with a TMS acetylide, but the subsequent reduction with $SnCl_2$ in acetone furnishes the hexaalkynyl **60** in a meager 3 %.

Conclusion

In conclusion, we have demonstrated the series of peralkynylated heterocycles and their heteroacene precursors. From these precursors, we can design our synthesis of these larger heteroacenes to be either symmetrical or asymmetrical. These routes allow for flexible construction of each of the molecules. These modules are aesthetically pleasing and also interesting molecules in that could be used in the synthesis of some novel PAEs. Since these heteroacenes have similar structures to the acenes, we can surmise that they possess the same potential applications. With the introduction of nitrogen atoms in the molecular framework, these materials should make these materials potential n-semiconductors, make the materials more stable to oxidation, and prohibit their Diels-Alder reactions with atmospheric oxygen. Even though we have not achieved any of the larger heterocyclic structures, we are currently working towards the goal.

7.3. Experimental

All compounds have been made according to the literature procedure. The only compound that will be listed are the peralkynylated phenazines and the peralkynyl-naphthalenes. Compounds were checked by NMR to ensure purity. All other work is currently pending at this time.

5,6,7,8-Tetrakis-(3,3-dimethyl-but-1-ynyl)-2,3-bis-[(triisopropylsilanyl)-ethynyl]-quinoxaline 41.

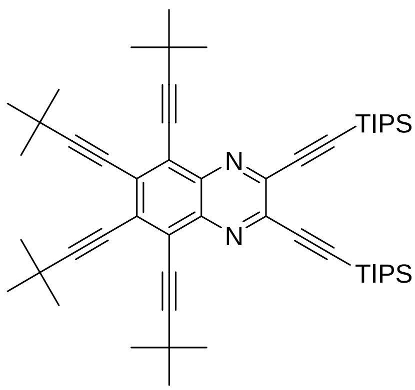

To a dry 50 mL round bottom flask, tetra(tert-butylethynyl)-o-phenylenediamine (0.204 g, 0.476 mmol), Bis(triisopropylsilylethynyl)dione (0.209 g, 0.500 mmol), toluene (10 mL), and an arbitrary amount of molecular sieves were added. The mixture was allowed to heat up to 80 °C for 4 hours. The reaction was then cooled, and the solvent was removed by reduced pressure to give a brownish black oil. Purification by column chromatography with eluent hexanes/CH_2Cl_2 (75:25) furnishes yellow crystals (0.143 g, 37 %). ^1H NMR ($CDCl_3$): δ = 1.43 (s, 18H), 1.37 (s, 18H) 1.18 (s, 42H). ^{13}C NMR ($CDCl_3$): δ = 141.53, 130.29, 126.08, 112.48, 108.94, 104.26, 99.52, 78.46, 75.23, 33.58, 29.16, 18.75, 11.89.

1,2,3,4-Tetrabromo-6,7,8,9-tetrakis-(3,3-dimethyl-but-1-ynyl)-phenazine

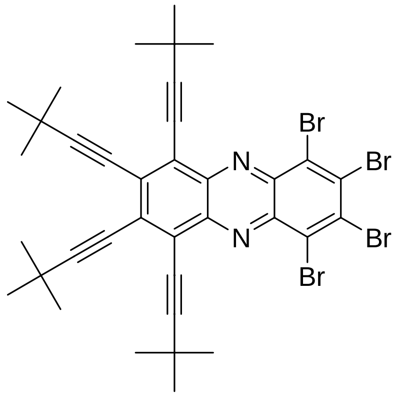

42. A 50 ml round bottom flask was charged with tetra(tert-butylethynyl)-o-phenylenediamine (0.274 g, 0.639 mmol), o-bromanil (0.273 g, 0.645 mmol), ethanol (10 mL), and 1 drop of H2SO4. The reaction was heated to reflux and stirred for 14 hrs. Filtration of a dark red solid followed by recrystallization from CH_3OH/CH_2Cl_2 yields a red crystalline solid (0.167 g, 32 %). ^1H NMR ($CDCl_3$): δ = 1.41 (s, 18H), 1.37 (s, 18H). ^{13}C NMR ($CDCl_3$): δ = 143.87, 139.54, 131.29, 127.99, 126.09, 112.62, 79.46, 75.09, 32.63, 28.35.

1,2,3,4,6,7,8,9-Octakis-(3,3-dimethyl-but-1-ynyl)-phenazine 43. To a flame

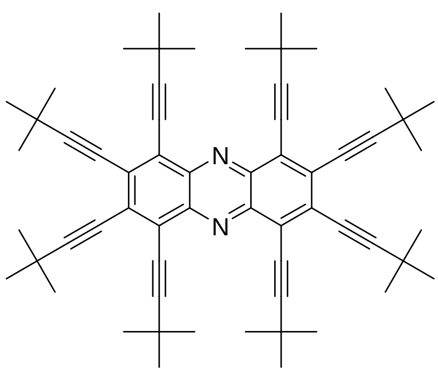

dried 100 mL pressure tube, tetrabromophenazine **42** (0.424 g, 0.519 mmol), $Pd(PPh_3)_2Cl_2$ (5 mol %), CuI (5 mol %), and triethylamine (7 mL) were added. The solution is flushed with nitrogen, and 3,3-dimethylbutyne (5 equivalents) was added via syringe. The reaction was sealed and allow to stir at 120 ^oC for 18 hrs. After heating, the reaction was allowed to stir and filtered. The solid was washed with diethyl ether. The organic layers were reduced to form a black oil. Purification by column chromatography with eluent hexanes/CH_2Cl_2 (80:20) furnished a red crystalline solid (0.098 g, 23 %). ^{1}H NMR ($CDCl_3$): δ = 1.46 (s, 36H), 1.32 (s, 36H). ^{13}C NMR ($CDCl_3$): δ = 141.82, 130.27, 124.71, 111.36, 110.00, 77.46, 75.92, 31.92, 30.84, 28.56, 28.31.

6,7-Bis-[(triisopropylsilanyl)-ethynyl]-2-thia-1,3-diaza-

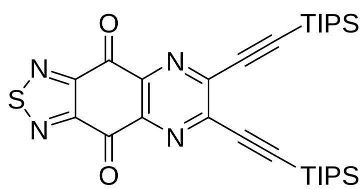

cyclopenta[b]naphthalene-4,9-dione 58. To a dry 50 mL round bottom flask, the diaminobenzothiadiazole **57** (0.209 g, 1.06 mmol), Bis(triisopropylsilylethynyl)dione (0.450 g, 1.07 mmol), toluene (15 mL), and an arbitrary amount of molecular sieves were added. This mixture was heated to 80 °C for 4 hours. The reaction was then allow to cool, and the solvent evaporated under reduced pressure to give a dark brown oil. Purification by column chromatography with eluent hexanes/ethyl acetate (85:15) yields a brown oil (0.130 g, 21 %). ^{1}H NMR ($CDCl_3$): δ = 1.17 (s, 42H). ^{13}C NMR ($CDCl_3$): δ = 172.50, 158.37, 142.38, 141.03, 109.64, 101.21, 18.34, 11.37.

6,7-Bis-[(triisopropylsilanyl)-ethynyl]-4,9-bis-trimethylsilanylethynyl-2-

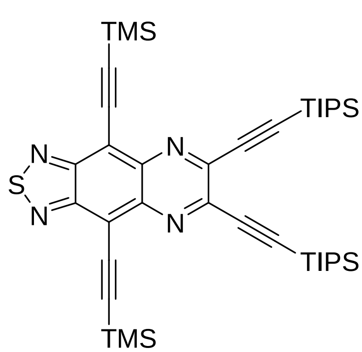

thia-1,3-diaza-cyclopenta[b]naphthalene 60. In a dry 100 mL round bottom schlenk flask, the naphthalene dione **58** (0.128 g, 0.221 mmol) and dry THF (10 mL) were added. A solution of TMS acetylide (2.1 equivalents) was added via syringe slowly at room temperature. The reaction was allowed to stir at room temperature for another 2 hrs. The solvent was evaporated under reduced pressure to give a dark brown oil. Purification by column chromatography with eluent hexanes/CH_2Cl_2 (80:20) yields a dark brown oil (4.00 mg, 3 %). ^{1}H NMR ($CDCl_3$): δ = 1.16 (s, 42H), 0.38 (s, 18H). ^{13}C NMR ($CDCl_3$): δ = 155.77, 146.68, 140.67, 102.255, 101.87, 98.32, 91.34, 19.06, 11.67, 1.32.

7.4. References

1. Boese, R.; Green, J. R.; Mittendorf, J.; Mohler, D. L.; Vollhardt, K. P. C., *Angew. Chem., Int. Ed. Engl.* **1992,** *31*, 1643.

2. Diercks, R.; Armstrong, J. C.; Boese, R.; Vollhardt, K. P. C., *Angew. Chem., Int. Ed. Engl.* **1986,** *25*, 268.

3. Neenan, T. X.; Callstrom, M. R.; Scarmoutzos, L. M.; Stewart, K. R.; Whitesides, G. M.; Howes, V. R., *Macromolecules* **1988,** *21*, 3525.

4. Bunz, U. H. F.; Rubin, Y.; Tobe, Y., *Chem. Soc. Rev.* **1999,** *28*, 107.

5. Bunz, U. H. F.; Enkelmann, V., *Angew. Chem.* **1993,** *32*, 1653.

6. Tovar, J. D.; Nux, N.; Jarrosson, T.; Khan, S. I.; Rubin, Y., *J. Org. Chem* **1997,** *62*, 3432.

7. Diederich, F.; Rubin, Y., *Angew. Chem., Int. Ed. Engl.* **1992,** *31*, 1101.

8. Gisselbrecht, J. P.; Moonen, N. N. P.; Boudon, C.; Nielsen, M. B.; Diederich, F.; Gross, M., *Eur. J. Org. Chem.* **2004**, 2959.

9. Diederich, F., *Chem. Commun.* **2001**, 219.

10. Martin, R. E.; Diederich, F., *Angew. Chem.* **1999,** *38*, 1350.

11. Tykwinski, R. R.; Diederich, F., *Liebigs, Ann. -Rec* **1997**, 649.

12. Anthony, J.; Boldi, A. M.; Rubin, Y.; Hobi, M.; Gramlich, V.; Knobler, C. B.; Seiler, P.; Diederich, F., *Helv. Chim. Acta.* **1995,** *78*, 13.

13. Tobe, Y.; Kubota, K.; Naemura, K., *J. Org. Chem* **1997,** *62*, 3430.

14. Bao, Z. N., *ACS Symp. Ser.* **2004,** *874*, 1.

15. Dimitrakopoulos, C. D.; Malenfant, P. R. L., *Adv. Mater.* **2002,** *14*, 99.

16. Dimitrakopoulos, C. D.; Mascaro, D. J., *IBM. J. Res. Development* **2001,** *45*, 11.

17. Witte, G.; Woll, C., *Mater. Res.* **2004,** *19*, 1889.

18. Horowitz, G., *J. Mater. Chem.* **2004,** *19*, 1946.

19. Xie, X. S., *Acc. Chem. Res.* **1996,** *29*, 598.

20. Moerner, W. E., *Acc. Chem. Res.* **1996,** *29*, 563.

21. Deleuze, M. S.; Claes, L.; Kryachko, E. S.; Francois, J. P., *J. Chem. Phys.* **2003,** *119*, 3106.

22. Herwig, P. T.; Mullen, K., *Adv. Mater.* **1999,** *11*, 480.

23. Keegstra, M. A.; DeFeyter, S.; DeSchryver, F. C.; Mullen, K., *Angew. Chem.* **1996,** *35*, 774.

24. Payne, M. M.; Delcamp, J. H.; Parkin, S. R.; Anthony, J., *Org. Lett.* **2004,** *6*, 1609.

25. Odom, S. A.; Parkin, S. R.; Anthony, J., *Org. Lett.* **2003,** *5*, 4245.

26. Anthony, J.; Eaton, D. L.; Parkin, S. R., *Org. Lett.* **2002,** *4*, 15.

27. Anthony, J.; Eaton, D. L.; Parkin, S. R., *J. Am. Chem. Soc.* **2001,** *123*, 9482.

28. Hegmann, F. A.; Tykwinski, R. R.; Lui, K. P. H.; Bullock, J. E.; Anthony, J., *Phys. Rev. Lett.* **2002,** *89*, 25.

29. Tokumoto, T.; Brooks, J. S.; Clinite, R.; Wei, X.; Anthony, J.; Eaton, D. L.; Parkin, S. R., *J. Appl. Phys.* **2002,** *92*, 5208.

30. Haddon, R. C.; Chi, X.; Itkis, M. E.; Anthony, J.; Eaton, D. L.; Siegrist, T.; Mattheus, C. C.; Palstra, T. T. M., *J. Phys. Chem. B* **2002,** *106*, 8288.

31. Brooks, J. S.; Vasic, R.; Tokumoto, T.; Graf, d.; Chung, O. H.; Anthony, J.; Odom, S. A., *Curr. Appl. Phys.* **2004,** *4*, 479.

32. Sheraw, C. D.; Jackson, T. N.; Eaton, D. L.; Anthony, J., *Adv. Mater.* **2003,** *15*, 2009.

33. Zhang, J. J.; Ho, D. M.; Pascal, R. A., *J. Am. Chem. Soc.* **2001,** *123*, 10919.

34. Qiao, X. X.; Padula, M. A.; Ho, D. M.; Vogelaar, N. J.; Schutt, C. E.; Pascal, R. A., *J. Am. Chem. Soc.* **1996,** *118*, 741.

35. Pascal, R. A.; Mcmillan, W. D.; Vanengen, D.; Eason, R. G., *J. Am. Chem. Soc.* **1987,** *109*, 4660.

36. Negishi, E.; Anastasia, L., *Chem. Rev.* **2003,** *103*, 1979.

37. Sonogashira, K., *J. Organomet. Chem.* **2002,** *653*, 46.

38. Bunz, U. H. F., *Chem. Rev.* **2000,** *100*, 1605.

39. Wenk, H. H.; Winkler, M.; Sander, W., *Angew. Chem.* **2003,** *42*, 502.

40. Grissom, J. W.; Gunawardena, G. U.; Klingberg, D.; Huang, D. H., *Tetrahedron* **1996,** *52*, 6453.

41. Nicoloaou, K. C.; Dai, W. M., *Angew. Chem.* **1991,** *30*, 1387.

42. Bergman, R. G., *Acc. Chem. Res.* **1973,** *6*, 25.

43. Jones, R. R.; Bergman, R. G., *J. Am. Chem. Soc.* **1972,** *94*, 660.

44. Dang, H.; Garcia-Garibay, M. A., *J. Am. Chem. Soc.* **2001,** *123*, 355.

45. Staab, H. A.; Ipaktschi, J., *Chem. Ber.* **1971,** *104*, 1170.

46. Ohkita, M.; Kawano, M.; Suzuki, T.; Tsuji, T., *Chem. Commun.* **2002**, 3054.

47. Ott, S.; Faust, R., *Synlett* **2004**, 1509.

48. Mitzel, F.; Fitzgerald, S.; Beeby, A.; Faust, R., *Eur. J. Org. Chem.* **2004**, 1136.

49. Winkelmann, E., *Tetrahedron* **1969,** *25*, 2427.

50. Entwistle, I. D.; Johnstone, R. A. W.; Povall, T. J., *J. chem. Soc. Perkin Trans. I* **1975**, 1300.

51. Smith, W. T.; Patterson, J. M.; Kovelesky, A. C., *J. Heterocycl. Chem.* **1990,** *27*, 549.

52. Suzuki, T.; Kabuto, C.; Yamashita, Y.; Saito, G.; Mukai, T.; Miyashi, T., *Chem. Lett.* **1987**, 2285.

Chapter 8

Conclusion

The synthesis of various types of conjugated heterocyclic systems, from PAEs to peralkynylated molecules, have been described and outlined in this manuscript. We determined that our original premise of created a conjugated system that would mimic a ladder polymer is viable, but does not have show much more improvement over the solubility issues that are present within the current ladder polymer systems.

With the advent of the conjugated quinoline PAEs, we were able to see that our vision towards the formation of the quinoxaline containing PAEs was a possibility. The solvochromic and ionochromic characteristics of the quinoline copolymers showed promising results. However, the data also showed that we were only able to obtain the conjugated system in the 3,6-positions and not the desired 5,8-positions. Since the alkynes were only present in the 3,6-positions we were unable to proceed to synthesize the simpler quinoline binding model. These quinoline systems proved to be the foundation which we used to prepare the benzothiadiazoles containing PAEs.

These benzothiadiazole copolymers showed interesting results in the solid state. The drop-cast films of the benzothiadiazole copolymers displayed differing results than previous PPE solid state properties in that they were more lustrous and also were nonfluorescent. The experience of performing reactions on the benzothiadiazoles assisted us to solve the problems of unreactivity with the HCSH coupling with these heterocycles and the subsequent quinoxaline based PAEs.

With the project of the benzothiadiazoles completed, we were able to progress to the quinoxaline containing PAEs. We demonstrated that the quinoxaline containing PAEs are very similar to the quinoline containing PAE in both ionochromic and solvochromic effects. However, our original premise for the formation of the “self assembling” ladder type polymers suffered the same drawback of insolubility just like the conventional ladder polymers. Currently, research in this area will likely lead to more soluble monomers for the formation of the multi-binding quinoxaline PAE.

The production of the peralkynylated molecules molecules produced many novel heterocyclic architectures. With the some extra synthetic steps these molecules would become interesting not only to expand its conjugation linearly through the alkynes, but also the expand the core of the molecule itself. These materials would be of some use as n-semiconducting materials.

APPENDIX A

CRYSTALLOGRAPHIC DATA

X-Ray Structure Determination $C_{27}H_{19}NO_2$ (6)

A colorless plate crystal was mounted on the end of a thin glass fiber with inert oil. X-ray intensity data were measured at 190(2) K using a Bruker SMART APEX CCD-based diffractometer system (Mo Kα radiation, λ = 0.71073 Å).[1] Crystal quality and initial unit cell parameters were determined based on reflections taken from a set of three scans measured in orthogonal regions of reciprocal space. Subsequently a hemisphere of frame data was collected with a scan width of 0.3° in ω and an exposure time of 10 sec. per frame. The first 50 frames were re-collected at the end of the data set to monitor crystal decay. The raw data frames were integrated into reflection intensity files using SAINT+,[1] which also applied corrections for Lorentz and polarization effects. The final unit cell parameters are based on the least-squares refinement of 2346 reflections with $I > 5(\sigma)I$ from the data set. Analysis of the data showed negligible crystal decay during data collection. No correction for absorption was applied. Systematic absences in the intensity data were uniquely consistent with the orthorhombic space group Pbcn. The structure was readily solved in this space group by a combination of direct methods and difference Fourier syntheses, and refined by full-matrix least-squares against F^2, using the

SHELXTL software package.[2] Solution of the structure in Pbcn yielded an asymmetric unit containing half of the molecule residing on a two-fold axis of rotation. The C_2 axis runs through the atoms C2 and C3 of the quinoline core. Two-fold symmetry is inconsistent with the molecular structure of quinoline, and therefore several models were tried. Refinement of the heteroatom (N1) as a carbon resulted in an unusually low anisotropic displacement parameter (adp) as well as a concentration of electron density around the atom. Similarly, refinement as a fully occupied nitrogen atom yielded a higher adp than the surrounding atoms, and significant hole in the electron density map near the atom. Therefore, and in agreement with the spectroscopic data (elsewhere), the structure was refined as possessing two-fold rotational disorder about the C_2 axis which runs through the atoms C2 and C3. The only affected atoms are C1 and the heteroatom N1. The site occupation factors (sofs) for C1 and N1 were each set at 0.5. The hydrogen atom attached to C1 was calculated by the standard method and given a sof of 0.5. Refinement of this model yielded reasonable adps as well as the lowest R-factors. Several refinements in lower symmetry space groups without crystallographically imposed two-fold molecular symmetry resulted in the same two-fold disorder as well as unstable refinements, and therefore the disorder model in the space group Pbcn was retained. Eventually, all non-hydrogen atoms were refined with anisotropic displacement parameters; C1 and N1 were constrained to the same atomic position with the same anisotropic displacement parameters. All hydrogen atoms (including the half-occupied H1) could be located in the Fourier difference map, but were placed in idealized positions and refined using a riding model.

(1) SMART Version 5.624 and SAINT+ Version 6.02a. Bruker Analytical X-ray Systems, Inc., Madison, Wisconsin, USA, 1998.

(2) Sheldrick, G. M. SHELXTL Version 5.1; Bruker Analytical X-ray Systems, Inc., Madison, Wisconsin, USA, 1997.

Table 1. Crystal data and structure refinement for **6**.

Identification code	**6**	
Empirical formula	C27 H19 N O2	
Formula weight	389.43	
Temperature	190(2) K	
Wavelength	0.71073 Å	
Crystal system	Orthorhombic	
Space group	Pbcn	
Unit cell dimensions	a = 21.263(2) Å	x= 90°.
	b = 6.7035(7) Å	x= 90°.
	c = 14.1510(15) Å	x = 90°.
Volume	2017.0(4) $Å^3$	
Z	4	
Density (calculated)	1.282 Mg/m^3	
Absorption coefficient	0.081 mm^{-1}	
F(000)	816	
Crystal size	0.78 x 0.42 x 0.05 mm^3	
Theta range for data collection	1.92 to 25.08°.	
Index ranges	-25<=h<=21, -7<=k<=7, -14<=l<=16	
Reflections collected	7687	
Independent reflections	1791 [R(int) = 0.0900]	
Completeness to theta = 25.08°	99.9 %	
Absorption correction	None	
Refinement method	Full-matrix least-squares on F^2	
Data / restraints / parameters	1791 / 0 / 138	
Goodness-of-fit on F^2	1.008	
Final R indices [I>2sigma(I)]	R1 = 0.0495, wR2 = 0.1053	

R indices (all data)	R1 = 0.0841, wR2 = 0.1160
Largest diff. peak and hole	0.168 and -0.115 e.$Å^{-3}$

Table 2. Atomic coordinates (x 10^4) and equivalent isotropic displacement parameters ($Å^2$x 10^3) for **6**. U(eq) is defined as one third of the trace of the orthogonalized U^{ij} tensor.

	x	y	z	U(eq)
C(1)	233(1)	-962(3)	3262(1)	61(1)
C(2)	0	107(5)	2500	45(1)
C(3)	0	2187(4)	2500	41(1)
C(4)	246(1)	3196(3)	3293(1)	50(1)
C(5)	486(1)	2138(3)	4039(1)	48(1)
C(6)	461(1)	60(4)	4005(1)	58(1)
C(7)	775(1)	3138(3)	4825(1)	54(1)
C(8)	1037(1)	3944(4)	5462(1)	56(1)
C(9)	1351(1)	4870(4)	6248(1)	54(1)
C(10)	1356(1)	3932(4)	7129(1)	65(1)
C(11)	1651(1)	4831(5)	7891(1)	73(1)
C(12)	1942(1)	6631(5)	7775(2)	72(1)
C(13)	1955(1)	7585(4)	6905(1)	65(1)
C(14)	1658(1)	6689(4)	6144(1)	56(1)
C(15)	2002(1)	9268(4)	5090(2)	74(1)
N(1)	233(1)	-962(3)	3262(1)	61(1)
O(1)	1651(1)	7485(2)	5255(1)	64(1)

Table 3. Bond lengths [Å] and angles [°] for **6**.

C(1)-C(6)	1.346(3)
C(1)-C(2)	1.387(2)
C(2)-N(1)#1	1.387(2)
C(2)-C(1)#1	1.387(2)
C(2)-C(3)	1.394(4)
C(3)-C(4)	1.411(2)
C(3)-C(4)#1	1.411(2)
C(4)-C(5)	1.371(3)
C(5)-C(6)	1.395(3)
C(5)-C(7)	1.436(3)
C(7)-C(8)	1.190(3)
C(8)-C(9)	1.438(3)
C(9)-C(14)	1.391(3)
C(9)-C(10)	1.396(3)
C(10)-C(11)	1.386(3)
C(11)-C(12)	1.366(3)
C(12)-C(13)	1.388(3)
C(13)-C(14)	1.385(3)
C(14)-O(1)	1.367(2)
C(15)-O(1)	1.428(3)
C(6)-C(1)-C(2)	118.3(2)
N(1)#1-C(2)-C(1)#1	0.0(2)
N(1)#1-C(2)-C(1)	117.8(3)
C(1)#1-C(2)-C(1)	117.8(3)
N(1)#1-C(2)-C(3)	121.12(14)
C(1)#1-C(2)-C(3)	121.12(14)
C(1)-C(2)-C(3)	121.12(14)
C(2)-C(3)-C(4)	118.65(14)
C(2)-C(3)-C(4)#1	118.65(14)
C(4)-C(3)-C(4)#1	122.7(3)
C(5)-C(4)-C(3)	120.2(2)
C(4)-C(5)-C(6)	118.44(18)
C(4)-C(5)-C(7)	120.9(2)

C(6)-C(5)-C(7)	120.60(18)
C(1)-C(6)-C(5)	123.30(19)
C(8)-C(7)-C(5)	177.4(2)
C(7)-C(8)-C(9)	178.4(2)
C(14)-C(9)-C(10)	119.1(2)
C(14)-C(9)-C(8)	120.93(18)
C(10)-C(9)-C(8)	120.0(2)
C(11)-C(10)-C(9)	120.2(3)
C(12)-C(11)-C(10)	119.7(2)
C(11)-C(12)-C(13)	121.5(2)
C(14)-C(13)-C(12)	118.8(2)
O(1)-C(14)-C(13)	123.5(2)
O(1)-C(14)-C(9)	115.75(18)
C(13)-C(14)-C(9)	120.8(2)
C(14)-O(1)-C(15)	118.13(17)

Symmetry transformations used to generate equivalent atoms:
#1 -x,y,-z+1/2

Table 4. Anisotropic displacement parameters ($Å^2 x 10^3$) for **6**. The anisotropic displacement factor exponent takes the form: $-2\pi^2[h^2 a^{*2}U^{11} + ... + 2 h k a^* b^* U^{12}]$

	U^{11}	U^{22}	U^{33}	U^{23}	U^{13}	U^{12}
C(1)	73(2)	46(1)	64(1)	9(1)	-12(1)	-2(1)
C(2)	53(2)	42(2)	42(2)	0	1(1)	0
C(3)	40(2)	39(2)	45(2)	0	1(1)	0
C(4)	52(1)	45(1)	53(1)	-1(1)	-3(1)	1(1)
C(5)	46(1)	57(2)	41(1)	1(1)	4(1)	1(1)
C(6)	56(2)	66(2)	53(1)	16(1)	-4(1)	-3(1)
C(7)	48(1)	74(2)	41(1)	0(1)	-1(1)	-2(1)
C(8)	47(1)	78(2)	42(1)	0(1)	3(1)	1(1)
C(9)	45(1)	79(2)	38(1)	-5(1)	2(1)	6(1)
C(10)	56(2)	97(2)	43(1)	1(1)	8(1)	-1(1)
C(11)	64(2)	120(3)	36(1)	-1(1)	4(1)	10(2)
C(12)	68(2)	106(2)	43(1)	-20(1)	-6(1)	7(2)
C(13)	65(2)	82(2)	49(1)	-12(1)	-9(1)	6(1)
C(14)	52(1)	77(2)	38(1)	-5(1)	-3(1)	7(1)
C(15)	79(2)	74(2)	70(1)	8(1)	-9(1)	-6(2)
N(1)	73(2)	46(1)	64(1)	9(1)	-12(1)	-2(1)
O(1)	71(1)	74(1)	48(1)	4(1)	-14(1)	-1(1)

Table 5. Hydrogen coordinates (x 10^4) and isotropic displacement parameters ($Å^2$x 10^3) for **6**.

	x	y	z	U(eq)
H(1)	232	-2379	3259	73
H(4)	245	4613	3310	60
H(6)	613	-671	4534	70
H(10)	1156	2675	7206	78
H(11)	1651	4198	8492	88
H(12)	2140	7244	8302	87
H(13)	2163	8829	6833	78
H(15A)	1857	10315	5521	111
H(15B)	1940	9703	4435	111
H(15C)	2449	9010	5200	111

X-Ray Structure Determination bis(triisopropylethynyl)-o-phenylenediamine, $C_{28}H_{48}N_2Si_2$

An irregular orange fragment sectioned from a larger crystal was mounted on the end of a thin glass fiber using inert oil. X-ray intensity data were measured at 150.0(2) K on a Bruker SMART APEX CCD-based diffractometer (Mo Kα radiation, λ = 0.71073 Å).[1] The raw data frames were integrated with SAINT+,[1] which also applied corrections for Lorentz and polarization effects. The final unit cell parameters are based on the least-squares refinement of 6325 reflections from the data set with $I > 5\sigma(I)$. Analysis of the data showed negligible crystal decay during data collection. No correction for absorption was applied. Systematic absences in the intensity data uniquely determined the space group $P2_1/n$. The structure was solved by a combination of direct methods and difference Fourier syntheses, and refined by full-matrix least-squares against F^2, using the SHELXTL software package.[2] The molecule is disordered over a center of symmetry. All non-hydrogen atoms were refined with anisotropic displacement parameters. Hydrogen atoms attached to carbon were placed in idealized positions and included as riding atoms. Amine hydrogens were located in the difference map and refined subject to a N-H = 0.84(2) distance restraint.

(1) SMART Version 5.625 and SAINT+ Version 6.02a. Bruker Analytical X-ray Systems, Inc., Madison, Wisconsin, USA, 1998.

(2) Sheldrick, G. M. SHELXTL Version 5.1; Bruker Analytical X-ray Systems, Inc., Madison, Wisconsin, USA, 1997.

Table 1. Crystal data and structure refinement for bis(triisopropylethynyl)-o-phenylenediamine.

Identification code	bis(triisopropylethynyl)-o-phenylenediamine	
Empirical formula	C28 H48 N2 Si2	
Formula weight	468.86	
Temperature	150.0(2) K	
Wavelength	0.71073 Å	
Crystal system	Monoclinic	
Space group	$P2_1/n$	
Unit cell dimensions	a = 7.4335(4) Å	x= 90°.
	b = 14.7432(8) Å	x= 100.9520(10)°.
	c = 13.8970(8) Å	x = 90°.
Volume	1495.28(14) Å^3	
Z	2	
Density (calculated)	1.041 Mg/m^3	
Absorption coefficient	0.135 mm^{-1}	
F(000)	516	
Crystal size	0.40 x 0.28 x 0.20 mm^3	
Theta range for data collection	2.03 to 25.02°.	
Index ranges	-8<=h<=8, -17<=k<=17, -16<=l<=14	
Reflections collected	10349	
Independent reflections	2641 [R(int) = 0.0368]	
Completeness to theta = 25.02°	100.0 %	
Absorption correction	None	
Refinement method	Full-matrix least-squares on F^2	
Data / restraints / parameters	2641 / 4 / 172	
Goodness-of-fit on F^2	1.032	
Final R indices [I>2sigma(I)]	R1 = 0.0513, wR2 = 0.1371	
R indices (all data)	R1 = 0.0592, wR2 = 0.1434	
Largest diff. peak and hole	0.367 and -0.144 e.Å^{-3}	

Table 2. Atomic coordinates (x 10^4) and equivalent isotropic displacement parameters ($Å^2$x 10^3) for bis(triisopropylethynyl)-o-phenylenediamine. U(eq) is defined as one third of the trace of the orthogonalized U^{ij} tensor.

	x	y	z	U(eq)
Si	1911(1)	7002(1)	1418(1)	37(1)
C(1)	3039(3)	6371(1)	2516(2)	42(1)
C(2)	3681(3)	5967(1)	3246(2)	41(1)
C(3)	4368(3)	5477(1)	4139(1)	39(1)
C(4)	6139(3)	5115(1)	4316(1)	39(1)
C(5)	6768(3)	4644(1)	5178(2)	40(1)
C(6)	3264(3)	6796(2)	427(2)	50(1)
C(7)	2895(4)	7483(2)	-417(2)	63(1)
C(8)	3086(5)	5833(2)	36(2)	87(1)
C(9)	-468(3)	6515(2)	1045(2)	51(1)
C(10)	-1432(3)	6266(2)	1879(2)	66(1)
C(11)	-1679(3)	7112(3)	289(2)	83(1)
C(12)	1977(3)	8232(2)	1746(2)	52(1)
C(13)	868(5)	8449(2)	2552(2)	76(1)
C(14)	3943(4)	8572(2)	2035(2)	82(1)
N(1)	7177(5)	5173(2)	3693(2)	39(1)
N(2)	8482(4)	4296(2)	5432(3)	40(1)

Table 3. Bond lengths [Å] and angles [°] for bis(triisopropylethynyl)-o-phenylenediamine.

Si-C(1)	1.848(2)
Si-C(12)	1.867(2)
Si-C(6)	1.877(2)
Si-C(9)	1.888(2)
C(1)-C(2)	1.195(3)
C(2)-C(3)	1.441(3)
C(3)-C(5)#1	1.397(3)
C(3)-C(4)	1.399(3)
C(4)-N(1)	1.267(4)
C(4)-C(5)	1.386(3)
C(5)-N(2)	1.357(4)
C(5)-C(3)#1	1.397(3)
C(6)-C(8)	1.518(4)
C(6)-C(7)	1.535(3)
C(9)-C(10)	1.519(3)
C(9)-C(11)	1.527(3)
C(12)-C(14)	1.525(4)
C(12)-C(13)	1.545(3)
C(1)-Si-C(12)	107.47(10)
C(1)-Si-C(6)	107.56(9)
C(12)-Si-C(6)	110.08(11)
C(1)-Si-C(9)	106.82(10)
C(12)-Si-C(9)	114.61(11)
C(6)-Si-C(9)	109.99(11)
C(2)-C(1)-Si	176.34(19)
C(1)-C(2)-C(3)	177.3(2)
C(5)#1-C(3)-C(4)	120.09(17)
C(5)#1-C(3)-C(2)	119.18(18)
C(4)-C(3)-C(2)	120.72(19)
N(1)-C(4)-C(5)	118.4(2)
N(1)-C(4)-C(3)	121.9(2)
C(5)-C(4)-C(3)	119.66(19)

N(2)-C(5)-C(4)	124.1(2)
N(2)-C(5)-C(3)#1	115.7(2)
C(4)-C(5)-C(3)#1	120.24(18)
C(8)-C(6)-C(7)	110.7(2)
C(8)-C(6)-Si	113.05(17)
C(7)-C(6)-Si	114.27(15)
C(10)-C(9)-C(11)	111.27(19)
C(10)-C(9)-Si	115.84(16)
C(11)-C(9)-Si	111.61(17)
C(14)-C(12)-C(13)	111.0(2)
C(14)-C(12)-Si	111.26(18)
C(13)-C(12)-Si	112.69(17)

Symmetry transformations used to generate equivalent atoms:

#1 -x+1,-y+1,-z+1

Table 4. Anisotropic displacement parameters ($Å^2$x 10^3) for joe117at. The anisotropic displacement factor exponent takes the form: $-2\square^2$[h^2 $a^{*2}U^{11}$ + ... + 2 h k a* b* U^{12}]

U^{11}	U^{22}	U^{33}	U^{23}	U^{13}	U^{12}	
Si34(1)	43(1)	33(1)	9(1)	2(1)	5(1)	
C(1)38(1)	42(1)	41(1)	9(1)	-1(1)	-1(1)	
C(2)38(1)	35(1)	45(1)	3(1)	-5(1)	-3(1)	
C(3)42(1)	29(1)	39(1)	3(1)	-10(1)	-3(1)	
C(4)40(1)	34(1)	38(1)	3(1)	-6(1)	-3(1)	
C(5)36(1)	33(1)	45(1)	0(1)	-10(1)	1(1)	
C(6)37(1)	66(1)	46(1)	8(1)	7(1)	13(1)	
C(7)56(1)	90(2)	46(1)	17(1)	18(1)	17(1)	
C(8)107(2)	74(2)	92(2)	-4(2)	44(2)	31(2)	
C(9)38(1)	68(2)	47(1)	4(1)	4(1)	-1(1)	
C(10) 5(1)	45(1)	88(2)	64(2)	30(1)	6(1)	-
C(11) 5(2)	38(1)	151(3)	57(2)	44(2)	-1(1)	-
C(12) 3(1)	71(2)	45(1)	35(1)	10(1)	-1(1)	
C(13) 17(2)	128(3)	57(2)	45(2)	2(1)	18(2)	
C(14) 20(2)	100(2)	60(2)	72(2)	13(1)	-21(2)	-
N(1)38(2)	49(2)	28(2)	5(1)	6(2)	-6(2)	
N(2)33(2)	45(2)	41(2)	6(2)	5(2)	1(1)	

Table 5. Hydrogen coordinates (x 10^4) and isotropic displacement parameters ($Å^2$x 10^3) for bis(triisopropylethynyl)-o-phenylenediamine.

	x	y	z	U(eq)
H(4)	6904	5176	3839	47
H(5)	7984	4411	5304	48
H(6)	4581	6875	742	59
H(7A)	3768	7385	-854	94
H(7B)	3039	8100	-152	94
H(7C)	1644	7403	-785	94
H(8A)	1840	5736	-332	131
H(8B)	3338	5405	585	131
H(8C)	3966	5736	-397	131
H(9)	-314	5933	700	62
H(10A)	-1661	6816	2232	99
H(10B)	-657	5851	2330	99
H(10C)	-2600	5968	1614	99
H(11A)	-2838	6799	43	125
H(11B)	-1050	7235	-256	125
H(11C)	-1927	7686	596	125
H(12)	1395	8572	1145	62
H(13A)	1308	8071	3128	115
H(13B)	-433	8324	2304	115
H(13C)	1024	9091	2733	115
H(14A)	3937	9224	2169	123
H(14B)	4597	8459	1497	123
H(14C)	4559	8250	2623	123
H(1N)	6720(60)	5530(30)	3250(30)	58
H(2N)	8260(30)	5290(30)	3890(30)	58
H(3N)	8830(70)	4140(30)	4920(20)	60
H(4N)	8640(70)	3890(30)	5880(30)	60

Table 6. Torsion angles [°] for bis(triisopropylethynyl)-o-phenylenediamine.

C(12)-Si-C(1)-C(2)	80(3)
C(6)-Si-C(1)-C(2)	-162(3)
C(9)-Si-C(1)-C(2)	-44(3)
Si-C(1)-C(2)-C(3)	9(7)
C(1)-C(2)-C(3)-C(5)#1	-10(5)
C(1)-C(2)-C(3)-C(4)	169(4)
C(5)#1-C(3)-C(4)-N(1)	176.5(2)
C(2)-C(3)-C(4)-N(1)	-2.4(3)
C(5)#1-C(3)-C(4)-C(5)	-0.8(3)
C(2)-C(3)-C(4)-C(5)	-179.80(17)
N(1)-C(4)-C(5)-N(2)	5.0(4)
C(3)-C(4)-C(5)-N(2)	-177.6(2)
N(1)-C(4)-C(5)-C(3)#1	-176.6(2)
C(3)-C(4)-C(5)-C(3)#1	0.8(3)
C(1)-Si-C(6)-C(8)	70.1(2)
C(12)-Si-C(6)-C(8)	-173.11(19)
C(9)-Si-C(6)-C(8)	-45.9(2)
C(1)-Si-C(6)-C(7)	-162.14(18)
C(12)-Si-C(6)-C(7)	-45.3(2)
C(9)-Si-C(6)-C(7)	81.9(2)
C(1)-Si-C(9)-C(10)	38.7(2)
C(12)-Si-C(9)-C(10)	-80.2(2)
C(6)-Si-C(9)-C(10)	155.11(18)
C(1)-Si-C(9)-C(11)	167.38(19)
C(12)-Si-C(9)-C(11)	48.5(2)
C(6)-Si-C(9)-C(11)	-76.2(2)
C(1)-Si-C(12)-C(14)	61.61(19)
C(6)-Si-C(12)-C(14)	-55.25(19)
C(9)-Si-C(12)-C(14)	-179.85(16)
C(1)-Si-C(12)-C(13)	-63.8(2)
C(6)-Si-C(12)-C(13)	179.35(17)
C(9)-Si-C(12)-C(13)	54.8(2)

Symmetry transformations used to generate equivalent atoms:
#1 -x+1,-y+1,-z+1

X-Ray Structure Determination of $C_{30}H_{36}N_2S$ (39a)

An irregular yellow crystal was mounted onto the end of a thin glass fiber using inert oil. X-ray intensity data were measured at 150(1) K on a Bruker SMART APEX CCD-based diffractometer (Mo Kα radiation, λ = 0.71073 Å).[1] The raw data frames were integrated with SAINT+,[1] which also applied corrections for Lorentz and polarization effects. The final unit cell parameters are based on the least-squares refinement of 7024 reflections from the data set with $I > 5(\sigma)I$. Analysis of the data showed negligible crystal decay during data collection.Systematic absences in the intensity data were consistent with the space group $P2_1/n$. The structure was solved by a combination of direct methods and difference Fourier syntheses, and refined by full-matrix least-squares against F^2, using SHELXTL.[2] All non-hydrogen atoms were refined with anisotropic displacement parameters; hydrogen atoms were placed in geometrically idealized positions and included as riding atoms with refined isotropic displacement parameters.

(1) SMART Version 5.625 and SAINT+ Version 6.02a. Bruker Analytical X-ray Systems, Inc., Madison, Wisconsin, USA, 1998.

(2) Sheldrick, G. M. SHELXTL Version 5.1; Bruker Analytical X-ray Systems, Inc., Madison, Wisconsin, USA, 1997.

Table 1. Crystal data and structure refinement for **39a**.

Identification code	**39a**	
Empirical formula	C30 H36 N2 S	
Formula weight	456.67	
Temperature	150(1) K	
Wavelength	0.71073 Å	
Crystal system	Monoclinic	
Space group	$P2_1/n$	
Unit cell dimensions	a = 9.0675(5) Å	x= 90°.
	b = 12.4366(6) Å	x= 91.7400(10)°.
	c = 24.6288(13) Å	x = 90°.
Volume	2776.1(3) Å^3	
Z	4	
Density (calculated)	1.093 Mg/m^3	
Absorption coefficient	0.135 mm^{-1}	
F(000)	984	
Crystal size	0.38 x 0.30 x 0.18 mm^3	
Theta range for data collection	1.65 to 24.12°.	
Index ranges	-9<=h<=10, -11<=k<=14, -27<=l<=28	
Reflections collected	14498	
Independent reflections	4428 [R(int) = 0.0410]	
Completeness to theta = 24.12°	99.9 %	
Absorption correction	None	
Refinement method	Full-matrix least-squares on F^2	
Data / restraints / parameters	4428 / 0 / 346	
Goodness-of-fit on F^2	1.046	
Final R indices [I>2sigma(I)]	R1 = 0.0437, wR2 = 0.1177	
R indices (all data)	R1 = 0.0564, wR2 = 0.1226	
Largest diff. peak and hole	0.319 and -0.202 e.Å^{-3}	

Table 2. Atomic coordinates (x 10^4) and equivalent isotropic displacement parameters ($Å^2$x 10^3) for **39a**. U(eq) is defined as one third of the trace of the orthogonalized U^{ij} tensor.

	x	y	z	U(eq)
S(1)	2238(1)	7276(1)	2138(1)	37(1)
N(1)	1354(2)	6158(1)	2176(1)	31(1)
N(2)	3551(2)	6950(1)	1740(1)	35(1)
C(1)	2090(2)	5453(2)	1870(1)	26(1)
C(2)	1708(2)	4345(2)	1794(1)	26(1)
C(3)	2621(2)	3731(2)	1479(1)	26(1)
C(4)	3913(2)	4189(2)	1233(1)	27(1)
C(5)	4279(2)	5264(2)	1296(1)	28(1)
C(6)	3343(2)	5904(2)	1623(1)	27(1)
C(7)	419(2)	3922(2)	2042(1)	27(1)
C(8)	-656(2)	3614(2)	2257(1)	31(1)
C(9)	-2029(2)	3274(2)	2517(1)	33(1)
C(10)	-3332(2)	3819(2)	2221(1)	44(1)
C(11)	-1960(2)	3633(2)	3112(1)	45(1)
C(12)	-2174(3)	2059(2)	2484(1)	50(1)
C(13)	2311(2)	2578(2)	1391(1)	25(1)
C(14)	2103(2)	1679(2)	1351(1)	34(1)
C(15)	1857(2)	495(2)	1306(1)	37(1)
C(16)	3315(3)	-83(2)	1430(1)	50(1)
C(17)	1298(3)	221(2)	734(1)	61(1)
C(18)	721(3)	157(2)	1719(1)	54(1)
C(19)	4878(2)	3475(2)	919(1)	26(1)
C(20)	5692(3)	2973(2)	700(1)	38(1)
C(21)	6851(2)	2319(2)	426(1)	43(1)
C(22)	8359(3)	2618(2)	693(1)	58(1)
C(23)	6859(3)	2602(2)	-179(1)	57(1)
C(24)	6557(3)	1134(2)	506(1)	66(1)
C(25)	5568(2)	5725(2)	1051(1)	29(1)

C(26)	6613(2)	6072(2)	843(1)	34(1)
C(27)	7948(2)	6465(2)	573(1)	37(1)
C(28)	7751(3)	7643(2)	409(1)	53(1)
C(29)	9275(2)	6331(2)	964(1)	57(1)
C(30)	8165(3)	5790(2)	61(1)	49(1)

Table 3. Bond lengths [Å] and angles [°] for **39a**.

S(1)-N(1)	1.6090(17)
S(1)-N(2)	1.6165(17)
N(1)-C(1)	1.346(2)
N(2)-C(6)	1.344(2)
C(1)-C(6)	1.420(3)
C(1)-C(2)	1.432(3)
C(2)-C(3)	1.381(2)
C(2)-C(7)	1.435(3)
C(3)-C(4)	1.452(3)
C(3)-C(13)	1.475(3)
C(4)-C(5)	1.384(3)
C(4)-C(19)	1.481(3)
C(5)-C(6)	1.430(3)
C(5)-C(25)	1.449(3)
C(7)-C(8)	1.188(3)
C(8)-C(9)	1.480(3)
C(9)-C(12)	1.519(3)
C(9)-C(10)	1.528(3)
C(9)-C(11)	1.531(3)
C(10)-H(10A)	0.9800
C(10)-H(10B)	0.9800
C(10)-H(10C)	0.9800
C(11)-H(11A)	0.9800
C(11)-H(11B)	0.9800
C(11)-H(11C)	0.9800
C(12)-H(12A)	0.9800
C(12)-H(12B)	0.9800
C(12)-H(12C)	0.9800

C(13)-C(14)	1.138(3)
C(14)-C(15)	1.493(3)
C(15)-C(17)	1.522(3)
C(15)-C(16)	1.527(3)
C(15)-C(18)	1.529(3)
C(16)-H(16A)	0.9800
C(16)-H(16B)	0.9800
C(16)-H(16C)	0.9800
C(17)-H(17A)	0.9800
C(17)-H(17B)	0.9800
C(17)-H(17C)	0.9800
C(18)-H(18A)	0.9800
C(18)-H(18B)	0.9800
C(18)-H(18C)	0.9800
C(19)-C(20)	1.118(3)
C(20)-C(21)	1.505(3)
C(21)-C(24)	1.512(3)
C(21)-C(23)	1.532(3)
C(21)-C(22)	1.545(3)
C(22)-H(22A)	0.9800
C(22)-H(22B)	0.9800
C(22)-H(22C)	0.9800
C(23)-H(23A)	0.9800
C(23)-H(23B)	0.9800
C(23)-H(23C)	0.9800
C(24)-H(24A)	0.9800
C(24)-H(24B)	0.9800
C(24)-H(24C)	0.9800
C(25)-C(26)	1.173(3)
C(26)-C(27)	1.483(3)
C(27)-C(29)	1.527(3)
C(27)-C(28)	1.529(3)
C(27)-C(30)	1.531(3)
C(28)-H(28A)	0.9800
C(28)-H(28B)	0.9800
C(28)-H(28C)	0.9800

C(29)-H(29A)	0.9800
C(29)-H(29B)	0.9800
C(29)-H(29C)	0.9800
C(30)-H(30A)	0.9800
C(30)-H(30B)	0.9800
C(30)-H(30C)	0.9800

N(1)-S(1)-N(2)	101.27(8)
C(1)-N(1)-S(1)	105.92(12)
C(6)-N(2)-S(1)	105.75(13)
N(1)-C(1)-C(6)	113.52(17)
N(1)-C(1)-C(2)	125.30(16)
C(6)-C(1)-C(2)	121.17(16)
C(3)-C(2)-C(1)	117.31(16)
C(3)-C(2)-C(7)	123.11(17)
C(1)-C(2)-C(7)	119.57(16)
C(2)-C(3)-C(4)	121.46(17)
C(2)-C(3)-C(13)	120.30(16)
C(4)-C(3)-C(13)	118.24(16)
C(5)-C(4)-C(3)	121.76(16)
C(5)-C(4)-C(19)	119.57(16)
C(3)-C(4)-C(19)	118.65(17)
C(4)-C(5)-C(6)	117.10(16)
C(4)-C(5)-C(25)	121.97(17)
C(6)-C(5)-C(25)	120.92(17)
N(2)-C(6)-C(1)	113.53(16)
N(2)-C(6)-C(5)	125.27(17)
C(1)-C(6)-C(5)	121.18(17)
C(8)-C(7)-C(2)	177.2(2)
C(7)-C(8)-C(9)	177.5(2)
C(8)-C(9)-C(12)	109.51(16)
C(8)-C(9)-C(10)	108.31(17)
C(12)-C(9)-C(10)	110.57(19)
C(8)-C(9)-C(11)	108.68(17)
C(12)-C(9)-C(11)	110.11(18)
C(10)-C(9)-C(11)	109.61(17)

C(9)-C(10)-H(10A)109.5
C(9)-C(10)-H(10B)109.5
H(10A)-C(10)-H(10B)
C(9)-C(10)-H(10C)109.5
H(10A)-C(10)-H(10C)
H(10B)-C(10)-H(10C)
C(9)-C(11)-H(11A)109.5
C(9)-C(11)-H(11B)109.5
H(11A)-C(11)-H(11B)
C(9)-C(11)-H(11C)109.5
H(11A)-C(11)-H(11C)
H(11B)-C(11)-H(11C)
C(9)-C(12)-H(12A)109.5
C(9)-C(12)-H(12B)109.5
H(12A)-C(12)-H(12B)
C(9)-C(12)-H(12C)109.5
H(12A)-C(12)-H(12C)
H(12B)-C(12)-H(12C)
C(14)-C(13)-C(3) 176.4(2)
C(13)-C(14)-C(15)178.8(2)
C(14)-C(15)-C(17)109.49(18)
C(14)-C(15)-C(16)108.83(18)
C(17)-C(15)-C(16)109.97(19)
C(14)-C(15)-C(18)108.91(17)
C(17)-C(15)-C(18)110.1(2)
C(16)-C(15)-C(18)109.55(19)
C(15)-C(16)-H(16A)109.5
C(15)-C(16)-H(16B)109.5
H(16A)-C(16)-H(16B)
C(15)-C(16)-H(16C)109.5
H(16A)-C(16)-H(16C)
H(16B)-C(16)-H(16C)
C(15)-C(17)-H(17A)109.5
C(15)-C(17)-H(17B)109.5
H(17A)-C(17)-H(17B)
C(15)-C(17)-H(17C)109.5

H(17A)-C(17)-H(17C)

H(17B)-C(17)-H(17C)

C(15)-C(18)-H(18A)109.5

C(15)-C(18)-H(18B)109.5

H(18A)-C(18)-H(18B)

C(15)-C(18)-H(18C)109.5

H(18A)-C(18)-H(18C)

H(18B)-C(18)-H(18C)

C(20)-C(19)-C(4) 174.9(2)

C(19)-C(20)-C(21)177.0(2)

C(20)-C(21)-C(24)109.86(18)

C(20)-C(21)-C(23)109.67(19)

C(24)-C(21)-C(23)110.9(2)

C(20)-C(21)-C(22)107.49(19)

C(24)-C(21)-C(22)109.6(2)

C(23)-C(21)-C(22)109.2(2)

C(21)-C(22)-H(22A)109.5

C(21)-C(22)-H(22B)109.5

H(22A)-C(22)-H(22B)

C(21)-C(22)-H(22C)109.5

H(22A)-C(22)-H(22C)

H(22B)-C(22)-H(22C)

C(21)-C(23)-H(23A)109.5

C(21)-C(23)-H(23B)109.5

H(23A)-C(23)-H(23B)

C(21)-C(23)-H(23C)109.5

H(23A)-C(23)-H(23C)

H(23B)-C(23)-H(23C)

C(21)-C(24)-H(24A)109.5

C(21)-C(24)-H(24B)109.5

H(24A)-C(24)-H(24B)

C(21)-C(24)-H(24C)109.5

H(24A)-C(24)-H(24C)

H(24B)-C(24)-H(24C)

C(26)-C(25)-C(5) 178.0(2)

C(25)-C(26)-C(27)177.6(2)

C(26)-C(27)-C(29)108.60(17)
C(26)-C(27)-C(28)110.09(18)
C(29)-C(27)-C(28)110.7(2)
C(26)-C(27)-C(30)108.43(18)
C(29)-C(27)-C(30)110.0(2)
C(28)-C(27)-C(30)108.97(19)
C(27)-C(28)-H(28A)109.5
C(27)-C(28)-H(28B)109.5
H(28A)-C(28)-H(28B)
C(27)-C(28)-H(28C)109.5
H(28A)-C(28)-H(28C)
H(28B)-C(28)-H(28C)
C(27)-C(29)-H(29A)109.5
C(27)-C(29)-H(29B)109.5
H(29A)-C(29)-H(29B)
C(27)-C(29)-H(29C)109.5
H(29A)-C(29)-H(29C)
H(29B)-C(29)-H(29C)
C(27)-C(30)-H(30A)109.5
C(27)-C(30)-H(30B)109.5
H(30A)-C(30)-H(30B)
C(27)-C(30)-H(30C)109.5
H(30A)-C(30)-H(30C)
H(30B)-C(30)-H(30C)

Symmetry transformations used to generate equivalent atoms:

Table 4. Anisotropic displacement parameters (Å^{2}x 10^3) for **39a**. The anisotropic displacement factor exponent takes the form: $-2\pi^2$[h^2 $a^{*2}U^{11}$ + ... + 2 h k a* b* U^{12}]

	U^{11}	U^{22}	U^{33}	U^{23}	U^{13}	U^{12}
S(1)	39(1)	27(1)	46(1)	-5(1)	11(1)	-1(1)
N(1)	31(1)	29(1)	35(1)	-2(1)	6(1)	2(1)
N(2)	34(1)	30(1)	40(1)	1(1)	6(1)	-3(1)
C(1)	24(1)	30(1)	24(1)	2(1)	2(1)	3(1)
C(2)	25(1)	27(1)	26(1)	2(1)	3(1)	1(1)
C(3)	26(1)	26(1)	26(1)	2(1)	2(1)	2(1)
C(4)	24(1)	33(1)	26(1)	1(1)	2(1)	4(1)
C(5)	25(1)	33(1)	26(1)	3(1)	3(1)	1(1)
C(6)	29(1)	26(1)	28(1)	1(1)	2(1)	-1(1)
C(7)	29(1)	23(1)	30(1)	0(1)	5(1)	2(1)
C(8)	31(1)	28(1)	34(1)	-1(1)	4(1)	6(1)
C(9)	26(1)	36(1)	37(1)	3(1)	9(1)	-1(1)
C(10)	31(1)	57(2)	43(2)	2(1)	6(1)	4(1)
C(11)	36(1)	63(2)	38(1)	2(1)	10(1)	5(1)
C(12)	40(2)	42(1)	67(2)	6(1)	19(1)	-7(1)
C(13)	22(1)	25(1)	28(1)	5(1)	11(1)	7(1)
C(14)	29(1)	43(1)	32(1)	1(1)	8(1)	5(1)
C(15)	42(1)	26(1)	43(1)	0(1)	9(1)	1(1)
C(16)	49(2)	31(1)	71(2)	5(1)	16(1)	5(1)
C(17)	86(2)	35(1)	60(2)	-9(1)	-6(2)	5(1)

C(18)	53(2)	35(1)	74(2)	3(1)	24(1)	-4(1)
C(19)	20(1)	32(1)	28(1)	4(1)	2(1)	-5(1)
C(20)	41(1)	38(1)	35(1)	3(1)	1(1)	-7(1)
C(21)	40(1)	41(1)	49(1)	-1(1)	17(1)	8(1)
C(22)	40(2)	64(2)	71(2)	8(1)	14(1)	14(1)
C(23)	63(2)	59(2)	51(2)	-5(1)	23(1)	14(1)
C(24)	69(2)	45(2)	84(2)	-6(1)	34(2)	7(1)
C(25)	27(1)	29(1)	29(1)	0(1)	6(1)	2(1)
C(26)	35(1)	37(1)	31(1)	4(1)	3(1)	3(1)
C(27)	26(1)	48(1)	37(1)	5(1)	9(1)	-5(1)
C(28)	54(2)	52(2)	53(2)	11(1)	18(1)	-10(1)
C(29)	36(1)	83(2)	51(2)	8(1)	5(1)	-10(1)
C(30)	43(2)	62(2)	44(1)	2(1)	16(1)	0(1)

Table 5. Hydrogen coordinates (x 10^4) and isotropic displacement parameters ($Å^2$x 10^3) for **39a**.

	x	y	z	U(eq)
H(10A)	-3217	4601	2245	56(7)
H(10B)	-4252	3606	2390	54(7)
H(10C)	-3361	3600	1839	54(7)
H(11A)	-1146	3263	3304	52(7)
H(11B)	-2892	3455	3282	53(7)
H(11C)	-1799	4412	3130	44(6)
H(12A)	-2210	1836	2102	45(6)
H(12B)	-3083	1833	2657	64(7)
H(12C)	-1324	1722	2671	61(8)
H(16A)	4046	142	1168	64(8)
H(16B)	3164	-862	1402	44(6)
H(16C)	3669	99	1798	91(11)
H(17A)	350	579	661	89(10)
H(17B)	1170	-559	701	62(7)
H(17C)	2015	466	471	74(9)
H(18A)	1080	352	2085	90(11)
H(18B)	572	-623	1699	61(7)
H(18C)	-216	525	1638	73(9)
H(22A)	8510	3396	667	89(10)
H(22B)	9147	2244	505	72(8)
H(22C)	8378	2403	1076	106(12)
H(23A)	5915	2394	-353	90(11)
H(23B)	7663	2216	-351	59(7)
H(23C)	7004	3378	-221	58(7)
H(24A)	6524	976	895	94(11)
H(24B)	7347	713	345	83(9)
H(24C)	5610	943	330	58(8)
H(28A)	6924	7706	145	72(9)
H(28B)	8655	7904	245	62(7)

H(28C)	7547	8073	731	63(8)
H(29A)	9123	6760	1292	67(8)
H(29B)	10169	6577	788	63(7)
H(29C)	9383	5572	1064	63(8)
H(30A)	8345	5039	164	65(8)
H(30B)	9011	6066	-134	55(7)
H(30C)	7276	5833	-174	73(9)

Table 6. Torsion angles [°] for **39a**.

N(2)-S(1)-N(1)-C(1)	0.61(15)
N(1)-S(1)-N(2)-C(6)	-0.78(15)
S(1)-N(1)-C(1)-C(6)	-0.3(2)
S(1)-N(1)-C(1)-C(2)	178.73(16)
N(1)-C(1)-C(2)-C(3)	-177.92(18)
C(6)-C(1)-C(2)-C(3)	1.0(3)
N(1)-C(1)-C(2)-C(7)	2.2(3)
C(6)-C(1)-C(2)-C(7)	-178.90(18)
C(1)-C(2)-C(3)-C(4)	-0.1(3)
C(7)-C(2)-C(3)-C(4)	179.77(18)
C(1)-C(2)-C(3)-C(13)	178.89(17)
C(7)-C(2)-C(3)-C(13)	-1.2(3)
C(2)-C(3)-C(4)-C(5)	-1.0(3)
C(13)-C(3)-C(4)-C(5)	179.94(18)
C(2)-C(3)-C(4)-C(19)	177.54(18)
C(13)-C(3)-C(4)-C(19)	-1.5(3)
C(3)-C(4)-C(5)-C(6)	1.2(3)
C(19)-C(4)-C(5)-C(6)	-177.33(17)
C(3)-C(4)-C(5)-C(25)	179.98(18)
C(19)-C(4)-C(5)-C(25)	1.4(3)
S(1)-N(2)-C(6)-C(1)	0.7(2)
S(1)-N(2)-C(6)-C(5)	-177.78(17)
N(1)-C(1)-C(6)-N(2)	-0.3(2)
C(2)-C(1)-C(6)-N(2)	-179.35(17)
N(1)-C(1)-C(6)-C(5)	178.25(17)
C(2)-C(1)-C(6)-C(5)	-0.8(3)

C(4)-C(5)-C(6)-N(2)	178.04(19)
C(25)-C(5)-C(6)-N(2)	-0.7(3)
C(4)-C(5)-C(6)-C(1)	-0.3(3)
C(25)-C(5)-C(6)-C(1)	-179.11(18)
C(3)-C(2)-C(7)-C(8)	177(100)
C(1)-C(2)-C(7)-C(8)	-4(5)
C(2)-C(7)-C(8)-C(9)	47(8)
C(7)-C(8)-C(9)-C(12)	146(5)
C(7)-C(8)-C(9)-C(10)	25(5)
C(7)-C(8)-C(9)-C(11)	-94(5)
C(2)-C(3)-C(13)-C(14)	-78(3)
C(4)-C(3)-C(13)-C(14)	101(3)
C(3)-C(13)-C(14)-C(15)	-25(13)
C(13)-C(14)-C(15)-C(17)	-149(11)
C(13)-C(14)-C(15)-C(16)	-29(11)
C(13)-C(14)-C(15)-C(18)	90(11)
C(5)-C(4)-C(19)-C(20)	42(3)
C(3)-C(4)-C(19)-C(20)	-137(2)
C(4)-C(19)-C(20)-C(21)	12(6)
C(19)-C(20)-C(21)-C(24)	114(4)
C(19)-C(20)-C(21)-C(23)	-123(4)
C(19)-C(20)-C(21)-C(22)	-5(5)
C(4)-C(5)-C(25)-C(26)	18(7)
C(6)-C(5)-C(25)-C(26)	-163(7)
C(5)-C(25)-C(26)-C(27)	-23(11)
C(25)-C(26)-C(27)-C(29)	-85(5)
C(25)-C(26)-C(27)-C(28)	154(5)
C(25)-C(26)-C(27)-C(30)	35(5)

Symmetry transformations used to generate equivalent atoms:

X-Ray Structure Determination $C_{60}H_{72}N_2$ (43)

An irregular orange-red fragment was sectioned from a larger crystalline aggregation and epoxied onto the end of a thin glass fiber. X-ray intensity data covering the full sphere of reciprocal space were measured at 293 K on a Bruker SMART APEX diffractometer (Mo Kα radiation, λ = 0.71073 Å).[1] The raw data frames were integrated and corrected for Lp effects with SAINT+.[1] Final unit cell parameters were determined by least-squares refinement of 7680 reflections from the data set with $I > 5(\sigma)I$. Analysis of the data showed negligible crystal decay during data collection. No correction for absorption was applied. $C_{60}H_{72}N_2$ crystallizes in the space group $P2_1/c$ as determined by the systematic absences in the intensity data. The structure was solved by a combination of direct methods[2] and difference Fourier syntheses, and refined by full-matrix least-squares against F^2 with SHELXTL.[3] The molecule is situated on a crystallographic inversion center. Three of the four crystallographically inequivalent t-butyl groups are rotationally disordered. Occupancies for the major and minor disorder components were constrained to sum to unity, and the minor component geometry was restrained to be similar to the major (19 restraints). Major component occupancies all refined to near 70%. Elongated displacement parameters and the presence of additional small electron density peaks near all four t-butyl groups indicate more than two disorder orientations exist throughout the crystal for theses groups - no attempt was made to model these. Eventually all non-hydrogen atoms were refined with anisotropic displacement parameters; hydrogen atoms were placed in geometrically idealized positions and included as riding atoms.

(1) SMART Version 5.625 and SAINT+ Version 6.22. Bruker Analytical X-ray Systems, Inc., Madison, Wisconsin, USA, 2001.

(2) Burla, M.C., Camalli, M., Carrozzini, B., Cascarano, G.L., Giacovazzo, C., Polidori, G., Spagna, R. Sir2002: a new Direct Methods program for automatic solution and refinement of crystal structures. J. Appl. Cryst. (2003), In preparation

(3) Sheldrick, G. M. SHELXTL Version 6.1; Bruker Analytical X-ray Systems, Inc., Madison, Wisconsin, USA, 2000.

Table 1. Crystal data and structure refinement for **43**.

Identification code	**43**	
Empirical formula	C60 H72 N2	
Formula weight	821.20	
Temperature	293(2) K	
Wavelength	0.71073 Å	
Crystal system	Monoclinic	
Space group	$P2_1/c$	
Unit cell dimensions	a = 19.4214(9) Å	x= 90°.
	b = 9.9650(5) Å	x= 112.6820(10)°.
	c = 15.4061(7) Å	x = 90°.
Volume	2751.0(2) Å^3	
Z	2	
Density (calculated)	0.991 Mg/m^3	
Absorption coefficient	0.056 mm^{-1}	
F(000)	892	
Crystal size	0.52 x 0.40 x 0.22 mm^3	
Theta range for data collection	2.27 to 23.26°.	
Index ranges	-21<=h<=21, -11<=k<=11, -17<=l<=17	
Reflections collected	18417	
Independent reflections	3950 [R(int) = 0.0338]	
Completeness to theta = 23.26°	100.0 %	
Absorption correction	None	
Refinement method	Full-matrix least-squares on F^2	
Data / restraints / parameters	3950 / 19 / 370	
Goodness-of-fit on F^2	1.040	

Final R indices [I>2sigma(I)]	R1 = 0.0518, wR2 = 0.1420
R indices (all data)	R1 = 0.0636, wR2 = 0.1536
Largest diff. peak and hole	0.195 and -0.185 e.Å^{-3}

Table 2. Atomic coordinates (x 10^4) and equivalent isotropic displacement parameters (Å^{2}x 10^3) for **43**. U(eq) is defined as one third of the trace of the orthogonalized U^{ij} tensor.

	x	y	z	U(eq)
N(1)	5248(1)	1224(1)	5480(1)	44(1)
C(1)	4524(1)	884(1)	5133(1)	42(1)
C(2)	3998(1)	1778(1)	5280(1)	47(1)
C(3)	3257(1)	1399(2)	4982(1)	51(1)
C(4)	2999(1)	167(2)	4461(1)	52(1)
C(5)	3491(1)	-680(2)	4279(1)	48(1)
C(6)	4273(1)	-353(1)	4645(1)	42(1)
C(7)	4236(1)	3042(2)	5734(1)	53(1)
C(8)	4386(1)	4134(2)	6073(1)	59(1)
C(9A)	4579(1)	5468(2)	6489(1)	71(1)
C(10A)	3895(3)	6408(4)	5925(4)	122(2)
C(11A)	4686(6)	5456(6)	7469(3)	134(3)
C(12A)	5221(5)	6060(10)	6303(7)	150(4)
C(9B)	4579(1)	5468(2)	6489(1)	71(1)
C(10B)	5238(9)	5088(11)	7490(7)	146(5)
C(11B)	4929(13)	6238(15)	6005(12)	187(12)
C(12B)	3993(6)	6096(18)	6753(18)	236(15)
C(13)	2739(1)	2217(2)	5205(1)	59(1)
C(14)	2342(1)	2886(2)	5452(1)	72(1)
C(15A)	1903(5)	3706(9)	5861(7)	83(2)
C(16A)	1231(4)	2960(6)	5841(8)	160(4)
C(17A)	1668(4)	4980(6)	5248(5)	131(3)
C(18A)	2379(3)	4097(7)	6843(3)	126(2)
C(15B)	1808(10)	3780(20)	5648(15)	83(2)

C(16B)	2177(8)	5042(17)	6140(20)	261(18)
C(17B)	1553(15)	2890(20)	6287(18)	270(20)
C(18B)	1116(8)	4081(19)	4804(9)	176(7)
C(19)	2220(1)	-149(2)	4134(1)	60(1)
C(20)	1573(1)	-380(2)	3872(1)	68(1)
C(21A)	769(1)	-644(2)	3567(2)	84(1)
C(22A)	410(2)	-671(7)	2500(3)	116(2)
C(23A)	680(2)	-2031(6)	3948(5)	129(3)
C(24A)	410(2)	404(7)	3970(5)	140(3)
C(21B)	769(1)	-644(2)	3567(2)	84(1)
C(22B)	607(6)	-840(20)	4438(8)	177(9)
C(23B)	406(6)	681(14)	3088(16)	193(11)
C(24B)	512(7)	-1800(20)	2882(16)	234(18)
C(25)	3219(1)	-1860(2)	3726(1)	57(1)
C(26)	2937(1)	-2804(2)	3242(1)	66(1)
C(27)	2579(1)	-3970(2)	2666(2)	81(1)
C(28)	2838(2)	-4132(3)	1875(2)	157(1)
C(29)	2764(2)	-5214(3)	3295(2)	151(1)
C(30)	1742(2)	-3741(4)	2260(3)	206(2)

Table 3. Bond lengths [Å] and angles [°] for **43**.

N(1)-C(6)#1	1.3394(18)
N(1)-C(1)	1.3414(18)
C(1)-C(6)	1.4279(19)
C(1)-C(2)	1.438(2)
C(2)-C(3)	1.384(2)
C(2)-C(7)	1.429(2)
C(3)-C(13)	1.434(2)
C(3)-C(4)	1.446(2)
C(4)-C(5)	1.382(2)
C(4)-C(19)	1.434(2)
C(5)-C(25)	1.428(2)
C(5)-C(6)	1.439(2)
C(6)-N(1)#1	1.3394(18)
C(7)-C(8)	1.193(2)

C(8)-C(9A)	1.461(2)
C(9A)-C(11A)	1.443(4)
C(9A)-C(12A)	1.503(6)
C(9A)-C(10A)	1.583(5)
C(10A)-H(10A)	0.9600
C(10A)-H(10B)	0.9600
C(10A)-H(10C)	0.9600
C(11A)-H(11A)	0.9600
C(11A)-H(11B)	0.9600
C(11A)-H(11C)	0.9600
C(12A)-H(12A)	0.9600
C(12A)-H(12B)	0.9600
C(12A)-H(12C)	0.9600
C(10B)-H(10D)	0.9600
C(10B)-H(10E)	0.9600
C(10B)-H(10F)	0.9600
C(11B)-H(11D)	0.9600
C(11B)-H(11E)	0.9600
C(11B)-H(11F)	0.9600
C(12B)-H(12D)	0.9600
C(12B)-H(12E)	0.9600
C(12B)-H(12F)	0.9600
C(13)-C(14)	1.187(2)
C(14)-C(15A)	1.487(3)
C(14)-C(15B)	1.487(5)
C(15A)-C(18A)	1.488(11)
C(15A)-C(16A)	1.492(12)
C(15A)-C(17A)	1.543(11)
C(16A)-H(16A)	0.9600
C(16A)-H(16B)	0.9600
C(16A)-H(16C)	0.9600
C(17A)-H(17A)	0.9600
C(17A)-H(17B)	0.9600
C(17A)-H(17C)	0.9600
C(18A)-H(18A)	0.9600
C(18A)-H(18B)	0.9600

C(18A)-H(18C)	0.9600
C(15B)-C(16B)	1.496(17)
C(15B)-C(18B)	1.496(17)
C(15B)-C(17B)	1.541(17)
C(16B)-H(16D)	0.9600
C(16B)-H(16E)	0.9600
C(16B)-H(16F)	0.9600
C(17B)-H(17D)	0.9600
C(17B)-H(17E)	0.9600
C(17B)-H(17F)	0.9600
C(18B)-H(18D)	0.9600
C(18B)-H(18E)	0.9600
C(18B)-H(18F)	0.9600
C(19)-C(20)	1.184(2)
C(20)-C(21A)	1.471(3)
C(21A)-C(24A)	1.516(5)
C(21A)-C(22A)	1.518(5)
C(21A)-C(23A)	1.537(5)
C(22A)-H(22A)	0.9600
C(22A)-H(22B)	0.9600
C(22A)-H(22C)	0.9600
C(23A)-H(23A)	0.9600
C(23A)-H(23B)	0.9600
C(23A)-H(23C)	0.9600
C(24A)-H(24A)	0.9600
C(24A)-H(24B)	0.9600
C(24A)-H(24C)	0.9600
C(22B)-H(22D)	0.9600
C(22B)-H(22E)	0.9600
C(22B)-H(22F)	0.9600
C(23B)-H(23D)	0.9600
C(23B)-H(23E)	0.9600
C(23B)-H(23F)	0.9600
C(24B)-H(24D)	0.9600
C(24B)-H(24E)	0.9600
C(24B)-H(24F)	0.9600

C(25)-C(26)	1.195(2)
C(26)-C(27)	1.464(3)
C(27)-C(28)	1.497(3)
C(27)-C(30)	1.517(4)
C(27)-C(29)	1.528(4)
C(28)-H(28A)	0.9600
C(28)-H(28B)	0.9600
C(28)-H(28C)	0.9600
C(29)-H(29A)	0.9600
C(29)-H(29B)	0.9600
C(29)-H(29C)	0.9600
C(30)-H(30A)	0.9600
C(30)-H(30B)	0.9600
C(30)-H(30C)	0.9600
C(6)#1-N(1)-C(1)	117.30(12)
N(1)-C(1)-C(6)	121.34(12)
N(1)-C(1)-C(2)	118.71(12)
C(6)-C(1)-C(2)	119.93(12)
C(3)-C(2)-C(7)	120.17(13)
C(3)-C(2)-C(1)	119.36(13)
C(7)-C(2)-C(1)	120.47(13)
C(2)-C(3)-C(13)	120.07(14)
C(2)-C(3)-C(4)	120.54(13)
C(13)-C(3)-C(4)	119.38(14)
C(5)-C(4)-C(19)	120.82(14)
C(5)-C(4)-C(3)	120.90(13)
C(19)-C(4)-C(3)	118.29(14)
C(4)-C(5)-C(25)	119.93(13)
C(4)-C(5)-C(6)	119.29(13)
C(25)-C(5)-C(6)	120.78(13)
N(1)#1-C(6)-C(1)	121.36(12)
N(1)#1-C(6)-C(5)	118.91(12)
C(1)-C(6)-C(5)	119.73(12)
C(8)-C(7)-C(2)	175.20(17)
C(7)-C(8)-C(9A)	179.22(18)

C(11A)-C(9A)-C(8)111.1(2)
C(11A)-C(9A)-C(12A)
C(8)-C(9A)-C(12A)111.4(4)
C(11A)-C(9A)-C(10A)
C(8)-C(9A)-C(10A)106.1(2)
C(12A)-C(9A)-C(10A)
C(9A)-C(10A)-H(10A)
C(9A)-C(10A)-H(10B)
H(10A)-C(10A)-H(10B)
C(9A)-C(10A)-H(10C)
H(10A)-C(10A)-H(10C)
H(10B)-C(10A)-H(10C)
C(9A)-C(11A)-H(11A)
C(9A)-C(11A)-H(11B)
H(11A)-C(11A)-H(11B)
C(9A)-C(11A)-H(11C)
H(11A)-C(11A)-H(11C)
H(11B)-C(11A)-H(11C)
C(9A)-C(12A)-H(12A)
C(9A)-C(12A)-H(12B)
H(12A)-C(12A)-H(12B)
C(9A)-C(12A)-H(12C)
H(12A)-C(12A)-H(12C)
H(12B)-C(12A)-H(12C)
H(10D)-C(10B)-H(10E)
H(10D)-C(10B)-H(10F)
H(10E)-C(10B)-H(10F)
H(11D)-C(11B)-H(11E)
H(11D)-C(11B)-H(11F)
H(11E)-C(11B)-H(11F)
H(12D)-C(12B)-H(12E)
H(12D)-C(12B)-H(12F)
H(12E)-C(12B)-H(12F)
C(14)-C(13)-C(3) 175.50(19)
C(13)-C(14)-C(15A)174.1(4)
C(13)-C(14)-C(15B)173.4(9)

C(15A)-C(14)-C(15B)
C(14)-C(15A)-C(18A)
C(14)-C(15A)-C(16A)
C(18A)-C(15A)-C(16A)
C(14)-C(15A)-C(17A)
C(18A)-C(15A)-C(17A)
C(16A)-C(15A)-C(17A)
C(15A)-C(16A)-H(16A)
C(15A)-C(16A)-H(16B)
H(16A)-C(16A)-H(16B)
C(15A)-C(16A)-H(16C)
H(16A)-C(16A)-H(16C)
H(16B)-C(16A)-H(16C)
C(15A)-C(17A)-H(17A)
C(15A)-C(17A)-H(17B)
H(17A)-C(17A)-H(17B)
C(15A)-C(17A)-H(17C)
H(17A)-C(17A)-H(17C)
H(17B)-C(17A)-H(17C)
C(15A)-C(18A)-H(18A)
C(15A)-C(18A)-H(18B)
H(18A)-C(18A)-H(18B)
C(15A)-C(18A)-H(18C)
H(18A)-C(18A)-H(18C)
H(18B)-C(18A)-H(18C)
C(14)-C(15B)-C(16B)111.7(13)
C(14)-C(15B)-C(18B)113.9(11)
C(16B)-C(15B)-C(18B)
C(14)-C(15B)-C(17B)101.9(13)
C(16B)-C(15B)-C(17B)
C(18B)-C(15B)-C(17B)
C(15B)-C(16B)-H(16D)
C(15B)-C(16B)-H(16E)
H(16D)-C(16B)-H(16E)
C(15B)-C(16B)-H(16F)
H(16D)-C(16B)-H(16F)

H(16E)-C(16B)-H(16F)
C(15B)-C(17B)-H(17D)
C(15B)-C(17B)-H(17E)
H(17D)-C(17B)-H(17E)
C(15B)-C(17B)-H(17F)
H(17D)-C(17B)-H(17F)
H(17E)-C(17B)-H(17F)
C(15B)-C(18B)-H(18D)
C(15B)-C(18B)-H(18E)
H(18D)-C(18B)-H(18E)
C(15B)-C(18B)-H(18F)
H(18D)-C(18B)-H(18F)
H(18E)-C(18B)-H(18F)
C(20)-C(19)-C(4) 178.3(2)
C(19)-C(20)-C(21A)178.5(2)
C(20)-C(21A)-C(24A)
C(20)-C(21A)-C(22A)
C(24A)-C(21A)-C(22A)
C(20)-C(21A)-C(23A)
C(24A)-C(21A)-C(23A)
C(22A)-C(21A)-C(23A)
C(21A)-C(22A)-H(22A)
C(21A)-C(22A)-H(22B)
H(22A)-C(22A)-H(22B)
C(21A)-C(22A)-H(22C)
H(22A)-C(22A)-H(22C)
H(22B)-C(22A)-H(22C)
C(21A)-C(23A)-H(23A)
C(21A)-C(23A)-H(23B)
H(23A)-C(23A)-H(23B)
C(21A)-C(23A)-H(23C)
H(23A)-C(23A)-H(23C)
H(23B)-C(23A)-H(23C)
C(21A)-C(24A)-H(24A)
C(21A)-C(24A)-H(24B)
H(24A)-C(24A)-H(24B)

C(21A)-C(24A)-H(24C)
H(24A)-C(24A)-H(24C)
H(24B)-C(24A)-H(24C)
H(22D)-C(22B)-H(22E)
H(22D)-C(22B)-H(22F)
H(22E)-C(22B)-H(22F)
H(23D)-C(23B)-H(23E)
H(23D)-C(23B)-H(23F)
H(23E)-C(23B)-H(23F)
H(24D)-C(24B)-H(24E)
H(24D)-C(24B)-H(24F)
H(24E)-C(24B)-H(24F)
C(26)-C(25)-C(5) 174.90(17)
C(25)-C(26)-C(27)178.2(2)
C(26)-C(27)-C(28)110.38(19)
C(26)-C(27)-C(30)108.25(19)
C(28)-C(27)-C(30)108.8(3)
C(26)-C(27)-C(29)108.64(18)
C(28)-C(27)-C(29)111.0(2)
C(30)-C(27)-C(29)109.6(3)
C(27)-C(28)-H(28A)109.5
C(27)-C(28)-H(28B)109.5
H(28A)-C(28)-H(28B)
C(27)-C(28)-H(28C)109.5
H(28A)-C(28)-H(28C)
H(28B)-C(28)-H(28C)
C(27)-C(29)-H(29A)109.5
C(27)-C(29)-H(29B)109.5
H(29A)-C(29)-H(29B)
C(27)-C(29)-H(29C)109.5
H(29A)-C(29)-H(29C)
H(29B)-C(29)-H(29C)
C(27)-C(30)-H(30A)109.5
C(27)-C(30)-H(30B)109.5
H(30A)-C(30)-H(30B)
C(27)-C(30)-H(30C)109.5

H(30A)-C(30)-H(30C)
H(30B)-C(30)-H(30C)

Symmetry transformations used to generate equivalent atoms:
#1 -x+1,-y,-z+1

Table 4. Anisotropic displacement parameters ($Å^2 x 10^3$) for **43**. The anisotropic displacement factor exponent takes the form: $-2\pi^2[h^2 a^{*2}U^{11} + ... + 2 h k a^* b^* U^{12}]$

	U^{11}	U^{22}	U^{33}	U^{23}	U^{13}	U^{12}
N(1)	47(1)	40(1)	44(1)	-4(1)	19(1)	-2(1)
C(1)	46(1)	41(1)	40(1)	0(1)	18(1)	-1(1)
C(2)	54(1)	42(1)	45(1)	0(1)	21(1)	3(1)
C(3)	53(1)	53(1)	52(1)	4(1)	25(1)	7(1)
C(4)	47(1)	56(1)	54(1)	5(1)	21(1)	0(1)
C(5)	48(1)	47(1)	49(1)	-1(1)	18(1)	-4(1)
C(6)	46(1)	40(1)	41(1)	0(1)	18(1)	-1(1)
C(7)	60(1)	49(1)	54(1)	-1(1)	26(1)	7(1)
C(8)	70(1)	51(1)	58(1)	-4(1)	28(1)	6(1)
C(9A)	90(1)	54(1)	74(1)	-19(1)	37(1)	-10(1)
C(10A)	158(4)	52(2)	136(4)	-14(3)	37(4)	24(2)
C(11A)	255(10)	87(3)	70(3)	-27(2)	75(4)	-34(5)
C(12A)	154(5)	121(5)	219(10)	-19(5)	118(6)	-47(4)
C(9B)	90(1)	54(1)	74(1)	-19(1)	37(1)	-10(1)
C(10B)	200(13)	111(7)	92(6)	-53(6)	18(7)	-7(8)
C(11B)	410(30)	73(7)	98(7)	-22(6)	123(13)	-113(14)
C(12B)	119(9)	216(17)	360(30)	-210(20)	74(15)	7(10)
C(13)	57(1)	59(1)	69(1)	4(1)	31(1)	9(1)
C(14)	70(1)	69(1)	89(1)	2(1)	43(1)	9(1)

C(15A)	86(3)	75(2)	108(5)	-3(3)	59(3)	18(2)
C(16A)	123(4)	117(5)	308(11)	-55(6)	158(6)	-19(4)
C(17A)	150(6)	104(4)	169(5)	20(4)	94(5)	61(4)
C(18A)	161(4)	130(4)	112(3)	-28(3)	80(3)	21(4)
C(15B)	86(3)	75(2)	108(5)	-3(3)	59(3)	18(2)
C(16B)	130(12)	157(16)	480(50)	-180(30)	100(20)	-9(12)
C(17B)	350(40)	240(20)	390(30)	180(20)	340(30)	190(30)
C(18B)	114(10)	162(14)	236(15)	-1(12)	49(10)	77(10)
C(19)	49(1)	66(1)	66(1)	2(1)	24(1)	1(1)
C(20)	53(1)	72(1)	79(1)	3(1)	26(1)	1(1)
C(21A)	44(1)	100(2)	106(2)	-5(1)	27(1)	-3(1)
C(22A)	66(2)	148(5)	110(3)	8(3)	9(2)	-8(3)
C(23A)	88(3)	131(4)	169(6)	26(4)	52(3)	-35(3)
C(24A)	72(2)	168(6)	181(7)	-30(5)	50(3)	27(3)
C(21B)	44(1)	100(2)	106(2)	-5(1)	27(1)	-3(1)
C(22B)	80(7)	280(30)	198(14)	13(15)	83(8)	-30(11)
C(23B)	76(6)	212(17)	270(20)	100(18)	42(10)	69(8)
C(24B)	88(9)	270(30)	310(40)	-170(30)	38(15)	-58(14)

C(25)	49(1)	58(1)	61(1)	-6(1)	19(1)	-8(1)
C(26)	54(1)	67(1)	75(1)	-13(1)	22(1)	-12(1)
C(27)	75(1)	71(1)	96(2)	-30(1)	32(1)	-24(1)
C(28)	234(4)	137(3)	132(2)	-65(2)	105(3)	-61(3)
C(29)	223(4)	82(2)	149(3)	-19(2)	73(3)	-54(2)
C(30)	79(2)	194(4)	295(5)	-135(4)	17(2)	-42(2)

Table 5. Hydrogen coordinates (x 10^4) and isotropic displacement parameters (Å^{2}x 10^3) for **43**.

	x	y	z	U(eq)
H(10A)	3458	6098	6012	183
H(10B)	3808	6384	5268	183
H(10C)	4005	7311	6153	183
H(11A)	4294	4946	7546	200
H(11B)	4676	6359	7680	200
H(11C)	5159	5054	7833	200
H(12A)	5364	6899	6630	226
H(12B)	5074	6207	5640	226
H(12C)	5637	5452	6521	226
H(10D)	5621	4591	7381	219
H(10E)	5036	4552	7853	219
H(10F)	5448	5896	7828	219
H(11D)	5280	5688	5868	280
H(11E)	5185	6982	6389	280
H(11F)	4559	6566	5427	280
H(12D)	4218	6735	7248	354
H(12E)	3745	5414	6965	354

H(12F)	3636	6544	6215	354
H(16A)	906	2786	5200	240
H(16B)	971	3489	6139	240
H(16C)	1382	2125	6171	240
H(17A)	2104	5439	5256	196
H(17B)	1391	5560	5493	196
H(17C)	1361	4733	4614	196
H(18A)	2541	3305	7223	189
H(18B)	2097	4655	7094	189
H(18C)	2807	4582	6845	189
H(16D)	1829	5557	6304	392
H(16E)	2338	5559	5724	392
H(16F)	2600	4816	6695	392
H(17D)	1287	2130	5938	404
H(17E)	1232	3403	6506	404
H(17F)	1982	2596	6816	404
H(18D)	1250	4455	4316	264
H(18E)	814	4711	4971	264
H(18F)	839	3266	4582	264
H(22A)	449	200	2257	173
H(22B)	-107	-912	2303	173
H(22C)	660	-1319	2264	173
H(23A)	904	-2701	3694	193
H(23B)	159	-2227	3766	193
H(23C)	920	-2030	4622	193
H(24A)	731	587	4611	210
H(24B)	-61	76	3948	210
H(24C)	333	1214	3607	210
H(22D)	938	-1502	4832	265
H(22E)	100	-1125	4264	265
H(22F)	681	-2	4774	265
H(23D)	665	1426	3469	289
H(23E)	-108	699	3016	289
H(23F)	433	743	2480	289
H(24D)	799	-1812	2494	352
H(24E)	-7	-1685	2493	352

H(24F)	582	-2625	3223	352
H(28A)	2684	-3368	1465	236
H(28B)	2624	-4931	1528	236
H(28C)	3372	-4201	2123	236
H(29A)	3295	-5292	3614	226
H(29B)	2572	-5998	2916	226
H(29C)	2539	-5134	3750	226
H(30A)	1558	-3779	2755	309
H(30B)	1504	-4422	1802	309
H(30C)	1635	-2875	1965	309

Table 6. Torsion angles [°] for **43**.

C(6)#1-N(1)-C(1)-C(6)	-0.3(2)
C(6)#1-N(1)-C(1)-C(2)	178.17(12)
N(1)-C(1)-C(2)-C(3)	-175.57(13)
C(6)-C(1)-C(2)-C(3)	2.9(2)
N(1)-C(1)-C(2)-C(7)	4.0(2)
C(6)-C(1)-C(2)-C(7)	-177.54(13)
C(7)-C(2)-C(3)-C(13)	-5.7(2)
C(1)-C(2)-C(3)-C(13)	173.90(13)
C(7)-C(2)-C(3)-C(4)	175.45(14)
C(1)-C(2)-C(3)-C(4)	-5.0(2)
C(2)-C(3)-C(4)-C(5)	2.4(2)
C(13)-C(3)-C(4)-C(5)	-176.51(14)
C(2)-C(3)-C(4)-C(19)	-177.28(14)
C(13)-C(3)-C(4)-C(19)	3.8(2)
C(19)-C(4)-C(5)-C(25)	2.6(2)
C(3)-C(4)-C(5)-C(25)	-177.07(14)
C(19)-C(4)-C(5)-C(6)	-177.97(14)
C(3)-C(4)-C(5)-C(6)	2.4(2)
N(1)-C(1)-C(6)-N(1)#1	0.3(2)
C(2)-C(1)-C(6)-N(1)#1	-178.14(12)
N(1)-C(1)-C(6)-C(5)	-179.78(12)
C(2)-C(1)-C(6)-C(5)	1.8(2)
C(4)-C(5)-C(6)-N(1)#1	175.54(13)

C(25)-C(5)-C(6)-N(1)#1	-5.0(2)
C(4)-C(5)-C(6)-C(1)	-4.4(2)
C(25)-C(5)-C(6)-C(1)	175.04(13)
C(3)-C(2)-C(7)-C(8)	-33(2)
C(1)-C(2)-C(7)-C(8)	148(2)
C(2)-C(7)-C(8)-C(9A)	-146(12)
C(7)-C(8)-C(9A)-C(11A)	-100(14)
C(7)-C(8)-C(9A)-C(12A)	28(14)
C(7)-C(8)-C(9A)-C(10A)	141(14)
C(2)-C(3)-C(13)-C(14)	-56(2)
C(4)-C(3)-C(13)-C(14)	123(2)
C(3)-C(13)-C(14)-C(15A)	2(6)
C(3)-C(13)-C(14)-C(15B)	160(8)
C(13)-C(14)-C(15A)-C(18A)	15(5)
C(15B)-C(14)-C(15A)-C(18A)	-153(7)
C(13)-C(14)-C(15A)-C(16A)	-107(5)
C(15B)-C(14)-C(15A)-C(16A)	84(6)
C(13)-C(14)-C(15A)-C(17A)	133(4)
C(15B)-C(14)-C(15A)-C(17A)	-36(6)
C(13)-C(14)-C(15B)-C(16B)	-101(8)
C(15A)-C(14)-C(15B)-C(16B)	69(6)
C(13)-C(14)-C(15B)-C(18B)	26(9)
C(15A)-C(14)-C(15B)-C(18B)	-164(8)
C(13)-C(14)-C(15B)-C(17B)	140(7)
C(15A)-C(14)-C(15B)-C(17B)	-50(6)
C(5)-C(4)-C(19)-C(20)	-177(100)
C(3)-C(4)-C(19)-C(20)	2(7)
C(4)-C(19)-C(20)-C(21A)	-24(14)
C(19)-C(20)-C(21A)-C(24A)	16(9)
C(19)-C(20)-C(21A)-C(22A)	139(9)
C(19)-C(20)-C(21A)-C(23A)	-103(9)
C(4)-C(5)-C(25)-C(26)	15(2)
C(6)-C(5)-C(25)-C(26)	-165(2)
C(5)-C(25)-C(26)-C(27)	-63(8)
C(25)-C(26)-C(27)-C(28)	179(100)
C(25)-C(26)-C(27)-C(30)	60(7)

C(25)-C(26)-C(27)-C(29)	-59(7)

Symmetry transformations used to generate equivalent atoms:

#1 -x+1,-y,-z+1